# Thin-bedded Facies Analysis of a Ferron Storm-dominated Delta Front and Prodelta: Cretaceous Ferron Sandstone, Utah

---

A Thesis

Presented to

the faculty of the Department of Earth and Atmospheric Sciences

University of Houston

---

In Partial Fulfillment

of the Requirements for the Degree

Masters of Science

---

By:

Darsel Seepersad

August 2012

# Thin-bedded Facies Analysis of a Ferron Storm-dominated Delta Front and Prodelta: Cretaceous Ferron Sandstone, Utah

Darsel Seepersad

APPROVED:

Dr. Janok P. Bhattacharya, Advisor

Dr. William Dupré, Committee Member

Dr. Kyle Strom, Committee Member

Dr. Mark Smith, Dean, College of Natural Sciences and Mathematics

## ACKNOWLEDGEMENTS

I would first and foremost thank God for blessing me with the opportunity to pursue my dreams. You have blessed me and given me the strength to continue each day even when times made me want to do the opposite.

I also offer the deepest gratitude to my advisor Dr. Janok Bhattacharya for his guidance throughout this project. He has been extremely patient and has given me his undivided attention throughout the past two years. I have learnt many skills from him, including being an effective research scientist. His passion for Geology and teaching is inspiring, and I have felt lucky to have an advisor like him. Special thanks also to my other committee members Dr. William Dupre, and Dr. Kyle Strom for their various inputs throughout the development of this thesis.

I would like to thank Yangyang Li, for his patience with me in the field as I learnt to take measured sections, as well as the time he took out of his schedule to help me put my thesis into perspective. Also thanks to Chris Campbell for being my research assistant in the field, who helped me set up rapelling stations, taught me to rapell, and sat there for many hours each day in the scorching sun until my field day was over. I am also grateful to my other housemates Danfix D'Souza and Omar Montes, for making three months in the desert seem like much less. We had many fun times roaming around Hanksville, finding ways to entertain ourselves.

Special thanks to Shawn Wright. I am grateful for the motivation given when this thesis got stressful. I am also grateful for the time taken to proof read my work, even when his

schedule seemed busier than mine. I also appreciate the time that he took out during Spring break to drive me to Hanksville, Utah, and help me with additional field work. I know there must have been many more enjoyable ways to spend your Spring break.

I would like to thank Sumiyyah Ahmed for the time she took out of her busy schedule to help me with the preparation for the proposal of this thesis. She guided me with many papers and discussions on how to get started.

Thanks to ExxonMobil, BP, Shell, Pioneer Resources, Nexen, Anadarko, and BHP Billiton for their contributions made to the funding of this project. Also thanks to the University of Houston for providing me with a Graduate Tuition Assistant Fellowship, as well as a Teaching Assistant position. Without their financial contribution, I would not have had the opportunity or resources to complete this thesis.

Lastly, but definitely not least, I would like to thank my mother Indera Seepersad, my father Ramchan Seepersad, my sister, Dana Seepersad and my brother Dale Seepersad for the support given through, not only this thesis, but my entire educational progress. They are not physically present here with me, but I have gotten financial support, guidance and love over many Skype phonecalls, and Whatsapp messages for which I am thankful. I was able to keep up with everything in Trinidad while I have spent the last two years in Houston.

August, 2012

# Thin-bedded Facies Analysis of a Ferron Storm-dominated Delta Front and Prodelta: Cretaceous Ferron Sandstone, Utah

---

An Abstract of a Thesis

Presented to

the faculty of the Department of Earth and Atmospheric Sciences

University of Houston

---

In Partial Fulfillment

of the Requirements for the Degree

Masters of Science

---

By:

Darsel Seepersad

August 2012

## Abstract

This study examines thin-bedded facies within shelf and prodelta deposits of the Cretaceous Ferron Notom Delta in central Utah. Thin beds may be the result of storms (tempestites), ignitive turbidity currents, or hyperpycnal flows. This study quantitatively evaluates the proportion of each facies types within heterolithic strata at the base of the sandier lithofacies to better characterize the relative proportion of formative processes.

Mud along shelves has traditionally been linked to suspension settling. This study also quantitatively compares structures initiated by traction deposition to those linked to suspension settling in an attempt to show that most mud deposited offshore is due to reworking by waves and storms, and hyperpycnal flows. Primary data were derived from well-exposed outcrops of parasequences 5a, 5b, 6, 11, and 16b, within the Notom deltaic wedge, which represent a spectrum of wave-dominated shorefaces to river-dominated deltas.

Parasequences 5a and 5b are comprised of over 60% HCS beds with subordinate amounts of wave-rippled strata. Parasequence 5a represents a high-energy wave environment. Parasequence 5b also reflects a wave-dominated environment; however, a greater proportion of massive to planar interbeds suggests fluvial and wave mixing. Parasequence 6 contains predominantly normal and inverse graded units with numerous Bouma sequences and starved ripples. Parasequence 6 is river/flood dominated, containing both ignitive turbidites and hyperpycnites. Parasequence 11 is dominated by graded bedding, and shows the highest degree of river/flood dominance with the highest

evidence of hyperpycnal deposits seen within the three parasequences. Parasequence 16 is dominated by massive units, along with graded beds, Bouma sequences, and rare HCS. Parasequence 16b shows evidence of all three processes, although ignitive turbidite deposits seem to dominate. Over 90% of all parasequences were represented by bedload deposits as opposed to suspended sediment settling.

Tempestites, ignitive turbidites, and hyperpycnites likely occur within the same system, interacting with each other, producing deposits which have remnant signatures of each. Results show it is possible to document the relative proportion of formative processes within heterolithic sequences, as well as to quantify them in terms of wave versus fluvial versus tidal dominance, as well as bedload versus suspended load transport.

# Table of Contents

# List of Figures

# List of Tables

# 1. Introduction and Motivation

Many oil and gas reservoirs contain some recoverable hydrocarbons in beds with thicknesses below the resolution of conventional logging tools (Passey, 2006, a). With the constant decline in the world's hydrocarbon production it is therefore necessary to understand these reservoirs, which are commonly bypassed.

## 1.1 Deltas

Deltas have traditionally been divided into three categories; river, wave, and tide dominated (Figure 1.1.1), based on the idea that the ratio of fluvial, wave, and tidal processes results in different and identifiable plan-view morphology of the resulting deposits, as well as characteristic internal facies successions (Galloway, 1975; Bhattacharya, 2006). Elongate shaped deltas were thought to be typical of fluvial dominance (e.g The Mississippi Delta), cuspate to arcuate systems were linked to being highly wave-influenced such as the Sao Francisco delta, while estuarine-shaped deltas were thought to be highly tidal dominated (e.g The Fly Delta). Most deltas however are mixed influence and do not fall into one category.

Ainsworth et al., (2011) modified Galloway's tripartite classification system to include secondary and tertiary processes which act on a system. He uses a lettered system, where W=wave, F=fluvial, and T=tidal. A bold upper case letter refers to the dominant process which acts on the system; a bold lower case letter refers to the secondary process, while a lower case italic letter refers to the tertiary process. An example of this is **Fw***t*, which represents a fluvial-dominated system, with some wave influence, and

minor tidal influence. Another example is **Wf**, which represents a wave-dominated system with some fluvial influence but no tidal processes.

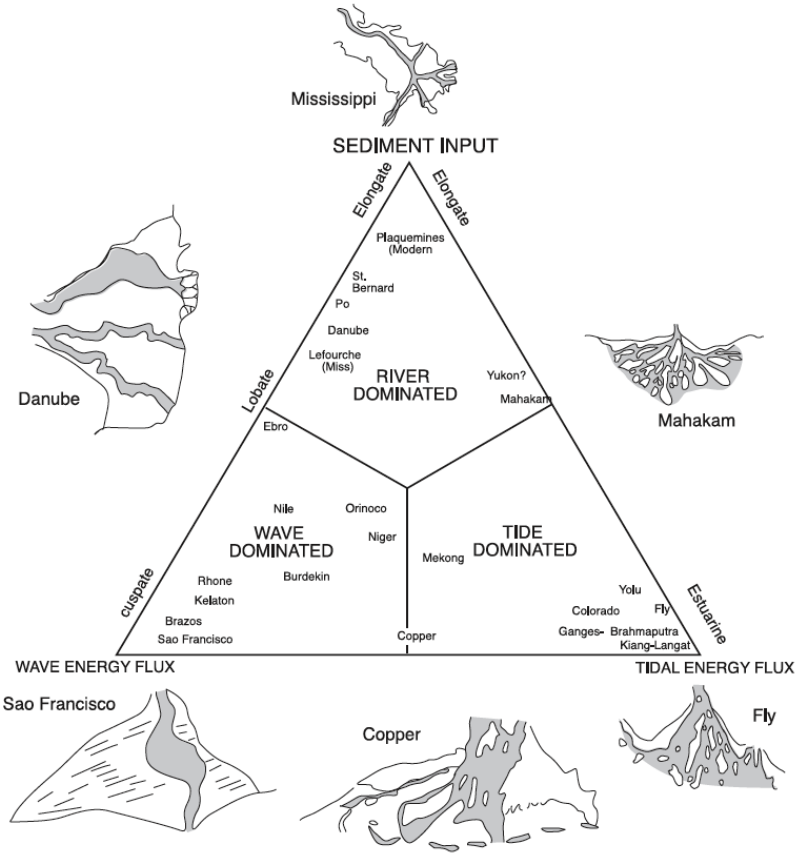


*Figure 1.1.1 The tripartite classification of deltas, into river-, wave-, and tide- dominated end members (Galloway, 1975)*

It is now recognized that the internal geometries may reflect a different dominance from plan view alone (Rodriguez et al, 2000; Lambiase et al., 2003; Gani and Bhattacharya, 2007). Lambiase et al. (2003) investigated the intertidal and subtidal lithofacies on the Trusan Delta with surface observations, trenches, and shallow cores, to show that commonly used delta classification schemes that rely heavily on surface morphology (e.g., Galloway, 1975; Coleman, 1982) to define hydrodynamic dominance and predict stratigraphic architecture are inappropriate for his example. Similarly, Rodriguez (2000)

looked at the Brazos delta, Texas. He showed that the facies architecture is not representative of the classic strandplain model for wave-dominated deltas, due to the strong influence of floods on the deltaic evolution.

Bhattacharya (2006) summarized common vertical facies present in river-dominated prodelta sediments. These are typically heterolithic laminated to thin-bedded mudstones with or without sandstones. Siltstones and sandstones are well stratified, and may show graded bedding. The graded bedding may reflect deposition from hyperpycnal density underflows generated at the river mouth during high-discharge floods (Mulder and Syvitski, 1995). Bioturbation varies depending on the rate of sedimentation, as well as the grain size of the supplied sediment (Bhattacharya, 2006). If there are high sedimentation rates, there may be sedimentary structures resulting from soft sediment deformation. Wave-formed structures may occur at the tops of graded sandstone beds, but are less abundant than in a more wave-influenced setting (Bhattacharya, 2006). If floods occur during major coastal storms, sets of highly aggrading wave ripples may be abundant.

Within wave-dominated delta fronts, there is an asymmetry that results from oblique wave approach, with amalgamated sandy beach-ridge and shoreface deposits on the updrift side, and muddier, more fluvial facies on the downdrift side (Bhattacharya and Giosan, 2003). Prodelta mudstones may be more bioturbated, thinner, and sandier than in river-dominated settings.

Tidally influenced deltas usually have abundant tidal indicators, including herring bone cross bedding, tidal bundles, and reactivation surfaces, although these features are found in many non-deltaic settings (Dalrymple, 1992). There is usually heterolithic wavy bedding (e.g flaser bedding), with abundant mud drapes and reactivation surfaces. Mudstones show abundant subaqueous shrinkage cracks, which may reflect salinity changes (Bhattacharya, 2006).

The purpose of this study is to use descriptions of the vertical facies successions of prodelta and delta-front facies successions on a millimeter to decimeter scale to predict the dominant delta classification (wave versus fluvial versus tidal) for multiple parasequences, as well as to quantitatively predict the relative proportions of the formative processes that produce heterolithic sections.

These parasequences have previously been described on a broader scale and interpreted by Zhu (2010) and Li (2009), where the heterolithic strata have been grouped as single facies units. In contrast, this study will also compare these previous interpretations with a lamina to thin-bedded scale interpretation to complete a more accurate and quantitative analysis. We are also interested in determining whether process-dominance changes when analyzing sandy versus muddy components of a facies succession. Sandy facies are commonly deposited above fair weather wave base and may show greater wave influence versus more distal, muddy facies.

## 1.2 Tempestites, Ignitive Turbidites, and Hyperpycnal flows

In order to better predict the dominance of wave, fluvial, and tidal influences on a delta, we must first understand the formative processes associated with the deposition of a deltaic system. These processes include tempestites, ignitive turbidites, and hyperpycnites.

The term tempestite is used as a synonym for a storm deposit. If a delta is influenced by many storm (tempestite), and flood deposits, they generally have a fairly characteristic signature, making their recognition in the rock record, in core, and in outcrop comparatively straight forward (Suter, 2006). During storms, waves, downwelling storm currents, or some type of combined flow may cut an initial erosional surface (Suter, 2006). This surface may be flat, undulatory, or channelized at a small scale (gutter casts) and may contain sole marks or tool marks in the form of flute casts, groove casts, or sole casts (Suter, 2006). Pebbles or a lag sometimes occur above the surface, which is overlain by low-angle laminated to hummocky cross-stratified sands (Harms et al., 1975).The term hummocky cross-stratification was introduced by Harms et al. (1975) for medium- to large-scale cross-stratification, mainly in coarse silt and fine sand, in which sets of fairly gently dipping laminae with erosional contacts suggest deposition on a bedding surface in the form of shifting three-dimensional hummocks and depressions (Figure1.2.1). Hummocky cross stratification forms under oscillatory flow conditions, with the addition of relatively minor unidirectional forcing causing a transition to low-angle laminae dipping in the direction of current flow. As the storm wanes, wave oscillation

ripples and/or combined-flow ripples form. Post storm deposits are generally characterized by suspension fallout, although this theory is currently being questioned (Macquaker et al., 2010). A typical vertical succession within a tempestite can be seen in Figure 1.2.2.

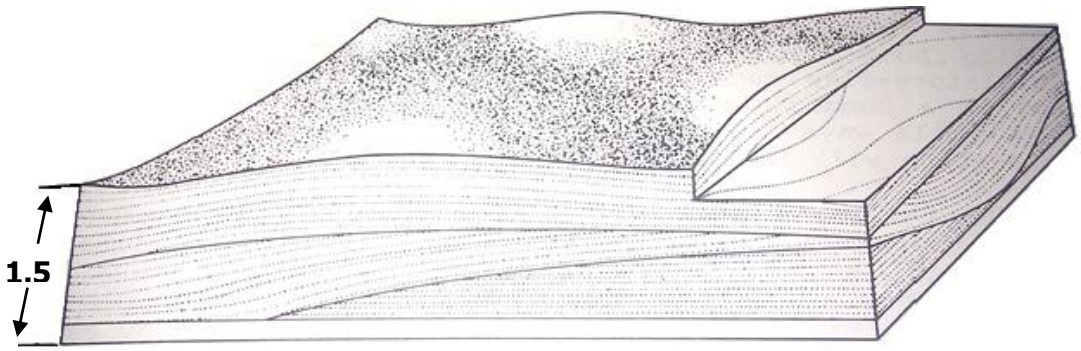


*Figure 1.2.1 A typical vertical cross section of hummocky cross stratification (Harms and Walker, 1982)*

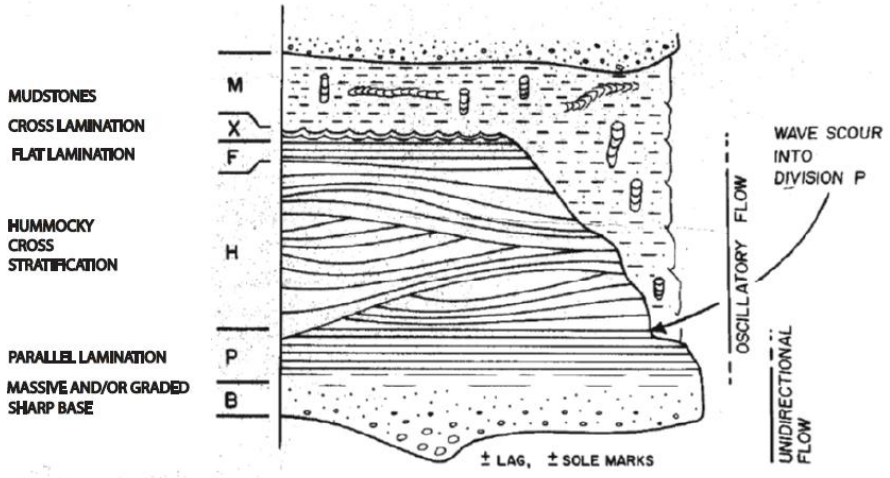


*Figure 1.2.2 A conceptualized sequence for the sedimentary structures within a tempestite deposit. (Lock et al., 2009, after Walker et al., 1983)*

Turbidites were first properly described by Arnold H. Bouma in 1962, who studied rocks deposited deep water and recognized particular fining up sandstone intervals within fine grained shales. Bouma described a characteristic vertical succession of facies within the turbidite, which can be seen in Fig 1.2.3, now termed the Bouma sequence.

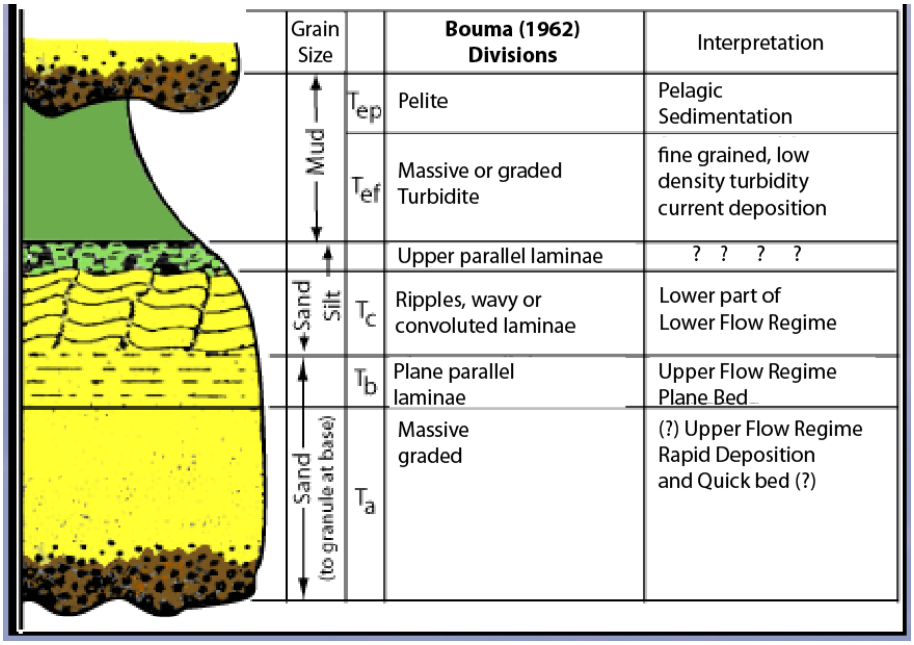


*Figure 1.2.3 An idealized Bouma Sequence*
*(http://sepmstrata.org/deepwater/DeepWatClasticSediments.html)*

Tempestite deposits bear superficial similarity to turbidites, because both result from waning currents and are therefore normally graded. Tempestites are combined flows in which storm-generated waves (oscillatory flow) overprint density-induced (unidirectional, geostrophic) flows (Myrow et al., 2001). Tempestites may pass downslope into true turbidites, and are commonly described as wave-modified turbidites (e.g., Myrow et al., 2001, 2002). (Figure 1.2.4).

Mulder and Syvitski (1995) differentiated between turbidity currents that are generated by ignitive transformation of a submarine slide into a turbulent flow (catastrophic), from flows that are generated by non-ignitive processes, such as a hyperpycnal discharge or a river during floods (Table1.2.1).

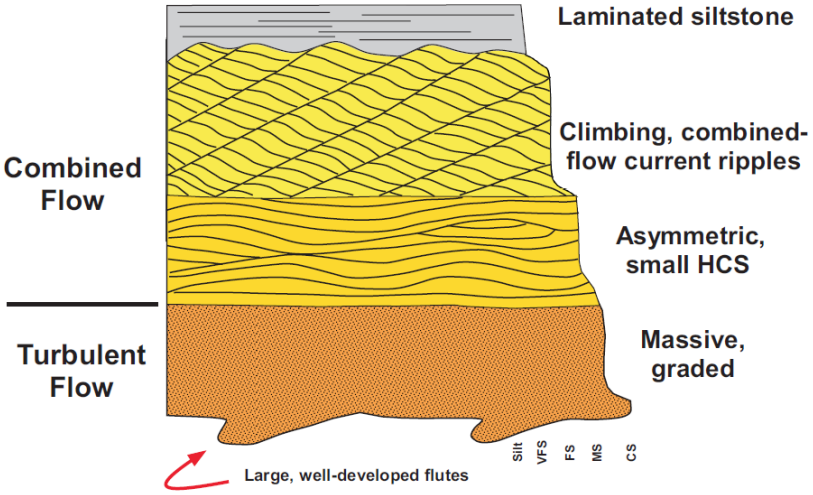


*Figure 1.2.4. A general model for a tempestite deposited by a wave-modified gravity flow (From Myrow et al., 2002 via: Suter, 2006)*

| Hyperpycnal Flows | Surge-induced flow |
|---|---|
| Minimum threshold of particle concentration for triggering: Initial concentration 5(?)-200kg $m^{-3}$ | No minimum threshold of particle concentration for triggering: Concentration: <1-15--kg $m^{-3}$ |
| Flow velocity: <2m $s^{-1}$ | Flow Velocity: < 4m $s^{-1}$, >10m $s^{-1}$ on steep slopes |
| Thick and long flow | Thick flow |
| No individual flow head | Well defined flow head, body and tail |
| Quasi steady flows | Unsteady flows |
| Duration: minutes to weeks | Duration: minutes to hours |

*Table 1.2.1 A comparison between hyperpycnites and ignitive turbidites (surge-induced) (Mulder et al., 2003)*

Hyperpycnal flows form in the marine environment when the density of the river water exceeds that of the marine water in which it enters. This flow usually occurs when a small- to medium-sized river floods (Mulder et al., 2003). This flow moves as a density

current that deposits its load along the gentle slopes of the delta front to form turbidites. Unlike ignitive turbidity current flows, hyperpycnal flows can be relatively long lived *and* travel long distances (Soyinka and Slatt, 2008; Nakajima, 2006). Hyperpycnites differ from other turbidites due to their well-developed inversely graded facies, as well as their intrasequence erosional contacts.

Posamentier and Walker (2006) looked at an ignitive turbidity current flows that produced massive slumps in Grand Banks (Newfoundland), in 1929. This slump, as with many ignitive tubidity currents, was triggered by earthquakes. They are linked to high flow velocities up to 20 m/s, and flow thicknesses of several hundred meters. Hyperpcynal flows however begin as inertial flows at the river mouth and transform into density underflows and ultimately turbidity flow on the slope. Such flows generally are of greater duration (i.e., days or weeks) than those that originate from large sediment slumps (i.e., hours) (Posamentier and Walker, 2006).

Nakajima (2006) described hyperpycnites in the central Japan Sea, where they were documented for up to 700 km downcurrent from linked river canyon fan systems. During the increasing or waxing period at the river mouth, the hyperpycnal flow develops a coarsening-up basal unit. During the decreasing or waning discharge period at the river mouth, the hyperpycnal flow develops a fining upward unit (Mulder et. al., 2003). Alternation of structureless to parallel-laminated sandstones may also indicate more sustained flows (Plink-Björklund and Steel, 2004). Also, since systems are usually not

hyperpycnal throughout the year, and most sediment discharge occurs during rare, large magnitude floods, we can expect to see some cyclicity within hyperpycnal deposits.

Mulder et al. (2003) also suggests that sedimentary structures, such as that related to ripple migration, may be indicative of hyperpycnal flows, with the most common being climbing ripples, suggesting particle deposition larger than particle transport. We can therefore use the different vertical successions created by ignitive turbidites, as opposed to hyperpycnal ones to distinguish them from each other. Table 1.2.2 shows the features that are expected to be associated with various storm and flood deposits.

The ideas that mud is transported and deposited primarily by simply suspension settling from suspended hypopycnal flows is under question. Hill et al. (2007) suggests that hypopycnal flows can only transport sediment up to 10 km initially from river mouths through the process of mud aggregate settling, although they may be deflected by coriolis in tidal processes. Suter (2006) suggests that they can be transported over 100 km. The presence of mud deposits many more kilometers away from the shoreline, with evidence of traction features, such as laminations and ripples, have suggested that bedload transport of mud may be a dominant process.

Many major delta complexes show major mud-dominated coastlines and inner-shelf mud belts, typically elongated downdrift of the river mouth, such as the Mekong in Vietnam (Ta et al. 2005), the Atchafalaya in the Gulf of Mexico (Augustinus 1989; Allison and Neil 2003; Rotondo and Bentley 2003), the Po in the Adriatic (Cattaneo et al. 2003 and Cattaneo et al. 2007), the Fly in Papua New Guinea (Walsh et al. 2004). Other

processes for the transport and deposition of mud are also possible. These include hyperpycnal flows from river mouths (Mulder et al., 2003; Nakajima, 2006 and others), as well as storm- and wave-reworked sediments (such as wave-enhanced sediment-gravity flows), which remobilize and transport mud further offshore. Mud flocculates at the seabed and forms low density sand- and silt-size floc particles that behave as bedload sand grains. Macquaker (2010) examined wave-enhanced sediment-gravity flows on the modern Eel shelf and described 3 components of mud beds related to their deposition. These include: homogenous or rippled, parallel-laminated, and bioturbated fabrics. Snedden and Nummedal (1991) looked at storm influenced shelves and their ability to re-suspend sediments to depths of over 100m through combined flows. These theories have been confirmed by laboratory experiments (Schieber et al., 2007; Schieber and Southard, 2009; Schieber and Yawner, 2009; Schieber et al., 2010) which show subtly cross-laminated mud current ripples (Macquaker and Bohacs, 2007; Macquaker et al., 2010).

My study compares the percentage of bedload transport from these vertical sections, to that from suspension fallout, associated with these storm and flood deposits.

| | IGNITIVE TURBIDITES | HYPERPYCNITES | TEMPESTITES |
|---|---|---|---|
| *Vertical Sequence* | Typical Bouma Sequence- Normally Graded | Inversely graded followed by normal grading | Normally Graded |
| *Bioturbation* | Minimal | Minimal | Mudstone commonly bioturbated |
| *Erosional Features* | flute casts, groove casts, or sole casts | flute casts, groove casts, or sole casts | Gutter Casts, flute casts, groove casts, or sole casts |
| *Thickness* | Up to a few meters | < 1m | Up to a few meters |
| *Lateral Extent* | Dependent on plume size, and viscosity | Dependent on plume size and viscosity | Dependent on storm size |
| *Sedimentary Structures* | Bouma Sequence | Inverse grading, followed by normal grading or repetition of Bouma sequence units in more sustained flows | symmetrical lamination, planar lamination, Hummocky cross-stratification, wave rippled |
| *Length of Time* | Short-lived (hours) | Sustained flow (days-weeks) | Short-lived (hours) |
| *Cause of Initiation* | Slope | Minimal threshold of particle concentration needed for triggering | Storm |
| *Velocity* | High (Up to 40 m/s) | Low (<2 m/s) | |

*Table 1.2.2 Expected characteristics of ignitive turbidites, hyperpycnites, and tempestite deposits (Harms et al., 1982; Myrow et al., 1992; Mulder and Syvitski, 1995; Mulder et al., 1998; Mulder et al., 2003; Plink-Björklund and Steel, 2004).*

## 1.3 Beds and Thin Beds

In order to understand the scale at which this mapping is done and why is it important, the concept of thin beds is discussed below.

A bed is defined as a layer of sedimentary rocks or sediments bounded above and below by bedding surfaces" (Campbell, 1967). The characteristics of a bed are given in Table 1.3.1. Beds represent the basic building blocks of larger sedimentary bodies. From smallest to largest, the component layers of a sedimentary body comprise laminae, lamina-sets, beds, and bed-sets (Campbell, 1967). Table 1.3.2 provides a more recent description of some of these terms. There are other component layers which are bigger than those mentioned above such as a barforms, bar assemblages, and others typically found in thicker sandstone units.

| | Characteristic | Lamina | Lamina Set | Bed | Bedset |
|---|---|---|---|---|---|
| | Name | Lamina surface | Laminaset surface | Bedding Surface | |
| Bounding Surface | Physical Nature | Sharp contact- may not be as sharp as bedding surface, often surface along which rocks part | Same as for bedding surfaces | Sharp Contact | |
| | Relation between Bounding Surfaces | Same as for bedding surfaces | | Parallel or non-parallel | |
| | Configuration of bounding surface | | | Even, wavy, or curved | |
| | Synchronous | Yes | Yes | Yes | |
| External Morphology | Geometry | Same as for bed | Same as for bed | Tabular, lens, or sometimes wedge shapes, also various forms bounded by curved surfaces | Same as for component beds |
| | Thickness | Usually measured in millimeters. | Usually measured in centimeters | Usually measured in centimeters or thicker units | Multiples of thickness of component beds |
| | Lateral Extent | Less than one inch in current ripples to a few miles in abyssal deposits | One inch in current ripples to few miles in turbidites | Few feet in fluvial festoons to few miles in turbidites | Tens of feet in fluvial deposits to hundred miles in some evaporite deposits |
| | Lateral Termination | (1) Intersection of laminar surfaces, (2) Gradation into another material in which laminar surfaces can no longer be recognized, (3) Abutting against an inconformity, (4) Truncation by bedding surfaces or abutting against | (1) Intersection of laminaset surfaces, (2) Truncation by laminaser or bedding surface or abutting against these surfaces (3) Gradation to another material in which laminaset surfaces can no longer be recognized | (1) Intersection of bedding surfaces, (2) Gradation to another material in which bedding surfaces can no longer be recognized, (3) Abutting against an unconformity | Termination of component beds in any of the three ways noted for bed |
| | Composition | Uniform (sometimes gradational) | Same as for bed | Uniform, rhythmic variation, or systematic gradation | |
| | Texture | Uniform (sometimes heterogeneous or gradational) | | Uniform, heterogenous, rhythmic variation or systematic gradation | |
| Internal Characteristics | Internal Structure | None (other than parallelism of component grains) | | Usually laminated (may not be laminated due to original depositional conditions or activity of organisms) | Same as for component beds |
| | Arrangement of internal layers | None | | Rhythmic or repetitive | Repetitive |
| | Relation of internal layers to bounding surfaces | None | | Parallel to or at an angle | Same as for component beds |

| | Adjacent layers | Same in repetitive laminae or different in rhythmic laminae | | Same or different | Different |
|---|---|---|---|---|---|
| Genesis | Conditions during formation | Constant | | Essentially constant overall but may fluctuate rhythmically, repetitively, or gradationally | Essentially constant overall but with repetition of the particular conditions prevailing during formation of a bed |
| | Time for formation | Instant of geologic time (a second for lamina in current ripples to years for lamina in abyssal oozes) | Moment of geologic time (a minute for some current ripple laminasets to a year for laminasets in aeolian festoons) | Many moments of geologic time ( a few minutes for some fluvial beds to years for some carbonate and evaporite beds) | Multiple of many moments (a few days for some fluvial bedsets to thousands of years for beach bedsets) |

*Table 1.3.1 Characteristics of a bed as defined by Campbell (1967).*

| Layer type | Definition | Time for deposition | Typical thicknesses |
|---|---|---|---|
| Lamina | Laminae are defined as the smallest megascopic geological layers. Laminae are uniform in composition and texture, and are never internally layered. | Min to hr | Less than 1 in. [2.5 cm] |
| Lamina-set | A relatively conformable succession of genetically related laminae bounded by surfaces of erosion, non-deposition, or their correlative conformities. Lamina-sets consist of a group or set of conformable laminae that compose distinctive structures in a bed. | Min to days | Less than 5 ft [1.5 m] |
| Bed | A relatively conformable succession of genetically related laminae or lamina-sets bounded by surfaces of erosion, non-deposition, or their correlative conformities. Not all beds contain lamina sets. | Min to yr | Inches to tens of ft |
| Bed-set | A relatively conformable succession of genetically related beds bounded by surfaces of erosion, non-deposition, or their correlative conformities. Beds above and below bed-sets always differ in composition, texture, or sedimentary structure from those composing the bed-set. | Longer period of time than beds | 1 to 50 ft [.3 to 15 m] |

*Table 1.3.2. A recent discussion of the terms laminae, lamina sets, beds, and bed-sets (Van Wagoner et al., 1990)*

In much of the geological literature, the term thin bed has been used in different contexts. Campbell (1967) limits the term ‘thin’ bed to a thickness between 3 and 10 cm (Figure 1.3.1). Bates and Jackson (1984) used the term to include sedimentary beds ranging from 5 to 60 cm. The geophysical literature defines a thin bed as the smallest resolvable bed which can be seen on seismic data. Model and field data examples reveal a practical limit of thin-bed resolution up to λ/16, promoting high-resolution correlation of stratigraphy and fine-scale reservoir geophysics beyond λ/4 (Zeng, 2008), which is the commonly accepted practical limit.

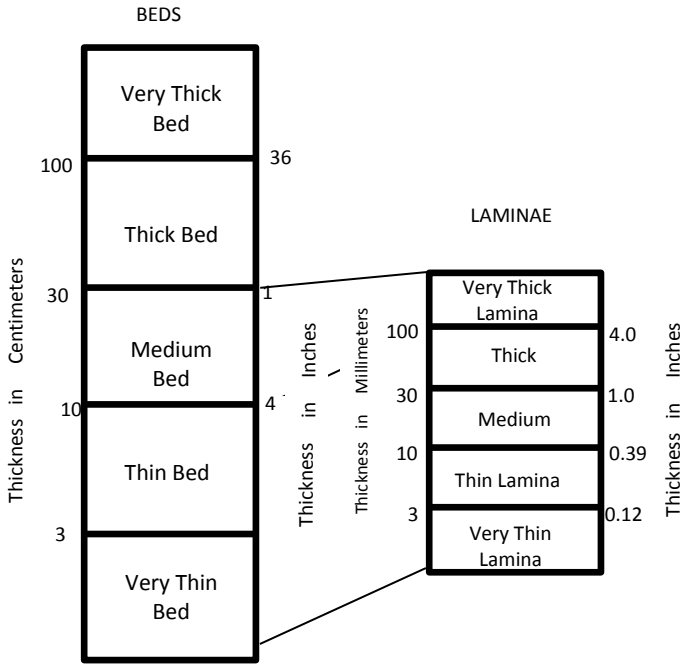


*Figure 1.3.1 The limits of thin beds as defined by Campbell in 1967. (Campbell, 1967, adapted from Ingram, 1954)*

In the petrophysical literature, the term bed has been defined as “any contiguous unit of rock with a narrow distribution of petrophysical characteristics that is bounded above and

below by units with significantly different petrophysical characteristics." (Passey et al., 2006, a,b). Petrophysical characteristics include porosity, grain density, permeability, and capillary pressure behavior. A petrophysical thin bed is one with a thickness of between 1 inch (2.5cm) and 2 feet (0.6m) (Passey et al., 2006, b).

There have been many studies of thin beds since the 1950's in the petrophysical literature, using the term 'shaly sand'. A 'shaly sand' is defined as a sandstone in which quartz is the primary mineral, but clay and other associated minerals may be present in varying amounts, distributions, and particle sizes (Passey et al., 2006, b). Thin beds have therefore historically also been called shaly sands. These thin beds, or shaly sands, are often below the resolution of seismic and well log data, and yields a lower resistivity response than thick sandstone units. If these units are predicted, they are known as low resistivity pay. If they are not recognized, they may end up being bypassed pay.

Petrophysical thin bed studies were first done in order to determine the amount of clay present in order to correct for porosity. Asquith (1990) describes the development in types of logging methods used since the 1950's, which allowed for an accurate determination in the volume of clay present and the ability to accurately derive porosity and water saturation values in shaly sandstone reservoirs.

The standard shaly sand analysis models were developed to address the effects of dispersed clays in sandstones, rather than macroscopically interbedded sandstones and shales. They therefore do not correctly account for the effect of thin beds on log

responses. In the early 1950's only electric logs were available (Asquith, 1990). These tools were inadequate to correctly resolve thin beds and once the response reached below a cutoff value, the formation was assumed to be shaly, despite possibly having a high net:gross value (Figure 1.3.2). Since then, higher resolution logs have become available, such as electronic borehole image (EBI) logs (Passey et al., 2006, a), which are better able to resolve bed thicknesses. The absolute resolution of a given log varies, depending on the specific tool's intrinsic resolution, the data sampling rate, logging speed, and data processing methods (Passey et al., 2006, a). Common logs may be ranked from lowest to highest vertical resolution as follows: Spontaneous potential, deep resistivity, gamma ray, bulk density, neutron porosity, acoustic, very shallow resistivity (e.g., microspherically focused log (MSFL)), dipmeters, sonic borehole image and electrical borehole image (EBI) logs (Passey et al., 2006, a).

Since then, the determination of original hydrocarbons in place (OOIP) now includes in its volumetric equation the hydrocarbon pore thickness (HPT), which is often referred to in the petrophysical literature as hydrocarbon pore volume (HPV). This quantity is a measure of thickness, rather than volume, and the total HPT is calculated by summing up the incremental HPT over the interval of interest (ie. thin bed intervals). Analysis and calculation of HPT is necessary in the creation of sand and shale maps.

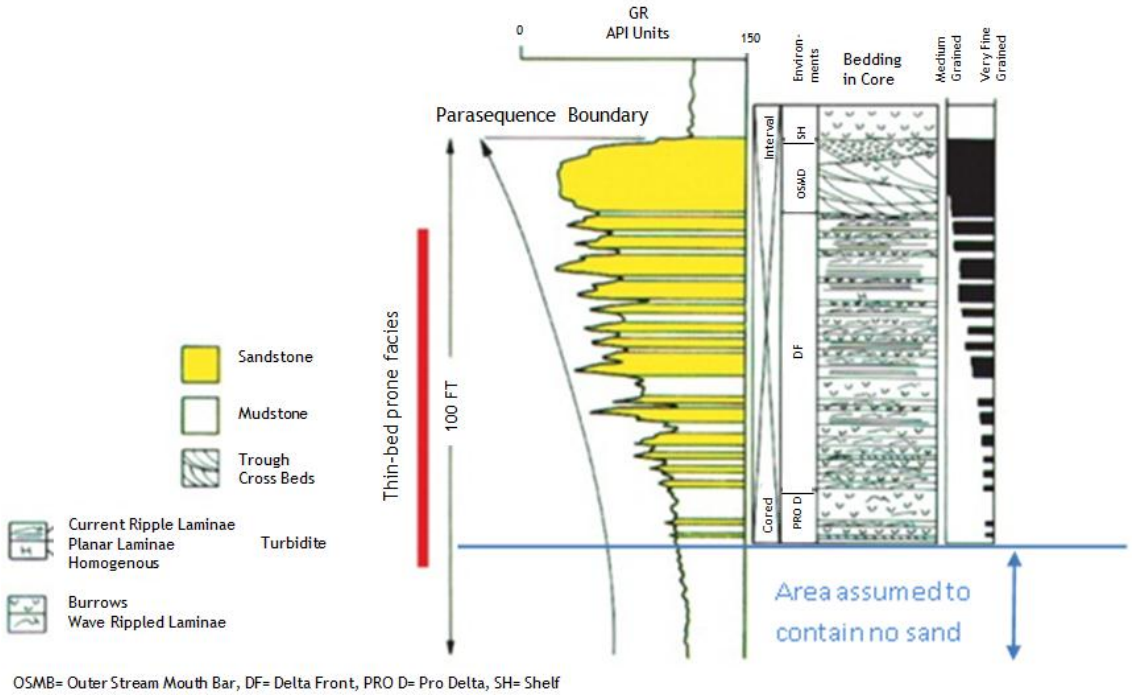


*Figure 1.3.2 A typical parasequence which forms in a deltaic environment on a sandy or wave dominated shoreline. The red bold line indicates where thin sandstone beds often occur. Figure also shows that below a certain depth, the formation is assumed to contain no more sandstone due to the lack of resolution taken by the tool. (Modified after Van Wagoner, 1990).*

Thin beds can occur in all siliciclastic environments, as can be seen in Table 1.3.3. The area of this study is the Ferron Sandstone in South central Utah, which occurs in a paleo-deltaic environment. Zhu (2010) described the Ferron Notom delta on a regional scale. He used many of the same methods used in this study. These are further described in Section 4. There has not, however, been any millimeter to decimeter scale mapping or millimeter to decimeter scale bedding diagrams created on the heterolithic lithofacies within this delta complex. This study will aim to provide a comprehensive look at heterolithic facies within multiple parasequences within the Ferron Notom delta complex in order to quantify formative mechanisms. It can be seen in Table 1.3.3 that

thin beds are common in delta-front and pro-delta areas. Parasequences in these deltaic regions are generally coarsening upward facies successions, as seen in the parasequences studied within the Ferron Notom delta complex. Figure 1.3.2 illustrates a parasequence that formed in a deltaic environment on a sandy fluvial, or wave dominated shoreline. The red bold line indicates where thin sandstone beds often occur (Passey et al., 2006).

| Depositional System | Thin-bed-prone | Not thin-bed-prone |
|---|---|---|
| Deep-water | Overbank/levee deposits<br>Distributary lobe<br>Channel margin<br>Hemipelagic | Channel axis<br>Debrites (sandy or muddy) |
| Beach/shoreface | Lower shoreface<br>Distal lower shoreface | Foreshore<br>Upper shoreface |
| Deltaic | Delta front<br>Prodelta | Stream-mouth bar |
| Tidal/estuarine | Sandy tidal channel<br>Intertidal sand flats | Subtidal |
| Fluvial | Point bars (meandering stream)<br>Levees<br>Terminal splay (overbank) | Braided streams<br>Channel sands<br>Channel lag deposits<br>Fluvial bars<br>Alluvial fans |
| Aeolian | Interdune<br>Wind-rippled deposits | Cross-bedded dunes |

*Table 1.3.3 Areas within depositional systems which are thin-bed prone. It illustrates that thin beds can occur in all siliiclastic environments. (Passey et al., 2006b)*

## 2. Geologic Setting

The Western Interior Seaway (Fig 2.1) split the continent of North America into two halves, Laramidia and Appalachia, during most of the mid- and late-Cretaceous period. Both Boreal waters from the Arctic Ocean and Tethyan waters from the Gulf of Mexico invaded the basin (Williams and Stelck, 1975). Aptian–Maastrichtian sedimentary deposits from the seaway crop out in the Western Interior Basin of Canada and the United States (Cumbaa et al., 2010).

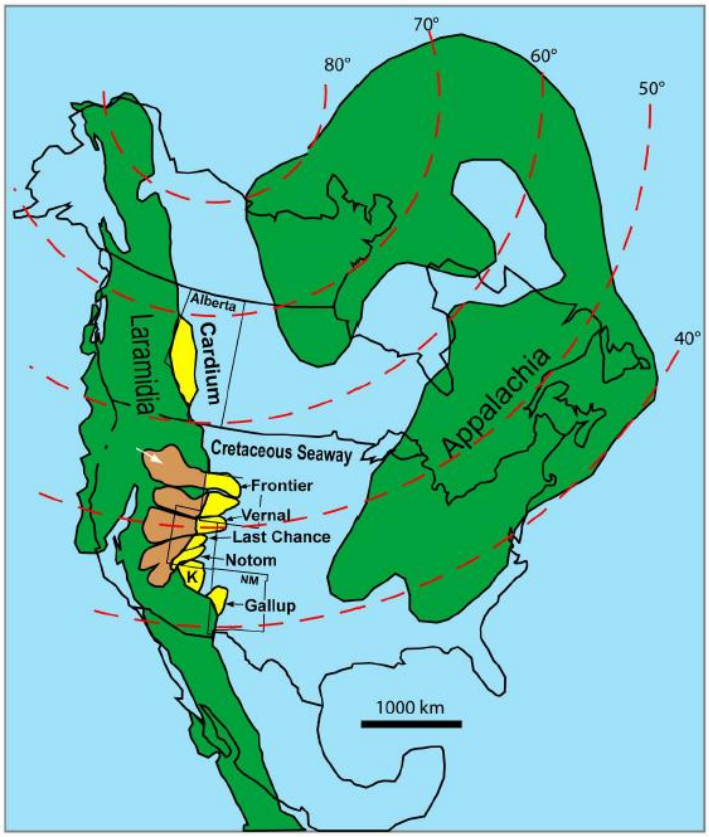


*Figure 2.1 Location of the Western Interior Seaway during the Turonian. Delta complexes within the Mancos shale can be seen here which includes the Ferron Notom Delta, The Ferron Last Chance Delta, as well as the Vernal Delta. (Bhattacharya and MacEachern, 2009)*

At its maximum, the Western Interior Seaway extended 4800 km from the present-day Arctic Ocean to the Gulf of Mexico, and had a maximum width of approximately 1600 km (Kauffman, 1984). Evidence from facies and faunal assemblages indicates maximum water depths of about 250 to 300 m (Kauffman, 1977), with fluctuations reflecting eustatic sea-level changes affected by seafloor spreading rates. It was therefore a relatively shallow sea. This seaway was formed as the young, buoyant Farallon plate subducted beneath the North American plate producing dynamic topography throughout most of Western North America. The seaway connected the Northern Boreal sea with the Gulf of Mexico. Two great continental watersheds drained into it from east and west, diluting its waters and bringing in eroded clay, silt, sand and gravel that formed shifting delta systems along its low-lying coasts. Numerous delta complexes have been deposited along the western margin, including the Ferron Delta complex.

The Ferron Delta complex includes the Notom, Last Chance, and Vernal deltas of Middle Turonian to Late Santonian age (Garrison and van den Bergh, 2004). The Notom Delta was the first to develop around 90.7Ma, in the Henry Mountain regions of Utah. At about 90.3Ma, there was a major river avulsion which shifted the depocenter north-northwestward to form the Last Chance Delta in the Castle Valley area (Gardner, 1995; Garrison and van den Bergh, 2004).

The Notom fluvial-deltaic system has both non-marine, fluvial-dominated delta plain facies association, and genetically related shallow marine facies associations (Peterson and Ryer, 1975; Garrison and van den Bergh, 2004). The Ferron Sandstone can be

seen in outcrop today in south central Utah, between Hanksville and Caineville. The Ferron Sandstone was first defined as a member of the Mancos Shale Formation by Lupton in 1914. It sits on top of the Tununk Shale Member and is overlain by the Blue Gate shale Member (Figure 2.2).

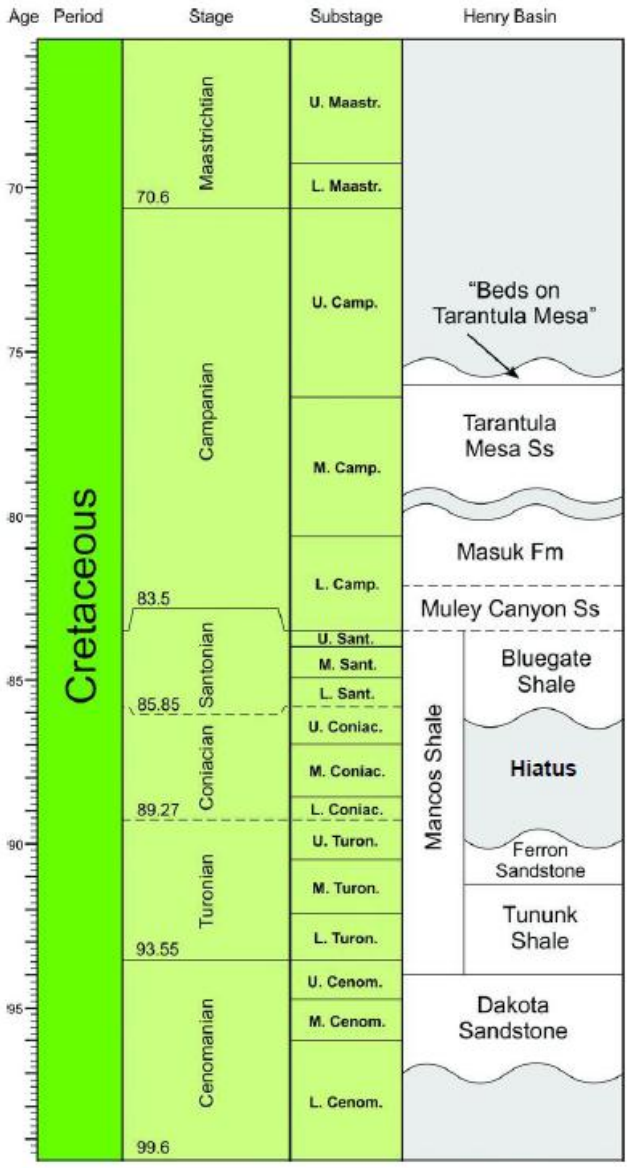


*Figure 2.2 The stratigraphic succession within the Mancos Shale, and the position of the Ferron sandstone within it. (Fielding, 2010)*

The Ferron Sandstone Member records the widespread regression of the Western Interior Seaway during the middle to late Turonian, as the shoreline prograded eastward, and there was a change in the shoreline configuration after the deposition of the Tununk Shale Member. A pronounced curve of the shoreline developed reflecting interaction between sediment supply and subsidence (Ryer, 2004).

## 3. Study Area/ Previous Interpretations

The Ferron Notom Delta complex consists of forty three (43) parasequences, eighteen (18) parasequence sets, and six (6) sequences (Zhu, 2010) (*Figure 3.1*). Table 3.1 shows a summary of this along with information about the sequence stratigraphy, shoreline trajectory and parasequence stacking patterns within the Ferron-Notom complex. Parasequences measured for this study are highlighted in pink.

Of the 43 parasequences, 5 were documented for this study; parasequences 5a, 5b, 6, 11, and 16b (*Figure 3.2*). These parasequences were previously measured by other students and were interpreted based on large meter-scale mapping techniques. They each showed various interpretations, with 5a and 5b being storm dominated, 6 being fluvial dominated, and 11 and 16b being of mixed influence (Zhu, 2010 and Li, 2010). These sections are well exposed, with thinly bedded sands, which are ideal for the measurement and analysis of millimeter to decimeter thick thin-bedded intervals. These parasequences were ideal for studying the processes that allowed for their deposition, and allowed for a comparison based on previous larger scale work.

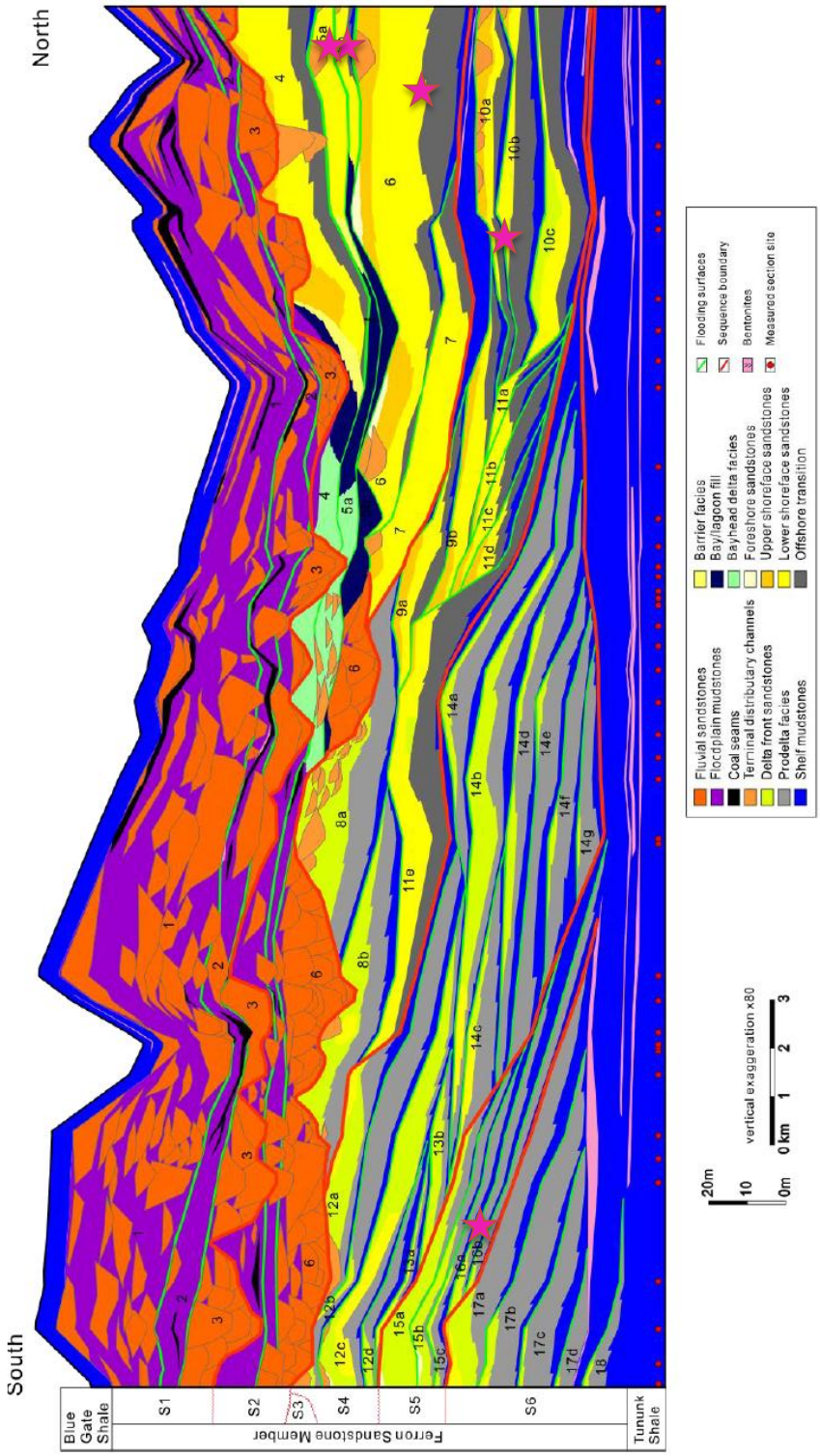


*Figure 3.1 Dip stratigraphy of the Ferron Notom Delta. Illustrated are the 43 parasequences, 18 parasequence sets, and 6 depositional sequences. (Zhu, 2010)*

| Sequence | System tract | Parasequence set | Parasequences | Stacking pattern | Shoreline trajectory | Shoreline translation distance (km) | Relative sea level change (m) |
|---|---|---|---|---|---|---|---|
| 1 | HST | 1 | 1 | Aggradation* | Ascending regressive | -- | ↑ 27.0* |
| | TST | 2 | 2 | Retrogradation* | Ascending transgressive | -- | ↑ 7.0* |
| | LST | 3 | 3 | Aggradation* | Ascending regressive | -- | ↑ 17.9* |
| 2 | HST | 4 | 4 | Progradation | Ascending regressive | 3.6 | ↓ 18.5* |
| | | 5 | 5a, 5b | Aggradation | Ascending regressive | -3.6 | ↑ 32.7 |
| | LST | 6 | 6 | Progradation-aggradation | Ascending regressive | 6.9 | ↑ 2.0 |
| | FSST | 7 | 7 | Degradation | Descending regressive | 9.6 | ↑ 20.0 |
| 3 | HST | 8 | 8a, 8b | Aggradation-progradation | Ascending regressive | 7.8 | ↓ 38.3 |
| | TST | 9 | 9a, 9b | Retrogradation | Ascending transgressive | -23.7 | ↑ 7.7 |
| | LST | 10 | 10a, 10b, 10c | Progradation-aggradation | Ascending regressive | 5.3 | ↑ 41.0 |
| | FSST | 11 | 11a, 11b, 11c, 11d, 11e | Degradation | Descending regressive | 20.2 | ↑ 12.5 |
| 4 | HST | 12 | 12a, 12b, 12c, 12d | Aggradation-progradation | Ascending regressive | 4.1 | ↓ 61.7 |
| | TST | 13 | 13a, 13b | Retrogradation | Ascending transgressive | -15.6 | ↑ 23.0 |
| | LST | 14 | 14a, 14b, 14c, 14d, 14e, 14f, 14g | Progradation-aggradation | Ascending regressive | 3.9 | ↑ 17.5 |
| 5 | HST | 15 | 15a, 15b, 15c | Aggradation-progradation | Ascending regressive | 9.0 | ↑ 32.0 |
| | | 16 | 16a, 16b | Aggradation | Ascending regressive | -2.9 | ↓ 47.2 |
| | LST | | | | | 1.9 | ↑ 14.6 |
| | | | | | | 0.2 | ↑ 2.0 |
| 6 | HST | 17 | 17a,17b, 17c, 17d | Aggradation-progradation | Ascending regressive | 0.8 | ↑ 8.1 |
| | | | | | | 3.5 | ↓ 8.5 |
| | LST | 18 | 18 | Progradation-aggradation | Ascending regressive | -1.5 | ↑ 32.0 |
| | | | | | | 0.5 | ↑ 4.1 |
| | | | | | | | ↑ 7.2 |

*Table 3.1 Summary of 43 parasequences, 18 parasequence sets and 6 sequences, along with information about sequence stratigraphy, shoreline trajectory, and parasequence stacking patterns within the Ferron Notom complex. Parasequences observed for this study are highlighted in green. "-"represents landward shoreline translation. "↑" represents relative sea-level rise, whereas "↓"represents relative sea-level fall. (Modified after Zhu, 2010)*

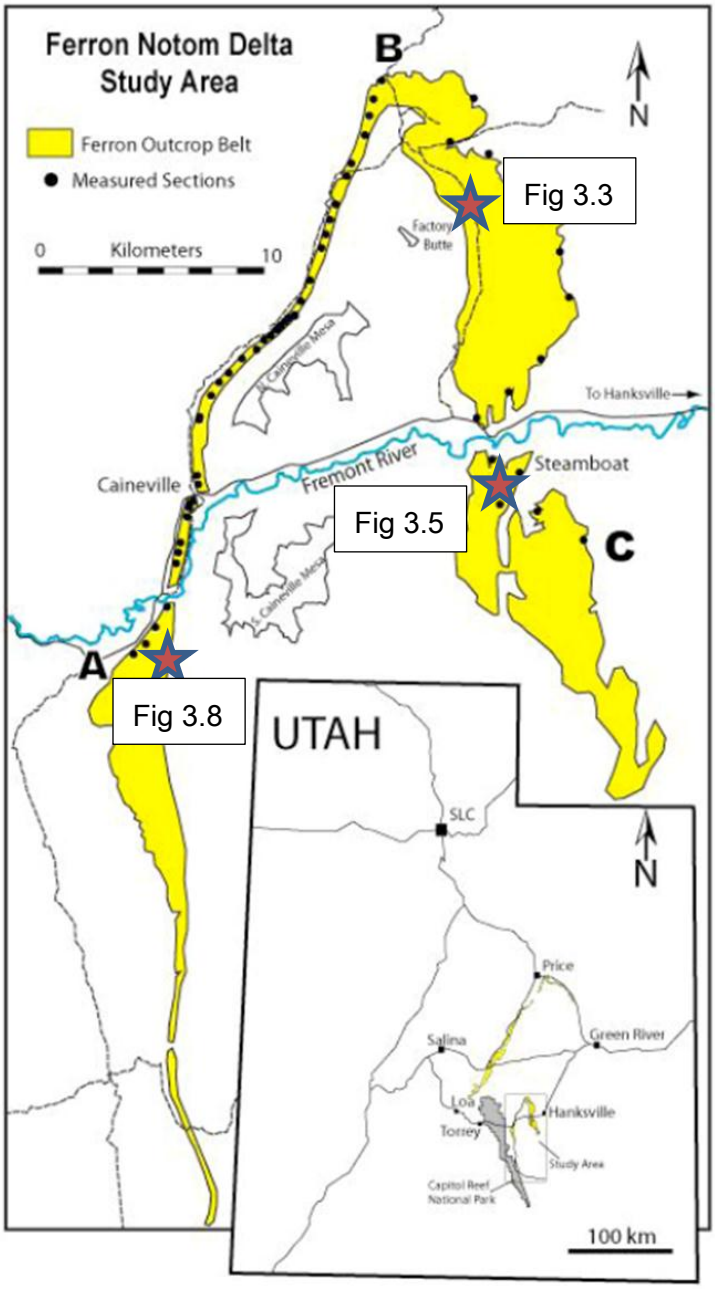


*Figure 3.2a showing the location of the Ferron Sandstone outcrop in South Central Utah, between Hanksville, and Caineville and locations of measured sections along west and east cliffs that surround the Caineville Mesa and Factory Butte. (Zhu, 2010)*

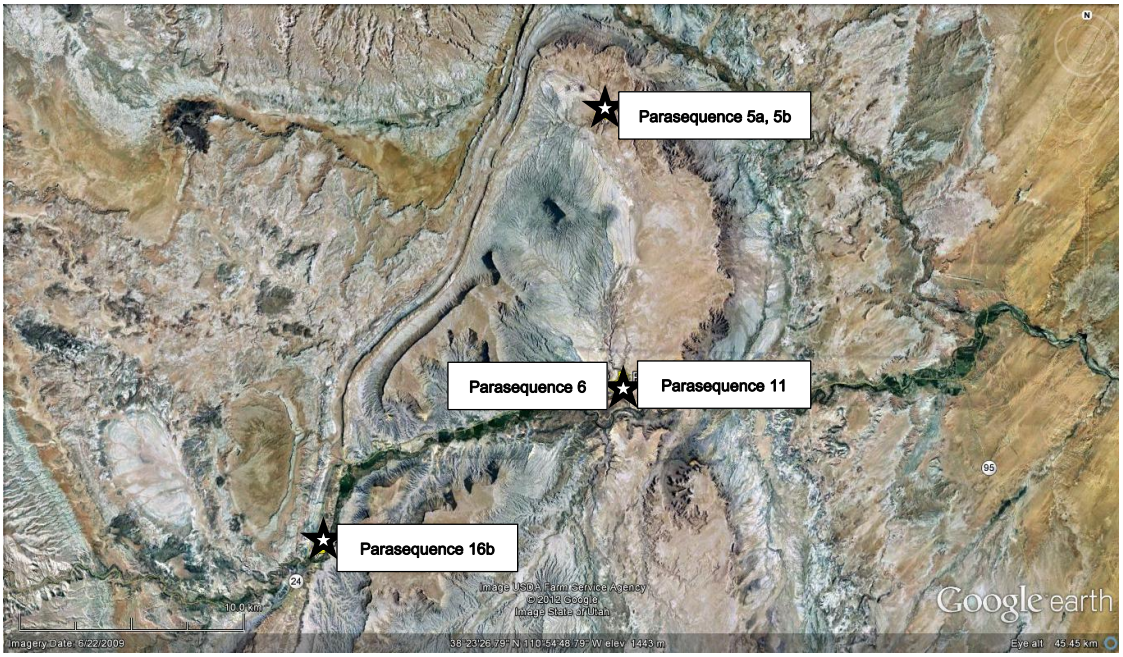


*Figure 3.2b Location of the various parasequences studied in this thesis (Google Earth, 2012)*

Parasequence 5 consists of two coarsening upward parasequences named 5a and 5b. These are located within Coalmine Wash (*Figure 3.3*). It overlies parasequence 6, and is underlain by parasequence set 4 (*Figure 3.4*). It was interpreted to be part of the highstand systems tract within sequence 2, showing an aggradational stacking pattern. All parasequences within parasequence set 5 show similar along-strike facies variations, changing from storm/wave-dominated shoreface facies associations in the NW to storm/wave- to river-dominated delta front facies associations to the SE, and back to storm/wave-dominated shoreface deposits farther south (Zhu, 2010).

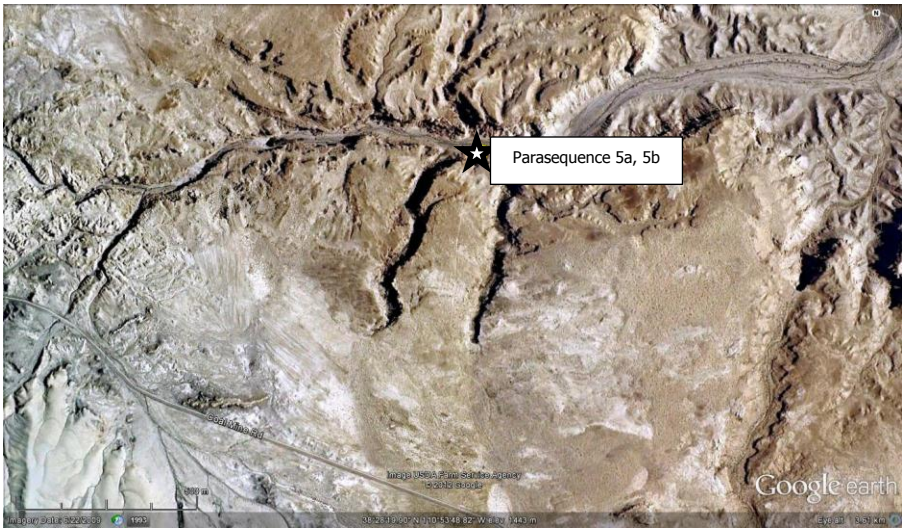


*Figure 3.3 The location of parasequence set 5 within Coalmine Wash (Google Earth, copyright 2012)*

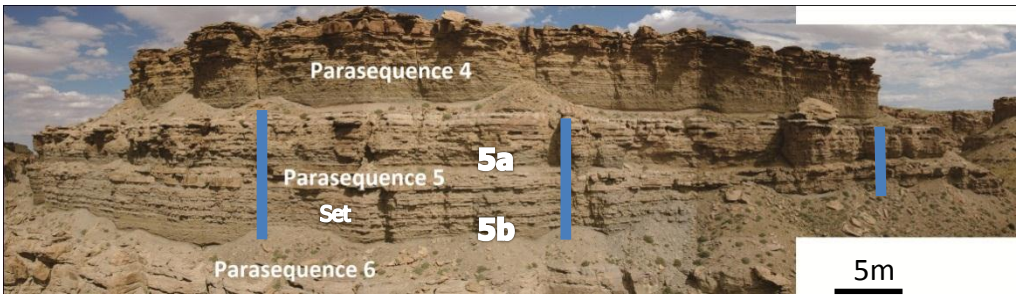


*Figure 3.4 Parasequence Set 5 (vertically exaggerated) overlying parasequence 6 and underlies parasequence 4. Parasequence 5 consists of two upward coarsening cycles; 5a and 5b. Blue bars represents length of recorded measured section*

Parasequences 6 and 7 were interpreted by Zhu et al. (2011) to be the lowstand systems tract within sequence 2, showing a progradational stacking pattern. Bedset 6-3 shows storm-, river-dominated delta front to prodelta facies. Bedsets 6-2 and 6-1 show along strike facies variations from storm/wave-dominated shoreface facies associations in the west, to storm/river-dominated delta-front facies associations (Zhu, 2010). Parasequence 6 for this study was documented along Highway 24 in the Steamboat area (*Figure 3.5 and Figure 3.6*).

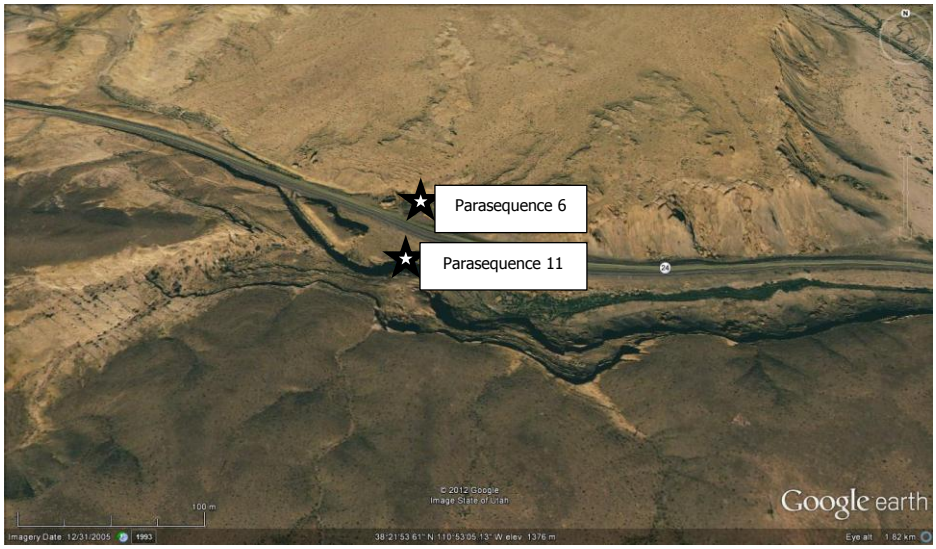


*Figure 3.5 Location of parasequence 6 and parasequence set 11. (Google Earth, copyright, 2012)*


*Figure 3.6 Photograph of location of measured section taken of parasequence 6. Blue bar represents length of recorded measured section.*

Parasequence Set 11 shows a marked sea-level drop from parasequence 12 which lies below it (Zhu, 2011). It was interpreted to represent the falling stage systems tract of sequence 3. Parasequence 11e was interpreted by Zhu et al. (2011) to consist primarily

of storm/wave-dominated shoreface sandstones and offshore transition mudstones with 3% river-influenced facies. The other four parasequences (11d-11a) consist of storm/ wave-dominated shoreface sandstones and offshore transition mudstones (Zhu, 2010). No significant facies variations between parasequences were observed in parasequence set 11. The sand/mud ratio for parasequences set 11 is about 1:1.2 (Zhu, 2010). Parasequence 11 was also documented along Highway 24 in the Steamboat Area (Figure 3.5, and 3.7).

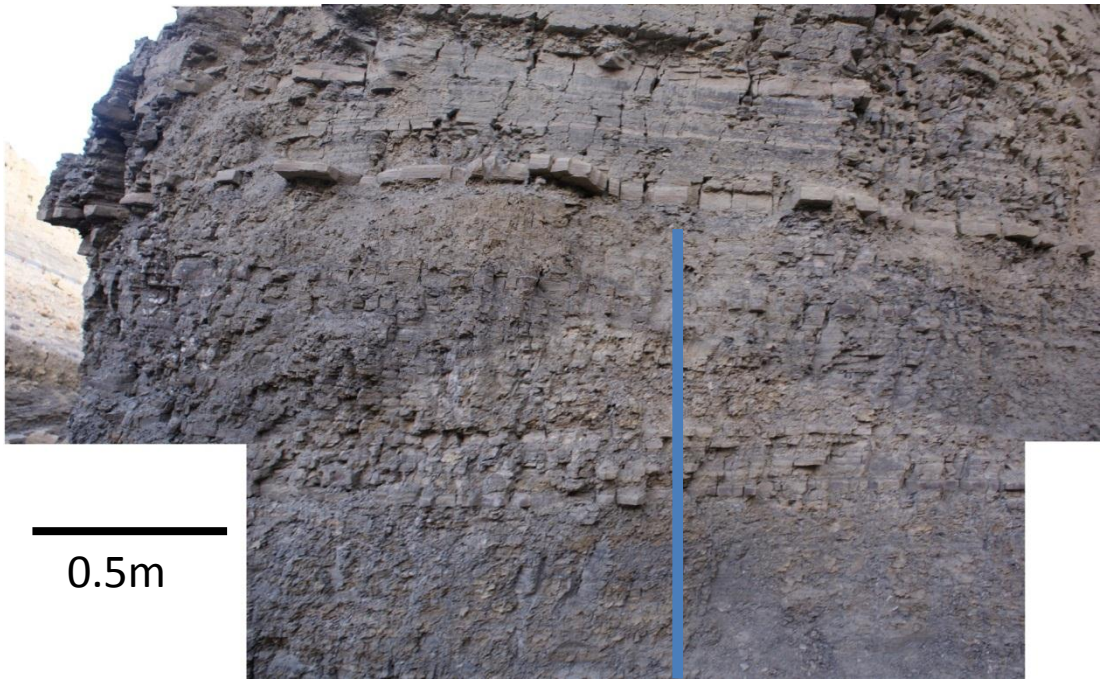


*Figure 3.7 Photograph of location of measured section taken of parasequence 11. Blue bar represents length of recorded measured section.*

Parasequence set 16 showed a basinward shift from parasequence 17 (Zhu et al., 2011). It shows an aggradational stacking pattern and was interpreted to represent the lowstand systems tract of sequence 5. Parasequences within parasequence set 16 primarily consists of storm/river-dominated distal delta front facies and prodelta

mudstone facies (Zhu, 2010). Parasequence 16 was documented in the Caineville area along County Rd (Figure 3.8 and 3.9).


*Figure 3.8 Map view of the location of the study area parasequence 16b within parasequence set 16 (Google Earth, copyright, 2012)*


*Figure 3.9 Photomosaic of location of measured section taken of parasequence 16. Blue bar represents length of recorded measured section.*

Zhu (2010) also observed the lateral variability of the facies within each parasequence and found that parasequence 5a, 5b, and 6, within the strike section, along-strike variations showed a district asymmetry. Zhu (2010) used the lateral and vertical facies variations to reconstruct the paleogeography of the Ferron Notom complex through its evolutional history. Figure 3.9 illustrates the results of this for parasequence 11 measured in this study. Parasequence 6 has been replaced with a more accurate model done by Li (in press).

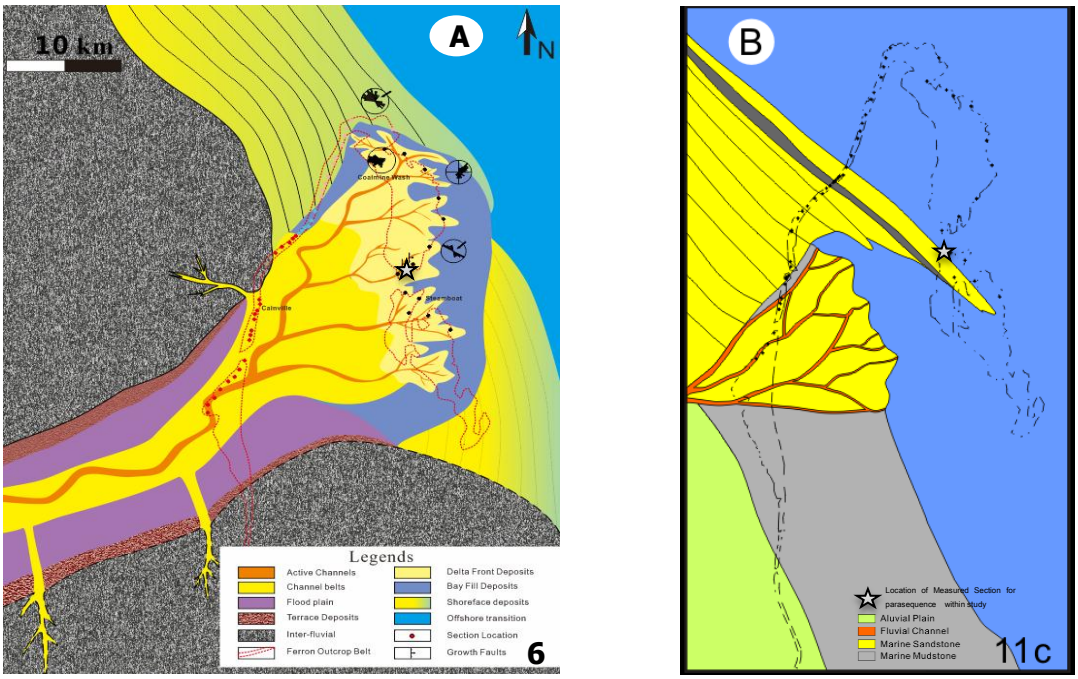


*Figure 3.9. Paleogeography maps for parasequence 6 and 11c. Measured sections were taken as shown by black stars. (Zhu, 2010 (B), and Li (personal communication)(A))*

## 4. Methodology

Primary data were derived from four well exposed outcrops of parasequences 5a, 5b, 6, 11, and 16b. Sedimentological and stratigraphic information was collected for each of these parasequences in the form of measured sections. Information gathered included grain size, lithofacies, degree of bioturbation, and plant material, as well as sedimentary structures. This data were collected on a millimeter to decimeter scale. An example of this is shown in Figure 4.1.

Grain sizes were recorded using the Wentworth classification. Clay and silt were differentiated based on texture using methods such as chewing, and color differentiation. Silt-sized particles in this area were characterized by a lighter color than clay-sized particles.

Rock samples were also collected from various sections within the parasequences for further analysis in slabs and thin sections. The measured sections for parasequence 5a and 5b were collected by rappelling on cliff faces, whereas 6, 11, and 16b were collected by walking laterally along the outcrop. Tools used included a rock hammer, hand lens, grain-size chart, measuring tape, field notebook, GPS to track all sections and a Brunton compass. A camera was also used to take over 1200 pictures along the exposed outcrops.

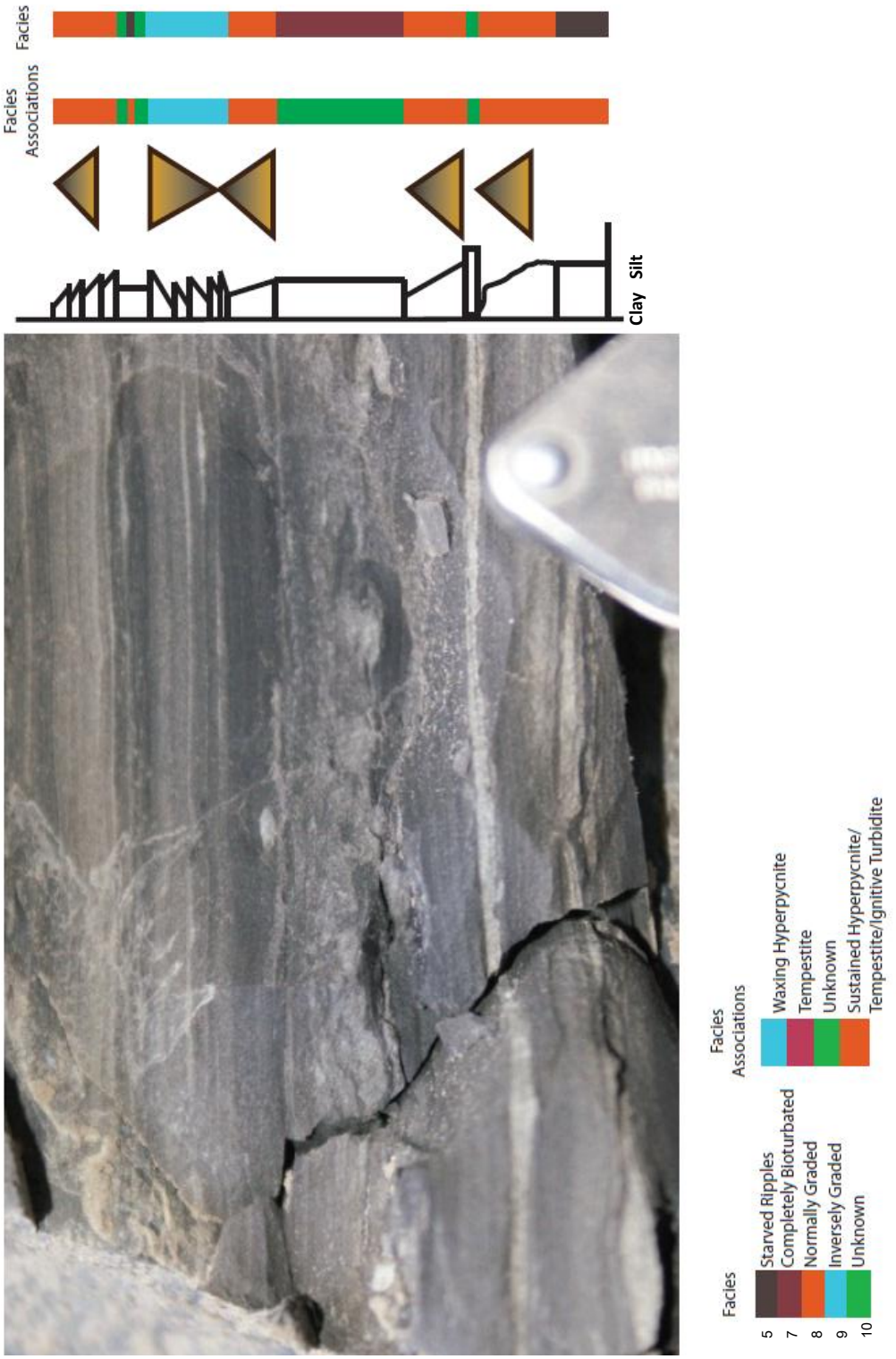


*Figure 4.1 An example of the types of data collected in a measured section. Examples of Facies 5,7,8,9, and 10 are shown.*

9 measured sections were collected in total. 3 sections were taken along parasequences 5a and 5b, and 1 section each for parasequences 6, 11, and 16b. These sections were digitized (as seen in Chapter 7), as well as entered into a spreadsheet for statistical analysis (See appendix as well as Chapter 7). Statistical analysis included grain size distributions, proportions of facies and bioturbated units within parasequences, as well as proportion dominance of wave versus tidal versus fluvial influence.

## 5. Facies

Within the 5 parasequences measured, 10 distinct facies were recognized, which are discussed below.

Facies 1: Hummocky Cross Stratification

Hummocky cross-stratification (HCS) (Fig. 5.1) was observed in sand-sized sediment ranging from very fine lower to fine lower. The modal and median distribution for this sedimentary structure however occurred in very fine lower sand-sized sediment. There was almost no bioturbation seen within these structures, however some (bioturbation index 2-3) was seen on the top of many of these units. The thicknesses of this facies ranged from 2cm (very thin beds or medium-scale lamina) to 70cm (thick bed) and within parasequence 5; many of these units were stacked upon each other. HCS was commonly seen topped with wave ripple beds (facies 4) which indicates waning of storm deposits, however since this was not always the case, wave rippled deposits were classified as a separate facies.

*Figure 5.1. Hummocky cross stratification observed at Caineville (parasequence 16b).*

## Facies 1: Interpretation

Hummocky cross stratification is widely used as an indicator of the lower shoreface environment, however, given that storm waves can entrain fine-grained sand sediments at depths of well over 100m (Porter-Smith et al., 2004, as referenced in Suter, 2006), these features can also occur in shelf settings. As the storm wanes, wave oscillation ripples and/or combined-flow ripples form 3-dimensional hummocks and depressions (Harms and Walker, 1982) (Figure 5.1). Hummocky cross stratification was observed in many of the parasequences measured, namely parasequence set 5, 6, and 16b.

**Association**: We can therefore note that these parasequences all had some form of wave influence, and is related to the deposition of tempestite deposits.

## Facies 2: Massive Bedding

Massive bedding was present in most parasequences measured (Figure 5.2, 5.3). This sedimentary structure was observed in units with sizes ranging from clay to very fine upper sand-sized sediments, with thicknesses of individual massive units ranging from 0.5cm (very thin beds or thin lamina scale) to 74.5cm (thick bed). Their overall proportion within various parasequences observed fluctuated between 0.7% and 44.6%. There was almost no bioturbation associated with these units, each having a modal and median distribution of a bioturbation index of 0, though bioturbation index ranged from 0-4 within this facies.

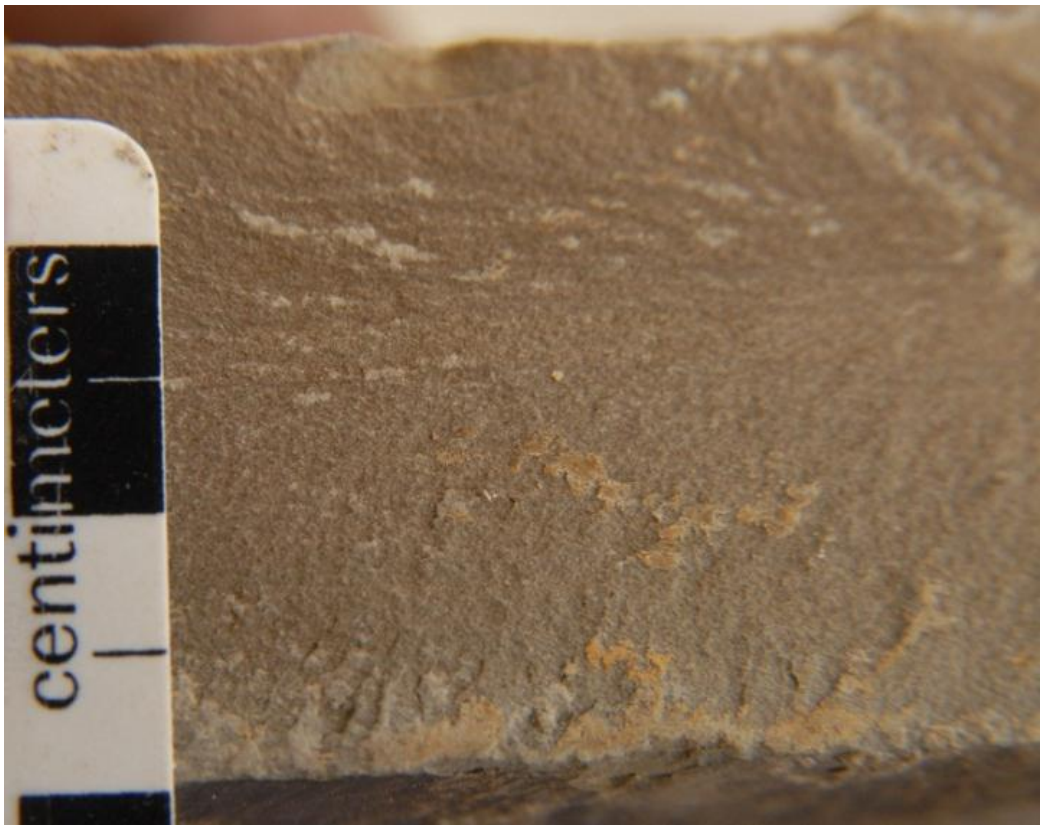


*Figure 5.2. Typical massive bedded facies observed within parasequences. This massive bedded unit was observed within parasequence 16.*

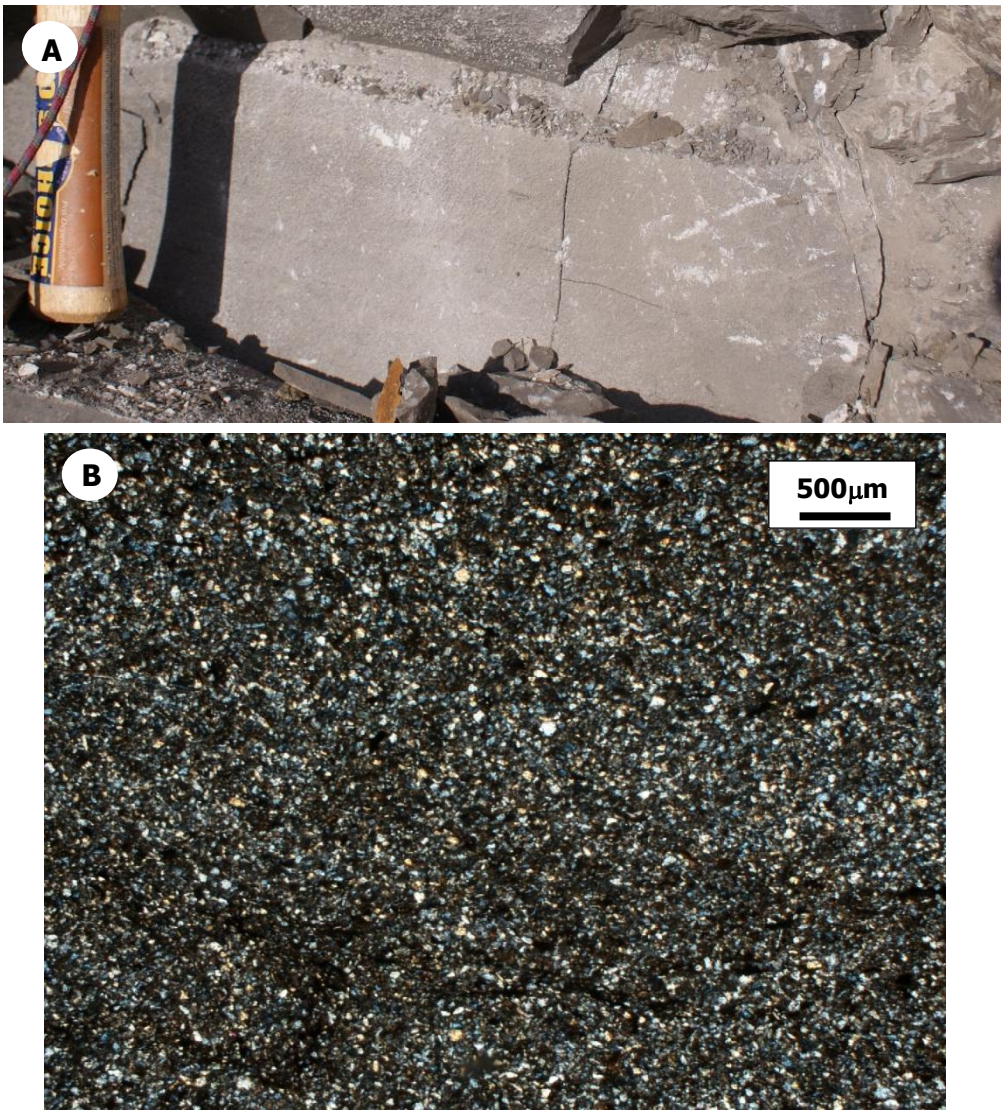


*Figure 5.3. Another typical example of a massive bedded unit observed within the Ferron sandstone. (parasequence 16b). A is taken from outcrop, and B is taken from thin section*

Facies 2: Interpretation

Massive bedded units have been variously attributed to: (1) turbidity currents (Bouma, 1962); (2) the antidune phase of the upper flow regime (Harms and Fahnestock, 1965; Walker, 1967); (3) grain flows (Stauffer, 1967); (4) pseudo-plastic quick bed (Middleton, 1967); (5) density- modified grain flows (Lowe, 1976); (6)

high-density turbidity currents (Lowe, 1982); (7) upper-plane-bed conditions under high rates of sediment feed (Amott and Hand, 1989); and (8) sandy debris flow (Shanmugam and Moiola, 1995; Shanmugam, 1996b) (Shanmugam, 1997). Therefore, for this study, the massive bedded structures were attributed to ignitive turbidites and hyperpycnal flow depending on the sedimentary structures observed immediately above.

**Association**: If Bouma sequence $T_A$ was followed by $T_B$- $T_E$, or a majority of it, it was attributed to ignitive turbidites; whereas if there were $T_A$-$T_B$, or $T_B$-$T_C$ repetition, it was attributed to either the presence of hyperpycnal flows, or ignitive turbidites.

Facies 3: Planar Laminations

Facies 3 (Figure 5.4) consisted of clay to very fine upper sand sized sediment. This sedimentary structure was present in units with thicknesses ranging from 0.5 cm (very thin bed or thin lamina scale) to 47cm to (thick bed). This facies was not observed in all sections measured, however where observed, their proportion of the total section ranged from 0.8% to 12.8%. There was little to no bioturbation associated with these units. The bioturbation index ranged with a mode and median distribution of 0, and a range from 0 to 4.

Facies 3: Interpretation

For this study, the planar bedded ($T_B$) structures were attributed to ignitive turbidites and hyperpycnal flows.

**Association**: If Bouma sequence $T_B$ was followed by $T_C$- $T_E$, or a majority of it, it was attributed to ignitive turbidites, whereas if there were $T_A$-$T_B$, or $T_B$-$T_C$ repetition, it was attributed to the presence of hyperpycnal flows, or ignitive turbidites.

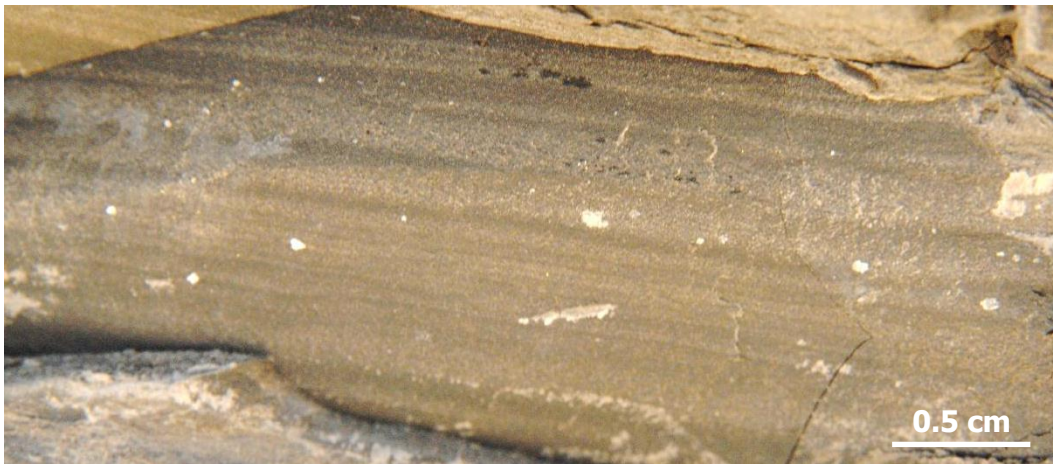


*Figure 5.4 An example of planar bedding seen within parasequence 16b.*

Facies 4: Wave-Ripple Cross Lamination

Wave-ripple cross lamination (Figure 5.7) was observed in every measured section. This facies occurred in sediments which ranged from clay to very fine lower sand sized sediment. Each unit measured of this facies had thicknesses which occurred between 0.5cm (very thin bed or thin lamina scale) to 41.5cm (thick bed); however total proportions observed within various parasequences ranged from 0.7% to 38.8% of the entire parasequence. Bioturbation for this facies was low, having a modal and median distribution of 0, within a bioturbation index range of 0 to 4. The mean bioturbation index was observed to be 0.94 amongst all parasequences.

Facies 4: Interpretation

Wave-ripple cross lamination is associated with the oscillatory movement of waves during the waning part of a storm event. Waves can also occur as fair-weather waves within the shoreface. Shoreface environments are associated with blocky sandstone deposits, and the heterolithic sediments, in which these wave ripple cross lamination were found were therefore assumed to be below fair-weather wave base, and linked to the occurrence of storm events (tempestites).

Facies 5: Starved Ripples

Starved ripples (Figure 5.5) were observed within all of the parasequences, however not in all of the measured sections. This facies was observed in silt to very fine lower sand sized sediment. Distribution of units which contained this facies ranged from 0.1cm (very thin bed or very thin lamina scale) to 3.5cm (thin bed or thick lamina scale). This facies was not present in abundant amounts, where the total proportion of each measured section observed ranged between 0.2% and 4.1%. Of the 32 units found in total which contained starved ripples, only one showed any sign of bioturbation, with a bioturbation index of 4.

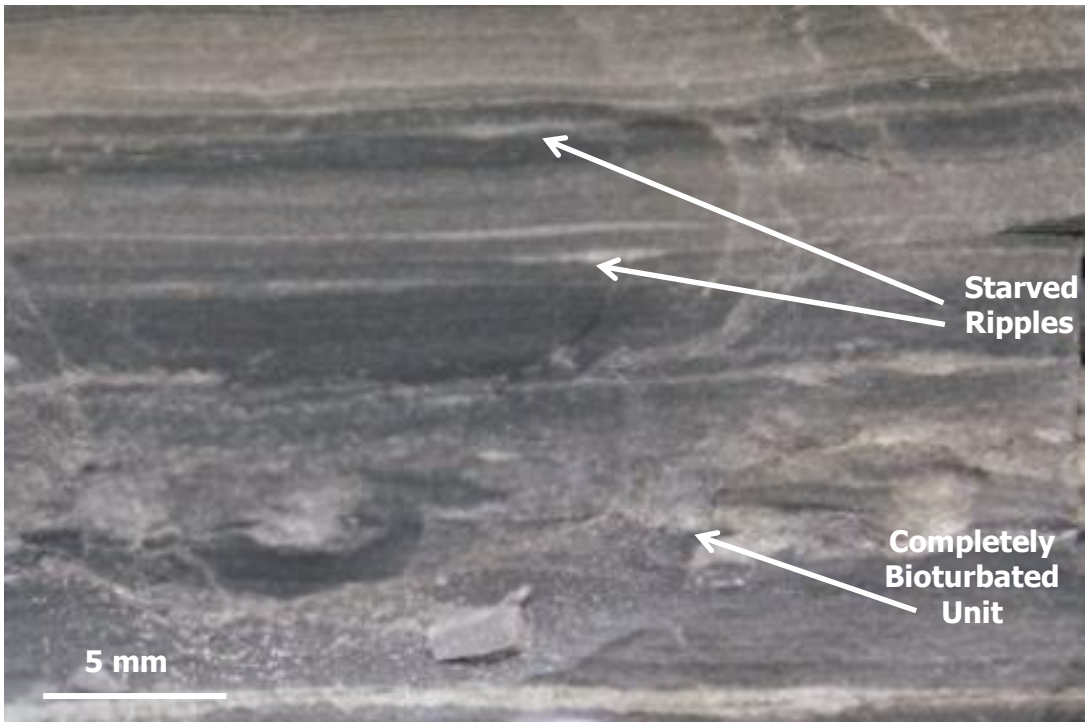


*Figure 5.5. Starved ripples observed within parasequence 11. A completely bioturbated unit (Facies 7) can also be seen here*

Facies 5: Interpretation

Sometimes the sediment supply is low within a region and even though there is enough energy to produce ripples, these ripples are formed largely spaced apart with a thin lamination connecting them. These sedimentary structures are known as starved ripples and were observed in many of the parasequences measured. Starved ripples are usually associated with tidal deposition or deposition due to wave action (symmetrical) or can be associated with unidirectional currents (asymmetrical).

Since there was no regular spacing of these starved ripples or any other evidence of tidal dominance or secondary contribution in these parasequences, and the starved ripples present were asymmetrical in nature, they were attributed to turbidite deposition.

Facies 6: Asymmetrical Cross Lamination (Current Ripples)

Current ripples were rarely seen in the measured sections, however they were observed in all parasequences with the exception of parasequence 5a. They were found in units ranging from clay to very fine lower sand-sized sediment. Thicknesses of units ranged from 1cm (very thin bed or medium scale lamina) to 20cm (medium scaled beds). They did not consist of a majority of any parasequence, with their total proportion, ranging from 0.2% to 1.4% of the total thickness. Bioturbation index for this parasequence ranged from 0 to 4, with a mean distribution of 1.5, a modal distribution of 0, and a median distribution of 1.

Facies 6: Interpretation

Current ripples are the result of unidirectional flow producing ripples with a steep lee side, with a lower gradient on the stoss side. These ripples can be due to the presence of ignitive turbidites, or hyperpcynites. Sustained hyperpcynal flows, and ignitive turbidies have $T_A$-$T_B$ or $T_B$-$T_C$ cyclicity, whereas ignitive turbidites can also have the majority of the $T_A$-$T_E$ sequence preserved.

**Association**: If Bouma sequence $T_B$ was followed by $T_C$- $T_E$, or a majority of it, it was attributed to ignitive turbidites, whereas if there were $T_A$-$T_B$, or $T_B$-$T_C$ repetition, it was attributed to the presence of hyperpycnites, or ignitive turbidites.

Facies 7: Completely Bioturbated

Within some of the units there were no sedimentary structures which could be positively identified, due to bioturbation. There were sometimes remnant sedimentary structures (Figure 5.5 and 5.6), however this was not enough to be grouped into another facies category. This facies was observed within sediment ranging from clay to very fine lower sand-sized particles. The units ranged in thicknesses from 0.25cm (very thin bed or medium scaled lamina to 25cm (medium scaled beds). Trace fossils present included *Planolites* within parasequences 5a, 5b, 6, and 11; *Paleophycus* within parasequences 5a, 5b, and 6; and *Ophiomorpha* within parasequence 6. Table 5.1 shows a summary of the environmental facies association after Zhu (2010).


*Figure 5.6. A completely bioturbated unit (bioturbation index 5-6) observed within parasequence 11. Some remnant starved ripples can be observed to the base of the unit.*

| Lithofacies associations | Proportion of total facies measured | Lithology and sedimentary structures | Lithofacies associations |
|---|---|---|---|
| **Shelf** | 20.0% | Mainly shale with very thinly interbedded very fine-grained sandstones. The sandstones are usually starved current ripple cross laminated. Local sandstone interbeds are hummocky/swaley cross stratified very fine-grained sandstones. Contains local massive or graded siltstone/mudstone beds. Ammonite, inoceramus, fish scales and shark teeth are common. | Low to intense. BI=2-5. *Zoophycos* ichnofacies. Common ichnogenera: *Phycosiphon*, *Helminthopsis*, *Zoophycos*, *Planolites* and *Chondrites*. |
| **Offshore transition** | 6.6% | Silty and sandy mudstones interbedded with thin layers (1-3cm) of lower-very fine- to lower-fine-grained sandstones. Relatively thick (around 5cm) sandstone beds are usually sharp and erosive based, and show hummocky/swaley cross stratified sandstones grading into wave ripple or combined-flow ripple cross laminated sandstones. | Low to moderate. BI=2-5. Distal *Cruziana* ichnofacies. Common ichnogenera: *Planolites*, *Thalassinoides*, *Helminthopsis*, *Chondrites* and *Phycosiphon*. |
| **Prodelta** | 14.5% | Massive or graded mudstones and siltstones interbedded with thin bedded very fine-grained sandstones. Structureless and organic rich siltstone beds reach up to 5m thick. "Bouma sequence" is common. Soft sediment deformation is often seen. Very fine-grained sandstone and siltstone beds are mainly hummocky cross stratified, current ripple or combine flow ripple cross laminated, or planar laminated, and are capped by thin layers of mud drapes. Abundant plant materials and | Absent to moderate, generally lacking. BI=0-3. Archetypal to distal Cruziana ichnofacies with local *Skolithos* Ichnofacies. Common ichnogenera: *Planolites*, *Palaeophycus*, *Thalassinoides*, *Ophiomorpha*, *Chondrites* and *Skolithos*. |
| **Delta front** | 6.6% | Prevalent soft sediment deformation (ball and pillow structures, convolute bedding, flame structures, slump), climbing current ripples, graded beds and growth faulting. Most sandstones are very muddy or silty with a lot of plant material. Thinly interbedded very fine-grained planar laminated sandstones with mudstones. Current ripple cross laminated or combined-flow ripple cross laminated very fine-grained sandstones. Abundant hummocky/swaley cross stratified or planar laminated lower-very fine to upper-fine-grained sandstones are usually associated with soft sediment deformation from mm to meters scale. Bar scale, tabular dune-scale or trough cross stratified lower-fine to lower-medium grained sandstones. | Absent to moderate overall with local intensely bioturbation intervals. BI=0-5. *Skolithos* ichnofacies. Common trace fossils: *Ophiomorpha*, *Planolites*, *Astrosoma*, *Chondrites*, *Thalassinoides* and *Arenicolites*. Less common ichnogenera: *Skolithos*, *Diplocraterion*, *Schaubcylindrichnus*, *Rosselia* and *Teredolites*. |

*Table 5.1 Summary of Facies associations in the Ferron, Notom Delta. (Zhu, 2010)*

| | | | |
|---|---|---|---|
| **Shoreface** | 12.4% | Lower shoreface: upper-very fine-grained to lower-fine-grained hummocky/swaley cross stratified, planar laminated and wave-ripple cross laminated sandstones. HCS beds made of 20-30 cm thick lamina sets reach up to a few meters thick. Combined flow ripples or wave ripples on top of the HCS beds. Rare mudstone drapes. | Low to complete overall but locally absent. BI=0-6. Mixed *Cruziana*-distal *Skolithos* ichnofacies. Common ichnogenera: *Ophiomorpha*, *Thalassinoides*, *Asterosoma*, *Rosselia*, *Skolithos*. Less common ichnogenera: *Cylindrichnus*, *Teichichnus*, *Schaubcylindrichnus*, *Planolites* and *Palaeophycus*. |
| | | Upper shoreface: upper-fine grained to lower-medium grained dune-scale tabular cross bedded and trough cross bedded and local planar laminated sandstones. Range from tens of centimeters to 6 meters. Cross-set thickness from 15 to 30cm. Contacts between the upper shoreface and lower shoreface are concordant and sharp, marked by an obvious increase of grain size. | Absent to low. BI=0-2. *Skolithos* ichnofacies. Common ichnogenera: *Skolithos*, *Ophiomorpha*, and *Macaronichnus*. |
| **Foreshore** | 0.2% | Parallel/subparallel to low angle (less than a few degrees) seaward dipping lower-fine-grained planar laminated sandstones. Some locally preserved lower-fine grained hummocky cross stratified sandstone beds. | Absent to sparse. BI=0-1. No ichnofacies identifiable. A few *Ophiomorpha* were observed. |
| **Distributary channels** | 1.3% | Bar scale, tabular dune-scale or trough cross stratified lower-fine to lower-medium grained sandstones. Mudstone rip-up clasts, allochthonous wood trunks, and dinosaur bones at erosional base. | Absent to locally moderate. BI =0-3. *Skolithos* ichnofacies. Common ichnogenera: *Planolites*, *Ophiomorpha* and *Palaeophycus*. |
| **Bayhead delta** | 1.4% | Upper-very fine to upper-fine-grained relatively thick (> 10cm) HCS beds, upper-fine to lower-medium-grained cross bedded sandstones, very fine-grained current ripple or combined-flow ripple cross laminated sandstones, plant-material-rich mudstones, local soft sediment deformation. Thin lower-very fine to upper-fine-grained HCS beds passing into wave ripple cross laminated sandstones, very thinly interbedded (< 5cm) lower-very fine-grained HCS sandstones with mudstones. | Absent to high. BI=0-4. Mixed *Cruziana*-*Skolithos* ichnofacies. Common ichnogenera: *Ophiomorpha*, *Planolites*, *Thalassinoides*, *Asterosoma*. Less common ichnogenera: *Skolithos*, *Palaeophycus*, *Arenicolites*. |
| **Lagoonal and bay fill** | 1.3% | Lower- very fine- to lower-fine-grained HCS beds (up to 1m) with local soft sediment deformation and wave rippled tops. Planar laminated, wave- or current-ripple cross laminated thin (< 5cm) sandstone. Mudstones facies are sandy/silty and locally coaly. | Low to intense. BI=2-5. *Teichichnus* ichnofacies. Common ichnogenera: *Teichichnus*, *Palaeophycus*, *Planolites*, *Thalassinodes*, *Chondrites*, *Ophiomorpha*. |

*Table 5.1 (continued) Summary of Facies associations in the Ferron, Notom Delta. (Zhu, 2010)*

## Facies 7: Interpretation

Disruption of the facies by bioturbation makes the original depositional sedimentary structures obscure. Assessment of the bioturbation index (Figure 5.7) in deltaic settings are typically a response of the dynamic interplay of fluvial influx, fluvial discharge types, tidal energy, wave action, and storms (MacEachern et al., 2005). Multiple studies have shown a link between completely (or almost completely) bioturbated facies and their direct link to wave derived processes within deltaic facies (MacEachern et al., 2005). Parasequences were compared quantitatively to test whether there was any correlation between wave dominated facies, and that which were highly bioturbated.

This facies was not linked to any facies association as bioturbation is the result of low sedimentation rates.

| Grade | Classification | Visual Representation |
|---|---|---|
| 0 | Bioturbation absent |  |
| 1 | Sparse bioturbation, bedding distinct, few discrete traces |  |
| 2 | Uncommon bioturbation, bedding distinct, low trace density | 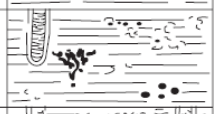 |
| 3 | Moderate bioturbation, bedding boundaries sharp, traces discrete, overlap rare |  |
| 4 | Common bioturbation, bedding boundaries indistinct, high trace density with overlap common |  |
| 5 | Abundant bioturbation, bedding completely disturbed (just visible) |  |
| 6 | Complete bioturbation, total biogenic homogenization of sediment |  |

*Figure 5.7 Visual representation of the bioturbation index classification scheme (MacEachern, et al., 2005)*

Facies 8: Normally Graded Bedding

In some of the units, there was an overall decrease in grain size from the base of the unit towards the top of the unit (Figure 5.8). These units were prominent in all parasequences measured. They occurred in sediment ranging from clay to very fine lower sand-sized particles. Thicknesses ranged from 0.5cm (very thin bed or thin lamina scale) to 14cm (medium-scaled bed). The total proportion of the entire section measured also ranged between 2.7% and 22.3%. There was little bioturbation associated with this facies, with a median and modal bioturbation index of 0. There was, however, bioturbation in units which fluctuated from a bioturbation index of 0 to 4.


*Figure 5.8 A sample taken from Parasequence 6. A measured section was constructed to illustrate the facies seen within this sample. There were many graded units as well as a starved ripple unit. The upright triangles on the diagram represent normally graded units, whereas the vertically flipped units represent inversely graded units. Wave ripple cross-lamination can also be seen here.*

Facies 8: Interpretation

Normally graded beds can be linked to the deposition of any waning flow. These can be associated with all formative processes being studied (tempestites, ignitive turbidites, and hyperpycnites)

Facies 9: Inversely Graded Bedding

In some of the units observed, there seemed to be an increase in grain size from the base of the unit towards the top of the unit (Fig 5.9). This sedimentary unit was classified as an inversely graded unit, and was seen in all but one measured section. Inversely graded units were seen in sediments ranging from clay to very fine lower sand-sized sediment. Thickness of units ranged from 0.5cm (very thin bed or thin lamina scale) to 9.5cm (thin bed or thick lamina scale). However, overall proportions of this facies within each measured section varied from 0.3% to 14.7%. There was little bioturbation associated with this facies. Only one of the 57 units showed any bioturbation, which had a bioturbation index of 2 with plant material. There was also no other inversely graded units which contained plant material.

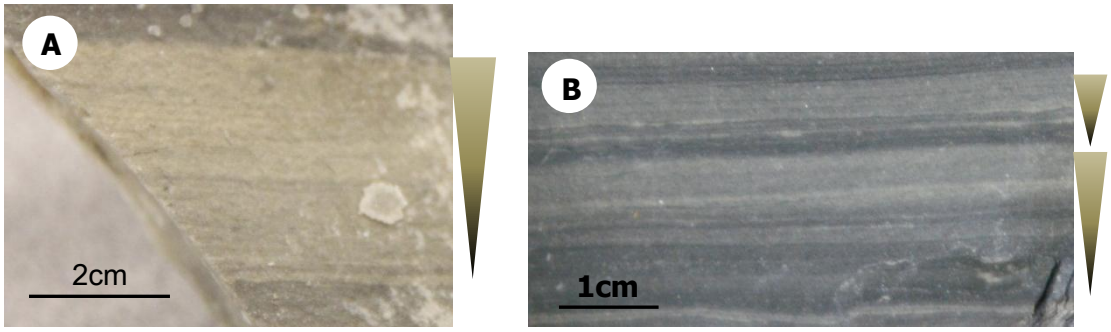


*Figure 5.9 Inverse grading seen in parasequence 6 (5.9A) and parasequence 11 (5.9B)*

Facies 9: Interpretation

This sedimentary unit was classified as an inversely graded unit, and was attributed to hyperpycnal turbidity flows. Although the origin of inverse grading in turbidites remains obscure (McLane, 1995), it is usually attributed to dispersive pressure caused by mutual impacts of grains behaving inertially within a rapidly shearing layer (Hand, 1997). Hyperpycnal flows are quasi-steady, which means that there are fluctuations with velocity over time. This characteristic is related to their flood origin, i.e. an event during which both river discharge and velocity increase, peak, and then decrease (Mulder et al., 2003). In the increase of velocity or the waxing part of the flow, these inversely graded beds are deposited. The complete sequence is explained by the shape of the flood hydrograph and predicted by the acceleration matrix of Kneller and Branney (1995), as seen in Figure 5.10.

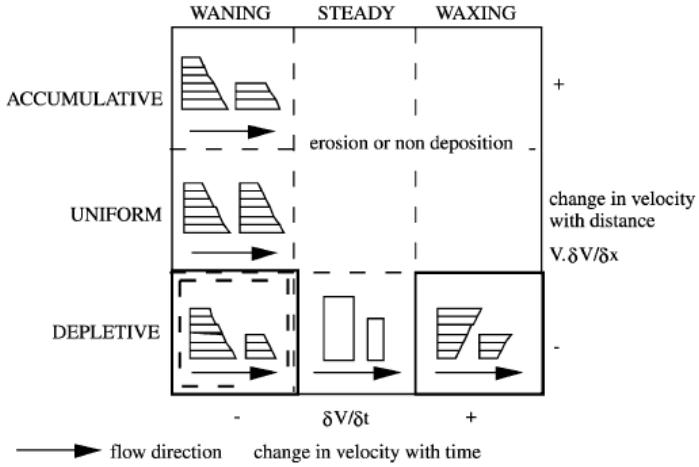


*Figure 5.10 Acceleration matrix from Kneller and Branney (1995). It illustrates the waxing part of the flood, and its association with the deposition of inversely graded beds.*

Facies 10: Unknown

Some units within the parasequences were difficult to identify. This was due to (1) high degree of weathered rock, (2) units too small, such that the sedimentary structure could not be identified with the naked eye, and (3) the units could not be followed laterally enough to tell the sedimentary structure due to poor outcrop conditions These occurred in units ranging from clay to very fine lower sand sized sediment. These units occurred in thicknesses ranging from 0.1cm (very thin bed or very thin lamina scale) to 8cm (thin bed or thick lamina scale). Their overall proportions varied within each section measured ranging from 0.5% to 25.5%.

Facies 10: Interpretation

These unknown units could not be given an interpretation, as were left as unknown.

A summary of each facies as well as their associations can be seen in Table 7.1.

## 6. Facies Associations as Applied to Measured Parasequences

Parasequence 5a

Parasequence 5a consisted of three measured sections, one of which is shown in Fig 6.1. Averages of proportions were used for analysis. This parasequence showed an overall coarsening upward succession, with a mean, modal, and median grain size of very fine lower sand-sized particles (Fig 6.2). Over 80% of this parasequence consisted of sand-sized particles (including very fine lower, very fine upper and fine lower grain size). Parasequence 5a showed an abundance of hummocky cross-stratified beds (over 76%) (Figure 6.3). Almost 4% of the beds were wave ripple cross-laminated units.

Parasequence 5a was interpreted as a high energy, wave/storm-dominated parasequence. There were also minimal amounts of grading, massive, and planar bedding present within this parasequence. 0.5% of the beds were unknown beds, and 16% had a bioturbation index of 5-6. On many of the HCS interfaces, there was a high degree of bioturbation, which were interpreted as ‘quiet periods’ between multiple storms affecting the depositional environment.

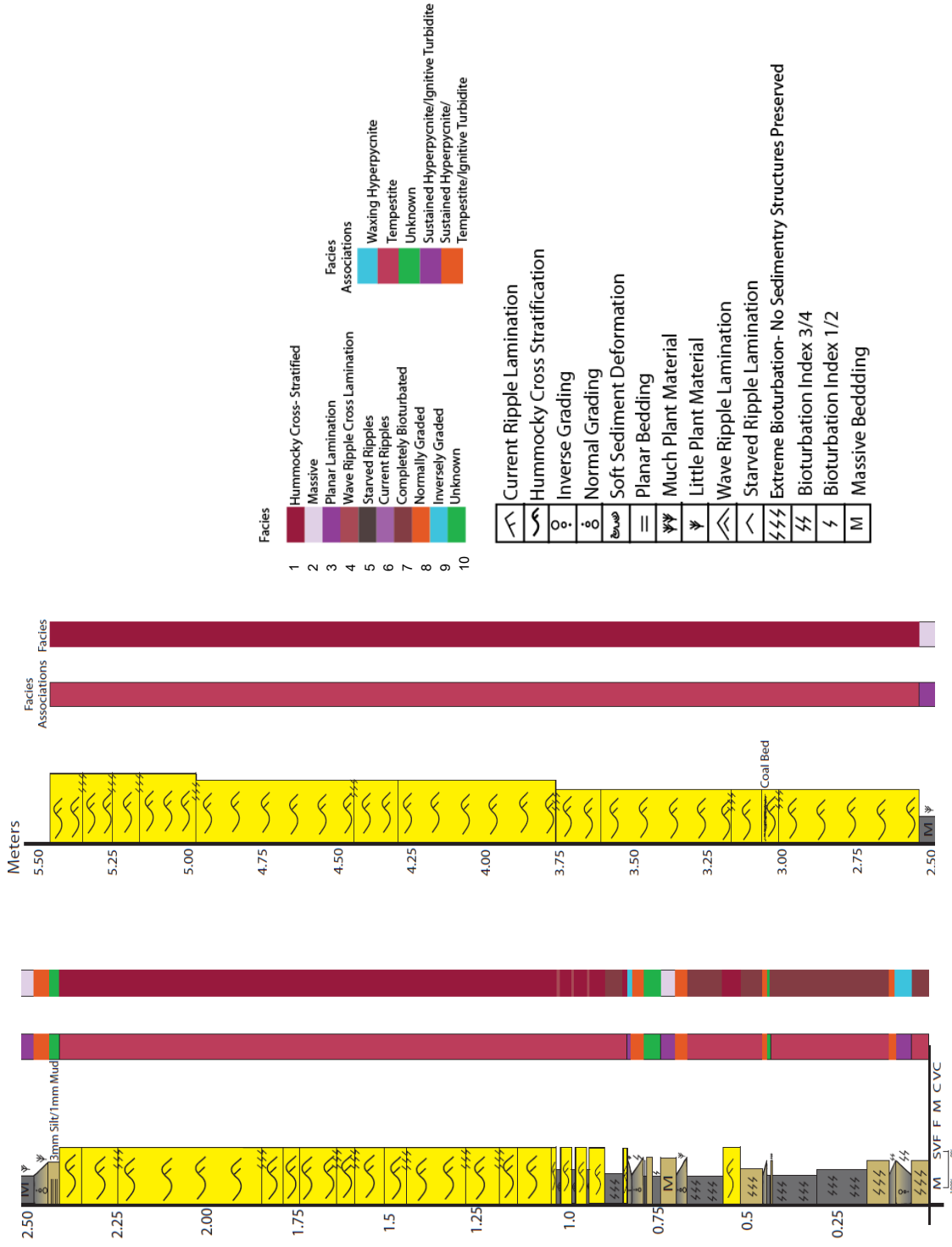


*Figure 6.1. Measured section of parasequence 5a, with associated sedimentary structures, facies, and facies associations.*

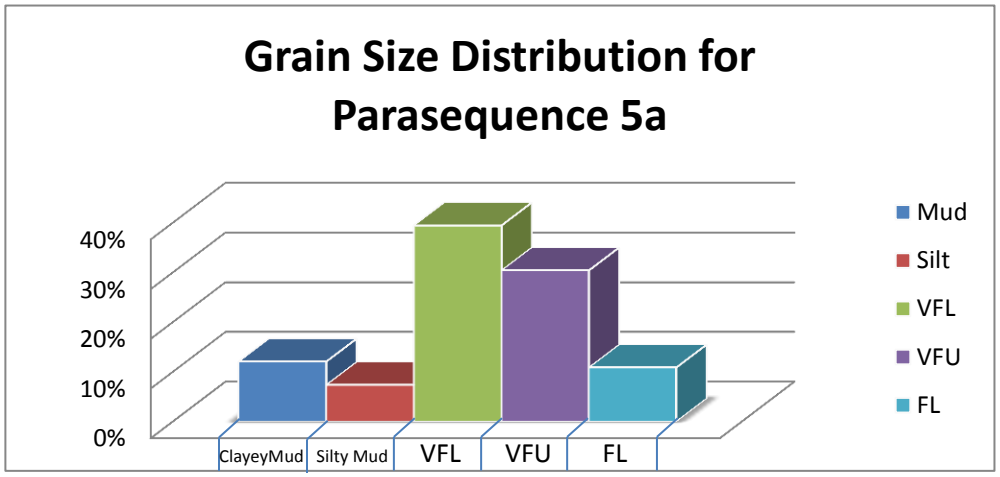


*Figure 6.2 Grain size distributions within parasequence 5a.*

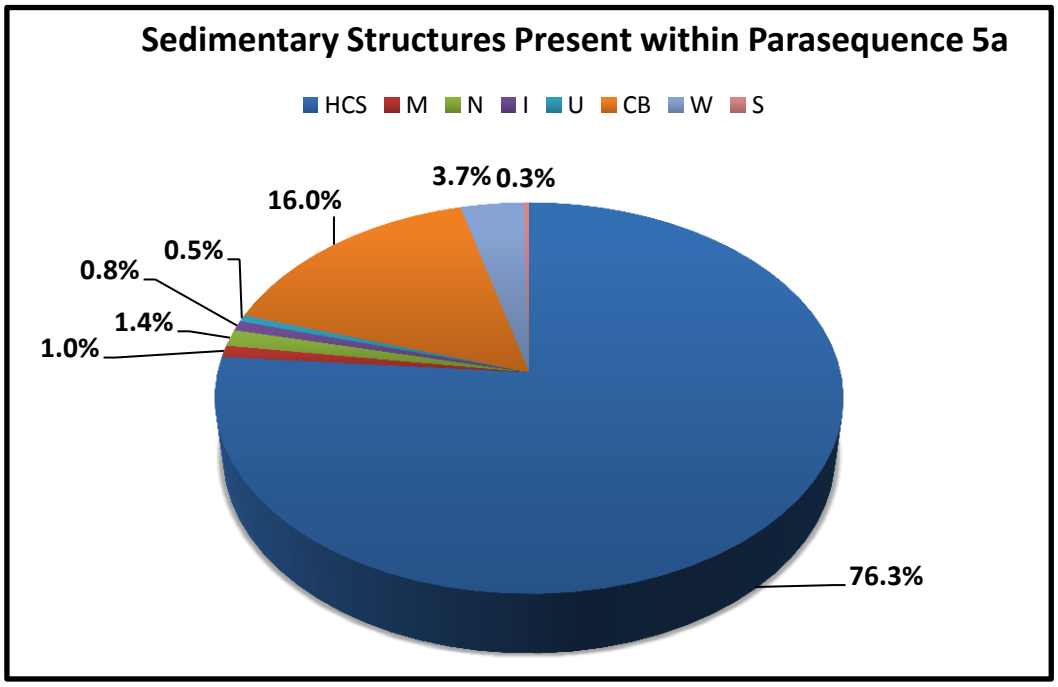


*Figure 6.3 Proportion of sedimentary structures present within parasequence 5a. M=Massive, N=Normal Grading, I=Inverse Grading, U=Unknown, CB=Completely Bioturbated, W=Wave Ripples, P=Planar Laminations, S= Starved Ripples, C=Current Ripples, HCS=Hummocky Cross Stratification.*

Parasequence 5b

Parasequence 5b also consisted of 3 measured sections (one shown in Fig 6.4). This parasequence lay stratigraphically below 5a. This parasequence also showed an overall coarsening upward succession, however it showed an average smaller grain size than 5a. The average grain size for this unit was silt-sized (Fig 6.5); however, the mode and median grain size were very fine lower sand. Only 58% of this parasequence consisted of sand-sized particles in comparison to parasequence 5a which consisted of over 80%. This lower average was associated with a more distal deposition of this unit. Parasequence 5b (Figure 6.6), also showed an abundance of HCS units (over 38%), however this is less than that of parasequence 5a. Wave ripples for this parasequence comprised 16% of the beds documented. This parasequence was therefore interpreted to be at least 54% wave/storm dominated. 7% of the beds documented were unknown in terms of sedimentary structure, and 18% being completely bioturbated units. There were also massive, planar, current ripples and normally graded beds present, which suggested that there was also the presence of ignitive turbidites within the parasequence. There were no complete Bouma sequences present however within this parasequence.

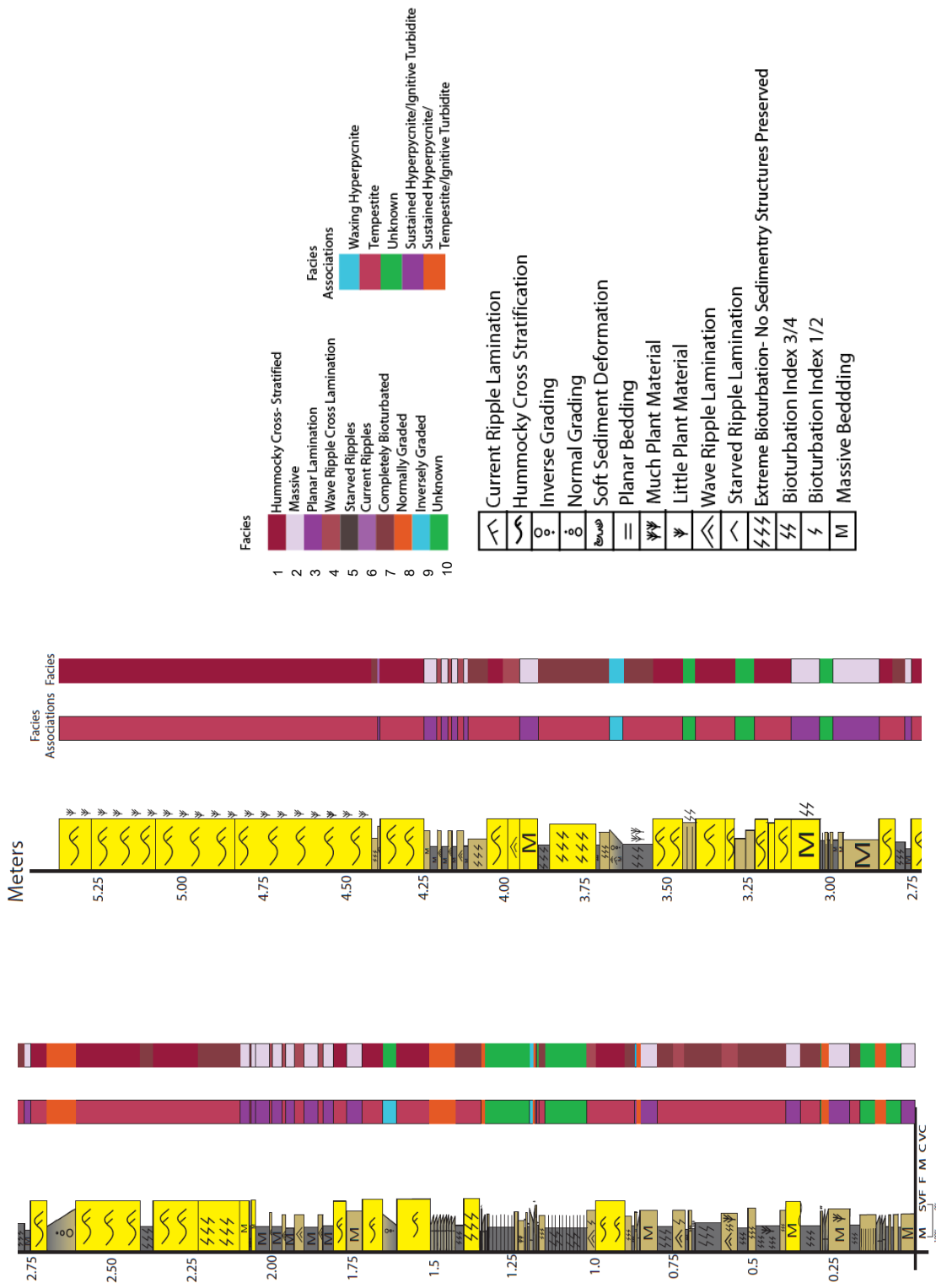


*Figure 6.4 Measured section of parasequence 5b, with associated sedimentary structures, facies, and facies associations.*

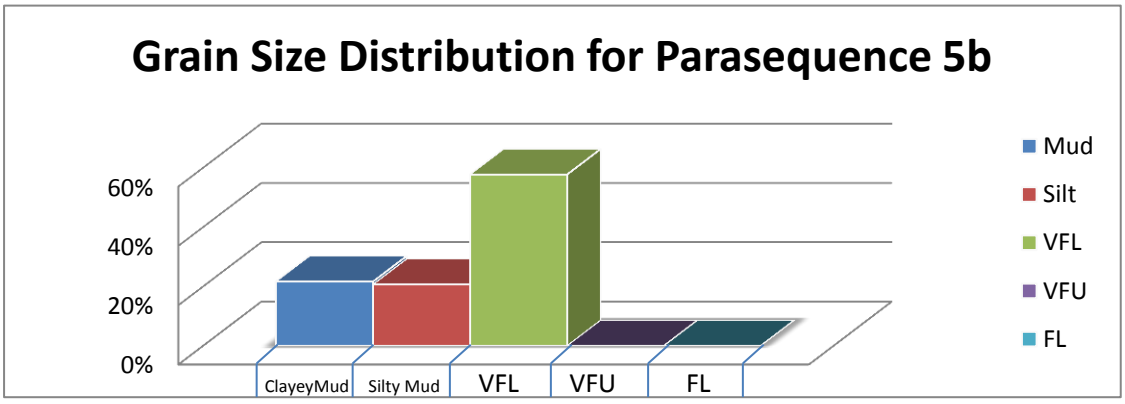


*Figure 6.5 Grain size distributions within parasequence 5b.*

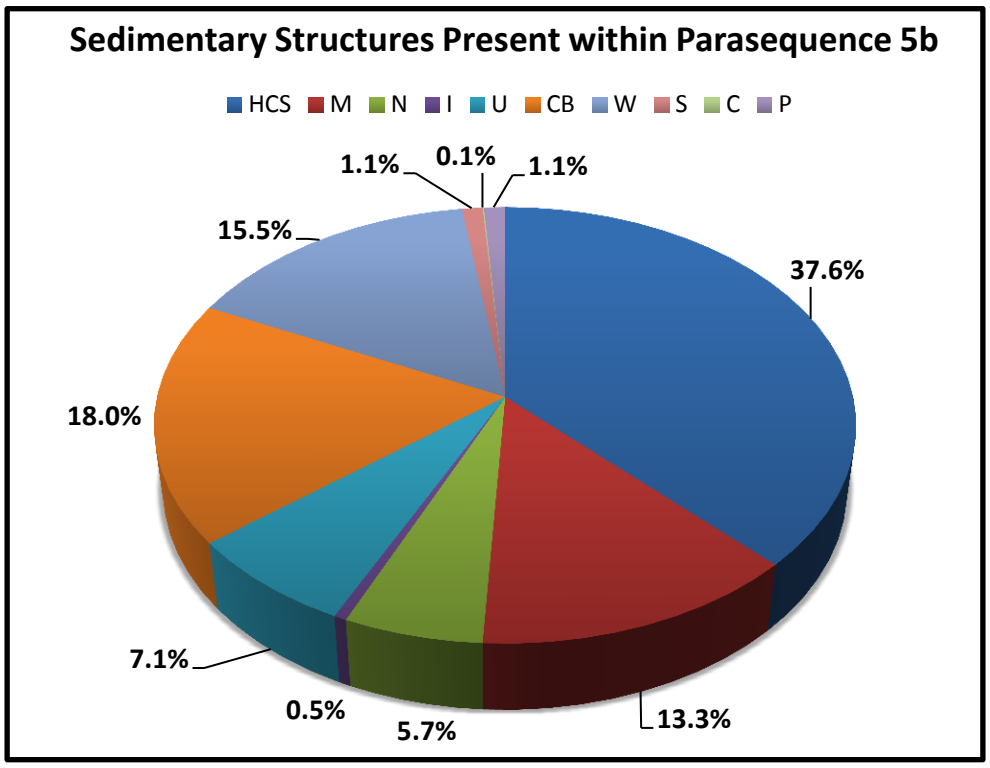


*Figure 6.6 Proportion of sedimentary structures present within parasequence 5b.*

*M=Massive, N=Normal Grading, I=Inverse Grading, U=Unknown, CB=Completely Bioturbated, W=Wave Ripples, P=Planar Laminations, S= Starved Ripples, C=Current Ripples, HCS=Hummocky Cross Stratification.*

Parasequence 6

This parasequence lies stratigraphically below parasequence 5b. This parasequence showed an overall coarsening upward facies succession (Fig 6.7) with the mean grain size being silt-sized particles (Figure 6.8). The modal and median grain size present was very fine lower sand-sized particles (Fig 6.8). The facies distribution (Figure 6.9) showed that 14.4% of the beds represented graded units (7.5% normally graded and 6.9% inversely graded). This was interpreted to represent hyperpycnal deposits (river dominated). 17% of the beds were wave-ripple cross lamination, which implies that at least 17% of this parasequence is wave/storm-dominated. 11.8% were massive and planar beds, which represents the possibility of either (1) sustained hyperpcynite deposits or (2) ignitive turbidite deposits proximal to deposition. 7.1% of beds were unknown facies, and 8.1% were completely bioturbated. 32.3% of the unit represented trough cross-bedded units, which is not shown in the measured section, but was present for 2 meters above the HCS beds.

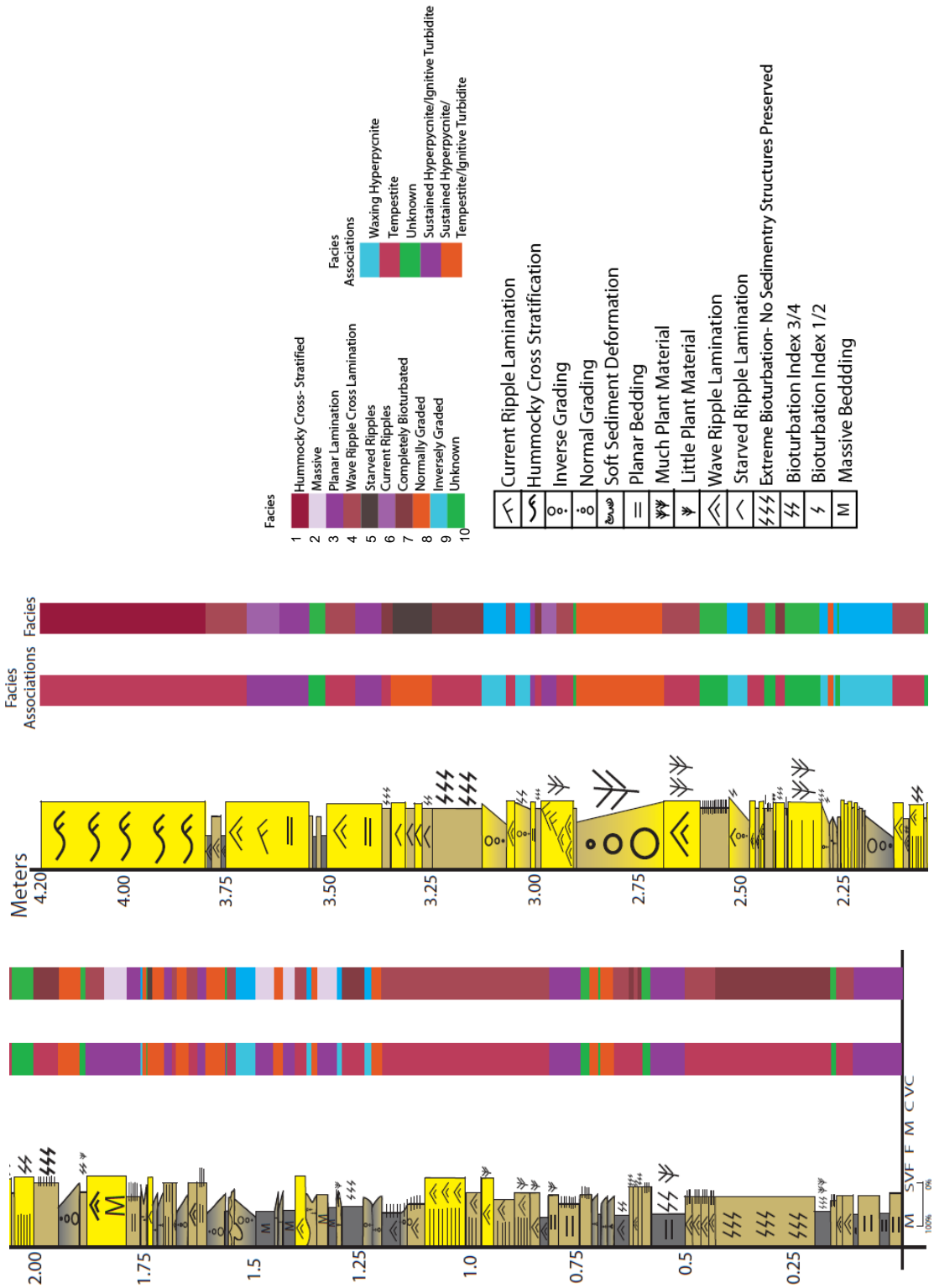


*Figure 6.7 Measured section of parasequence 6, with associated sedimentary structures, facies, and facies associations.*

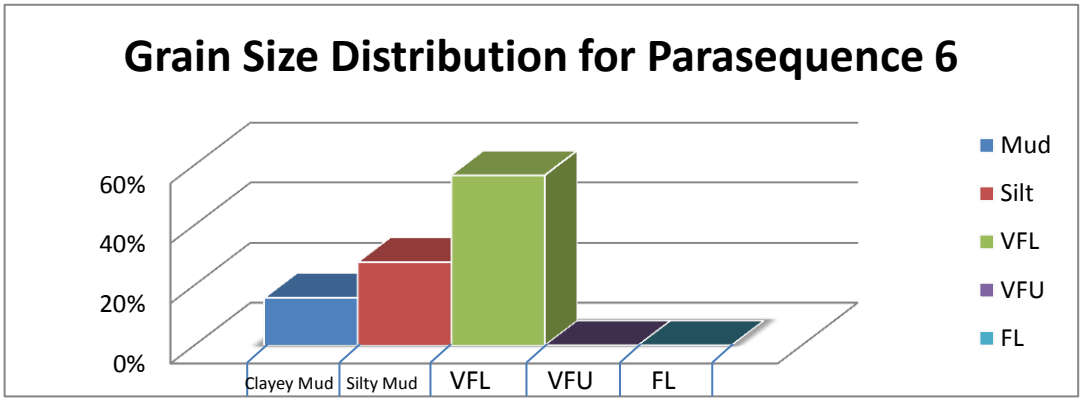


*Figure 6.8 Grain size distributions within parasequence 6.*

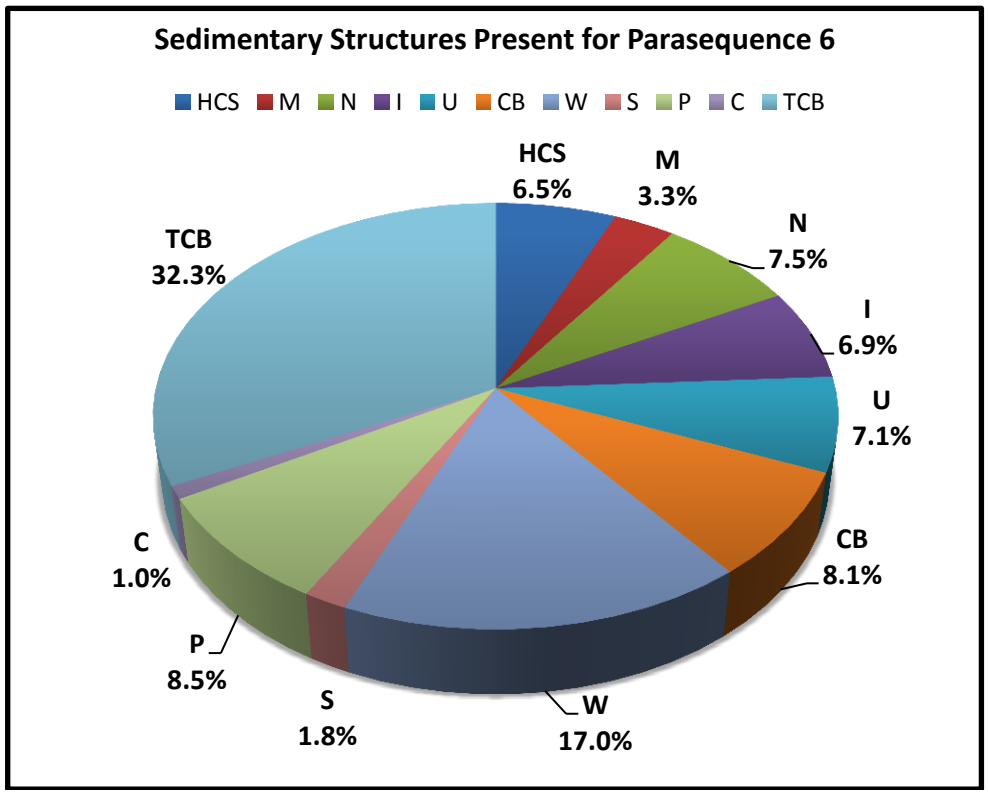


*Figure 6.9 Proportion of sedimentary structures present within parasequence 6.*

*M=Massive, N=Normal Grading, I=Inverse Grading, U=Unknown, CB=Completely Bioturbated, W=Wave Ripples, P=Planar Laminations, S= Starved Ripples, C=Current Ripples, HCS=Hummocky Cross Stratification, TCB=Trough Cross Bedding*

Parasequence 11

Parasequence 11 was documented in one measured section (Fig. 6.10), which showed an overall coarsening upward facies succession; however, it had the smallest grain sizes of all parasequences, with a mean, modal, and median distribution of clay-sized particles (Fig 6.11). In this parasequence, only 3% of the beds documented were sand-sized particles, whereas 51% were clay-sized, and 46% were silt-sized. The distribution within facies was significantly dominated by unknown sedimentary structures (26%), (with an additional 20% which were completely bioturbated) (Fig 6.12). This was due to the high degree of weathering present in the outcrop as well as the thickness size of beds which were too small to identify with the naked eye, even with the use of a hand lens. Of the remaining 54%, 22% were normally graded beds, and 15% were inversely graded beds. This suggests a high proportion of hyperpycnites. The other 17% were minor amounts of massive beds, planar beds, starved ripples, current ripples, and wave ripples. This means that there was some, but minor amounts of wave-storm influence as well as ignitive turbidites.

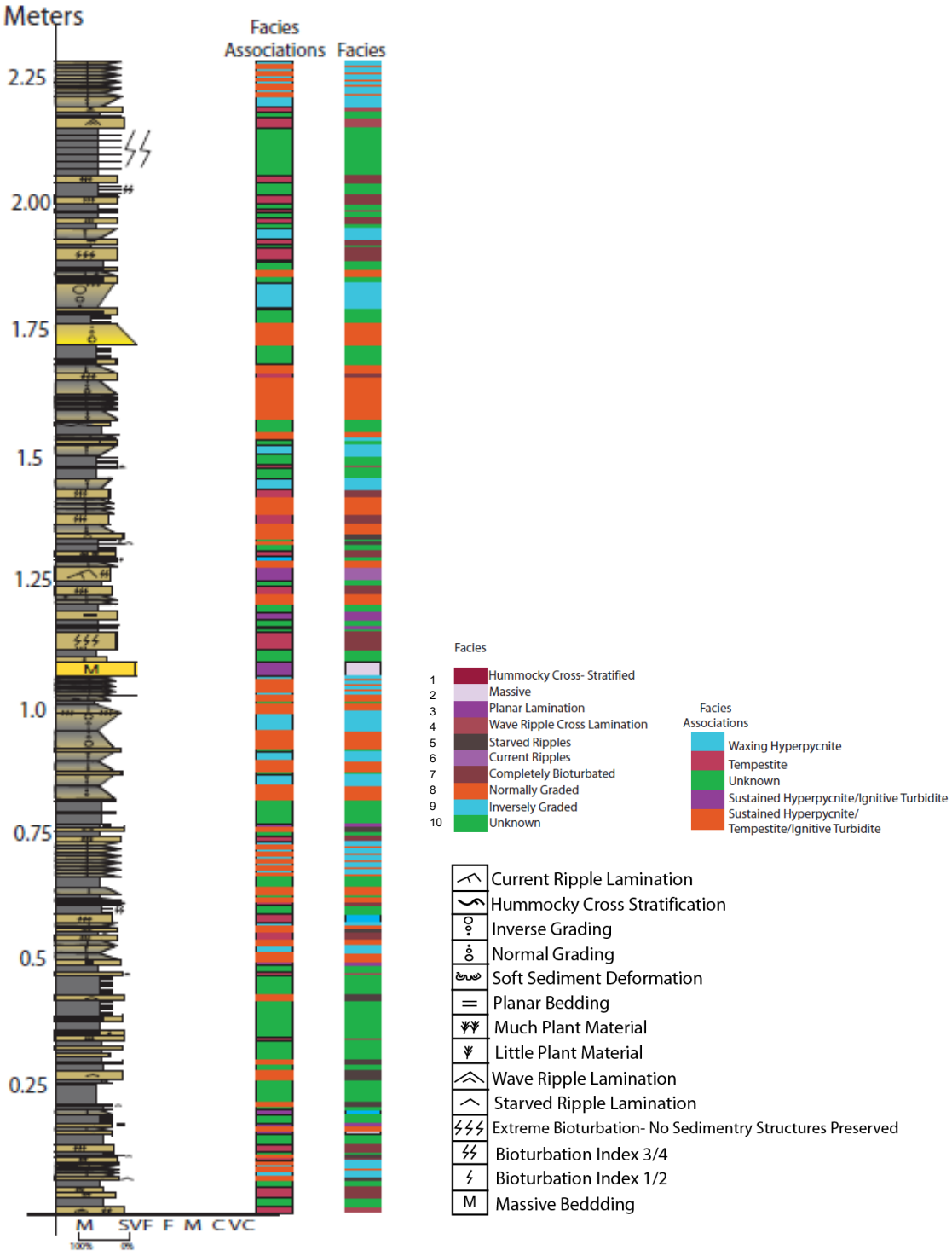


*Fig 6.10 Measured section of parasequence 11, with associated sedimentary structures, facies, and facies associations.*

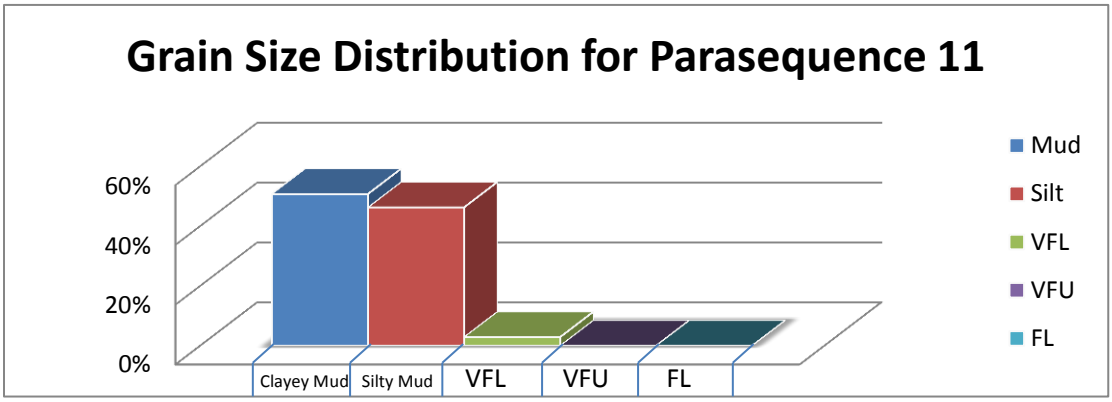


*Figure 6.11 Grain size distribution within parasequence 11*

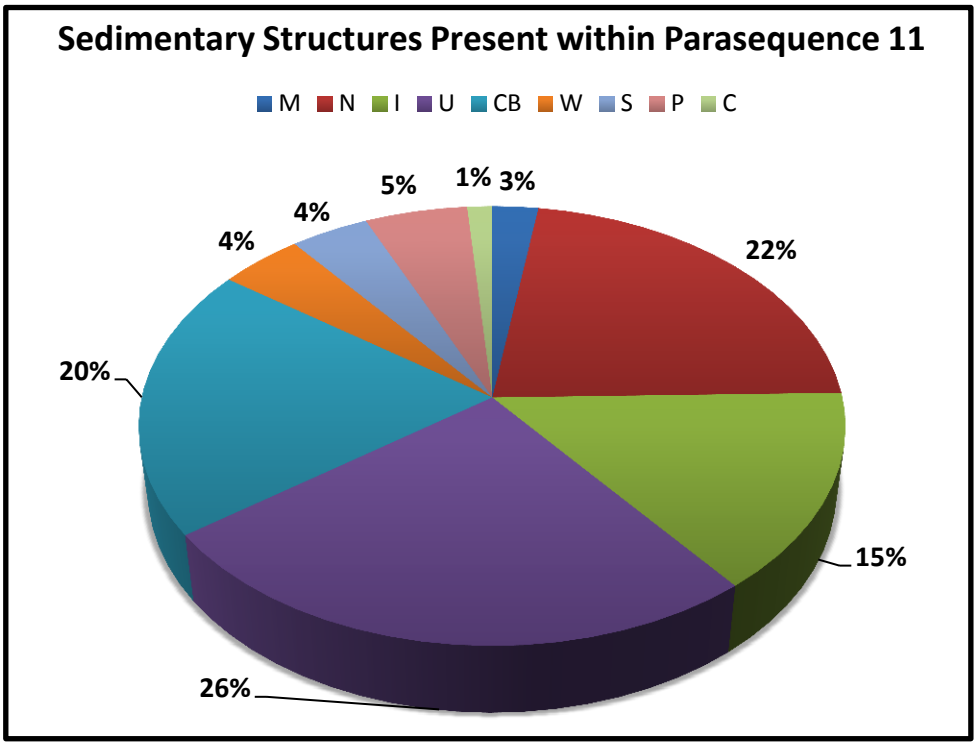


*Figure 6.12 Proportion of sedimentary structures present within parasequence 11. M=Massive, N=Normal Grading, I=Inverse Grading, U=Unknown, CB=Completely Bioturbated, W=Wave Ripples, P=Planar Laminations, S= Starved Ripples, C=Current Ripples, HCS=Hummocky Cross Stratification.*

Parasequence 16b

Parasequence 16b was documented in one measured section (Fig 6.13) in the Caineville area (Fig 3.8). This parasequence showed an overall coarsening upward succession, with a mean grain size of silt/very fine lower sand-sized grains. The median and modal distribution was very fine lower sand-sized grains (Fig 6.14). 54% of this unit consisted of sand-sized particles. The distribution of facies present within the parasequence was dominated by massive beds (45%) (Fig 6.15).

Figure 6.16 summarizes the proportions of each facies present within the parasequence. It shows the high dominance of storm/wave influence indicated by HCS beds, as well as wave-rippled beds. Parasequence 6 and 11 shows a high degree of river influence indicated by the high proportions of inversely graded beds. However parasequence 11 is more river-dominated than parasequence 6, which has at least 25% dominance from storm/wave influence. Parasequence 16b shows dominance by ignitive turbidites with 21% storm/wave influence, and at least 40% ignitive turbidite influence.

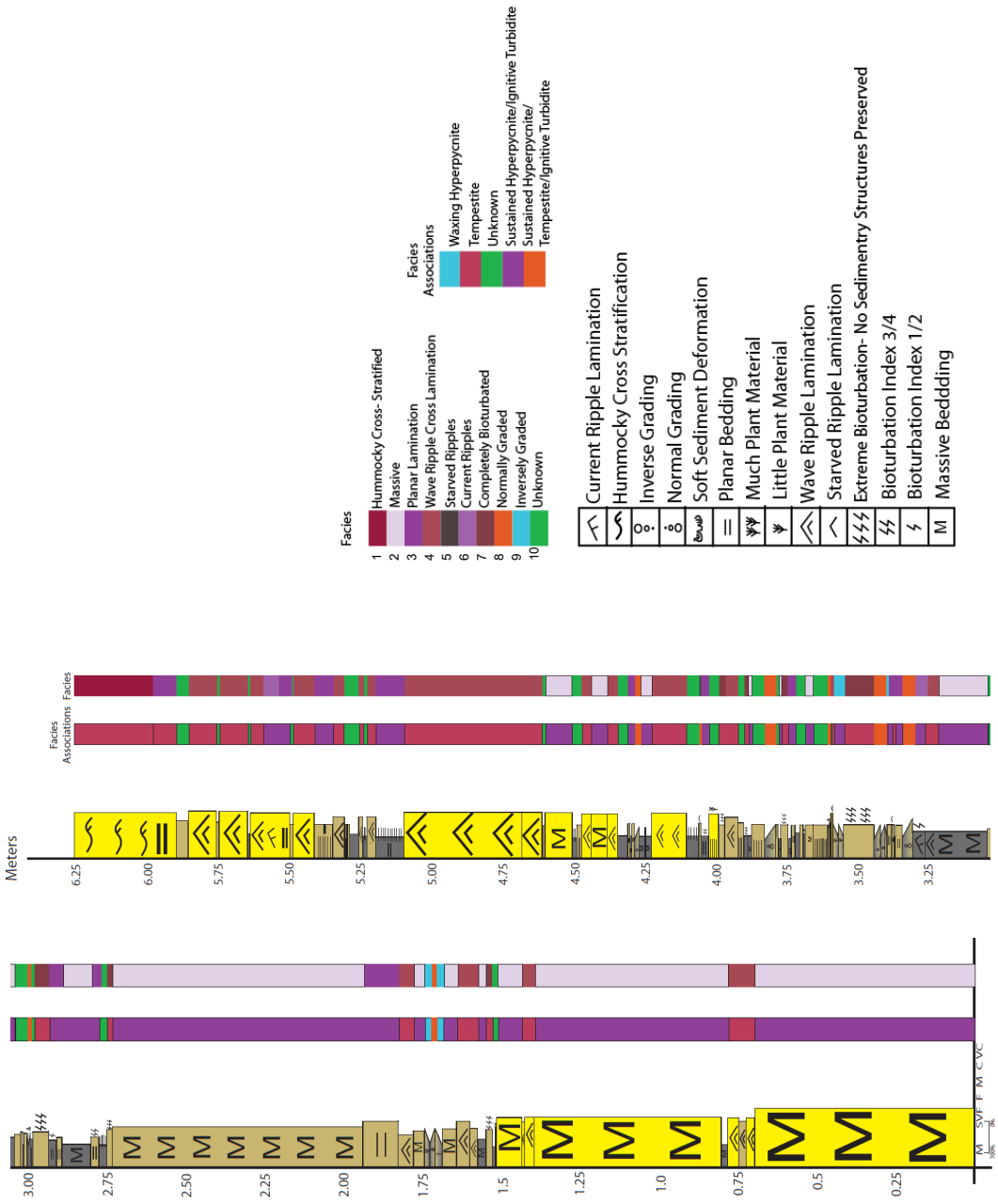


*Figure 6.13. Measured section of parasequence 16b with associated sedimentary structures, facies, and facies associations.*

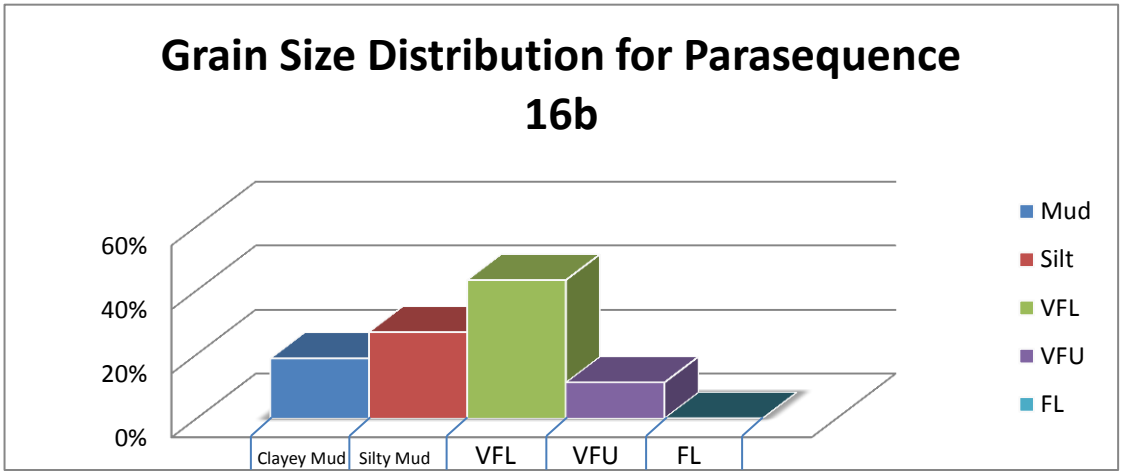


*Figure 6.14 Grain size distributions within parasequence 16.*

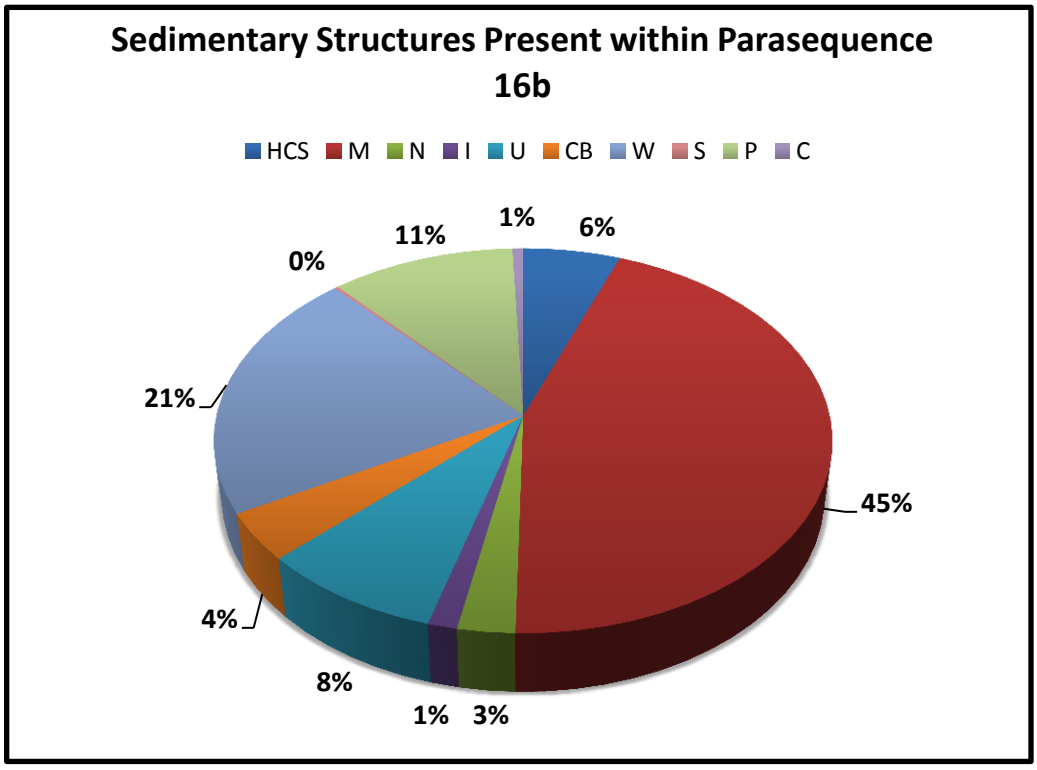


*Figure 6.15 Proportion of sedimentary structures present within parasequence 16. M=Massive, N=Normal Grading, I=Inverse Grading, U=Unknown, CB=Completely Bioturbated, W=Wave Ripples, P=Planar Laminations, S= Starved Ripples, C=Current Ripples, HCS=Hummocky Cross Stratification.*

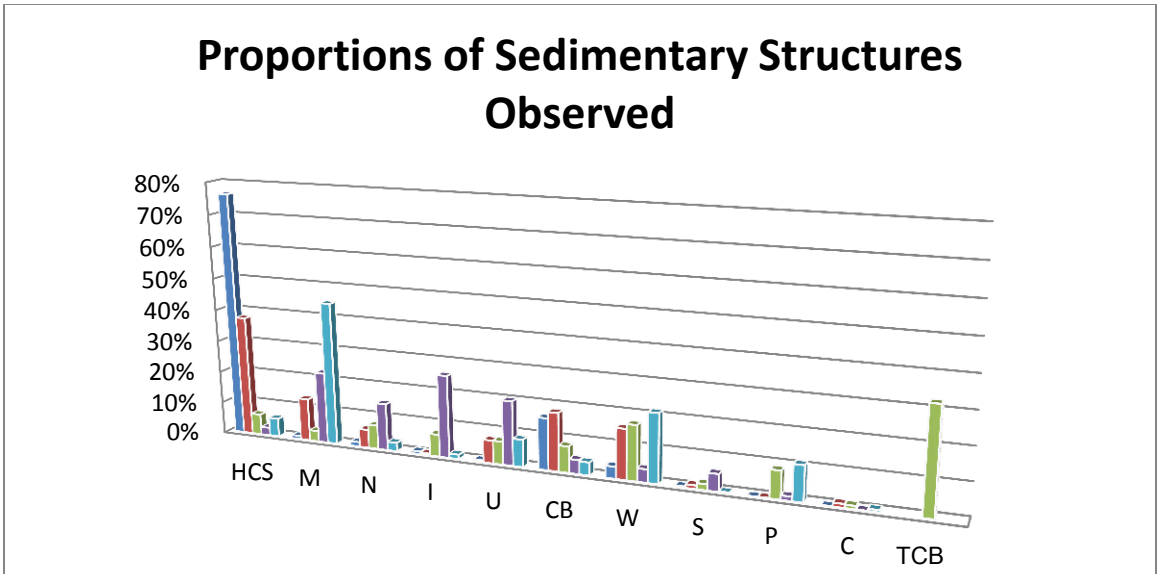


| | HCS | M | N | I | U | CB | W | S | P | C | TCB |
|---|---|---|---|---|---|---|---|---|---|---|---|
| PS5a | 76% | 1% | 1% | 1% | 1% | 16% | 4% | 0% | 0% | 0% | |
| PS5b | 38% | 13% | 6% | 1% | 7% | 18% | 16% | 1% | 0% | 1% | |
| PS6 | 6% | 3% | 7% | 7% | 7% | 8% | 17% | 2% | 9% | 1% | 32% |
| PS11 | 2% | 22% | 15% | 26% | 20% | 4% | 4% | 5% | 1% | 0% | |
| PS16 | 6% | 45% | 3% | 1% | 9% | 4% | 21% | 0% | 11% | 1% | |

*Figure 6.16 Proportion of sedimentary structures present within all measured parasequences.* HCS=Hummocky Cross Stratification, M=Massive Bedding, N=Normal Grading, I=Inverse Grading, U=Unknown Units, CB=Completely Bioturbated, W=Wave Ripples, S=Starved Ripples, P=Planar Laminations, C=Current Ripples, TCB=Trough Cross Bedding

## 7. Application to Environmental Classification, using Vertical Facies Associations

Based on Galloway's 1975 classification, along with work by Ainsworth et al. (2011), the facies identified during this study were plotted within the tripartite delta diagram to compare the dominant process (wave, fluvial, tidal) which were acting on the various parasequences.

Using sedimentary structures and dominant depositional process (ignitive turbidite, hyperpycnite, and tempestite) the dominance was determined as a proportion, ignoring the unknown facies (Table 7.1).

| Sedimentary Structure | Depositional Process | Dominance | 5a | 5b | 6 | 11 | 16 |
|---|---|---|---|---|---|---|---|
| *Massive Bedding* | Hyperpycnite/ Ignitive turbidite | Fluvial | 1% | 14% | 3% | 3% | 49% |
| *Wave Ripples* | Tempestite | Wave | 4% | 27% | 17% | 6% | 23% |
| *HCS* | Tempestite | Wave | 77% | 40% | 6% | 0% | 6% |
| *Current Ripples* | Hyperpycnite/ Ignitive turbidite | Fluvial | 0% | <1% | 33% (Includes Trough Cross beds) | 2% | 1% |
| *Starved Ripples* | Turbidites | Fluvial | <1% | 1% | 2% | 5% | <1% |
| *Planar Lamination* | Hyperpycnite/ Ignitive turbidite | Fluvial | <1% | 1% | 9% | 7% | 12% |
| *Normal Grading* | Hyperpycnite/ Ignitive turbidite | Fluvial | 1% | 6% | 7% | 30% | 3% |
| *Inverse Grading* | Hyperpycnite | Fluvial | 1% | 1% | 7% | 20% | 1% |
| *Completely Bioturbated* | Reworking by Bioturbation | Wave? | 16% | 19% | 8% | 27% | 4% |

*Table 7.1 Distribution of facies observed within various parasequences.*

Based on Table 6.1, the relative proportion dominance observed is as seen in Table 6.2 and 6.3

| | 5a | 5b | 6 | 11 | 16 |
|---|---|---|---|---|---|
| Fluvial | 4% | 29% | 72% | 92% | 69% |
| Wave | 96% | 71% | 28% | 8% | 31% |

*Table 7.2 Fluvial versus wave dominance for each parasequence observed excluding bioturbation.*

| | 5a | 5b | 6 | 11 | 16 |
|---|---|---|---|---|---|
| Fluvial | 3% | 23% | 57% | 71% | 66% |
| Wave | 97% | 77% | 43% | 28% | 34% |

*Table 7.3 Fluvial versus wave dominance for each parasequence observed including bioturbation.*

The data from table 7.2 were then plotted onto a tripartite diagram, using Ainsworth et al. (2011) classification (Fig 7.1).

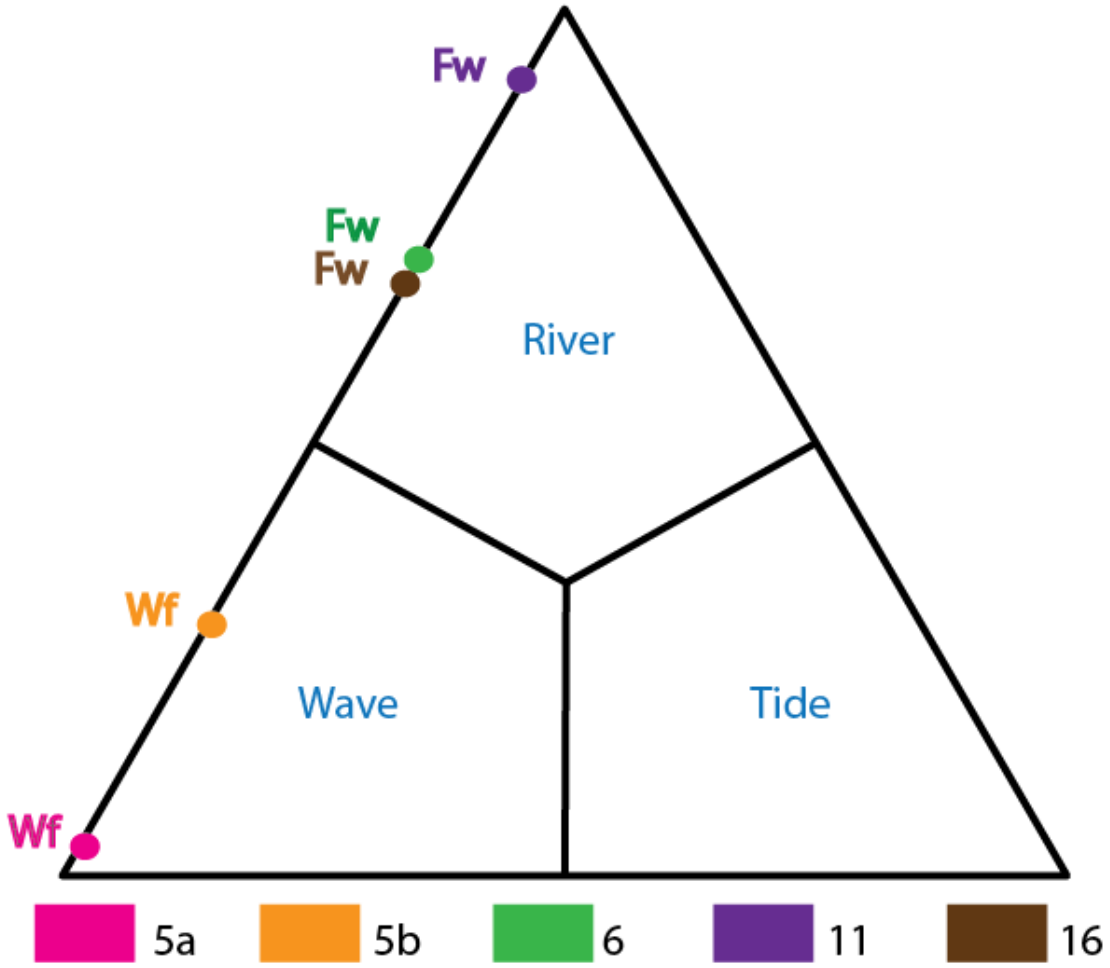


*Figure 7.1 Tripartite diagram showing the relative proportions of wave, fluvial and tidal influence within each parasequence.*

The data were plotted again, using only the heterolithic portions of each parasequence, as shown in Table 7.4, and Figure 7.2

| | 5a | 5b | 6 | 11 | 16 |
|---|---|---|---|---|---|
| Fluvial | 18% | 37% | 68% | 92% | 69% |
| Wave | 82% | 63% | 32% | 8% | 31% |

*Table 7.4 The proportion dominance of the heterolithic portion of each parasequence*

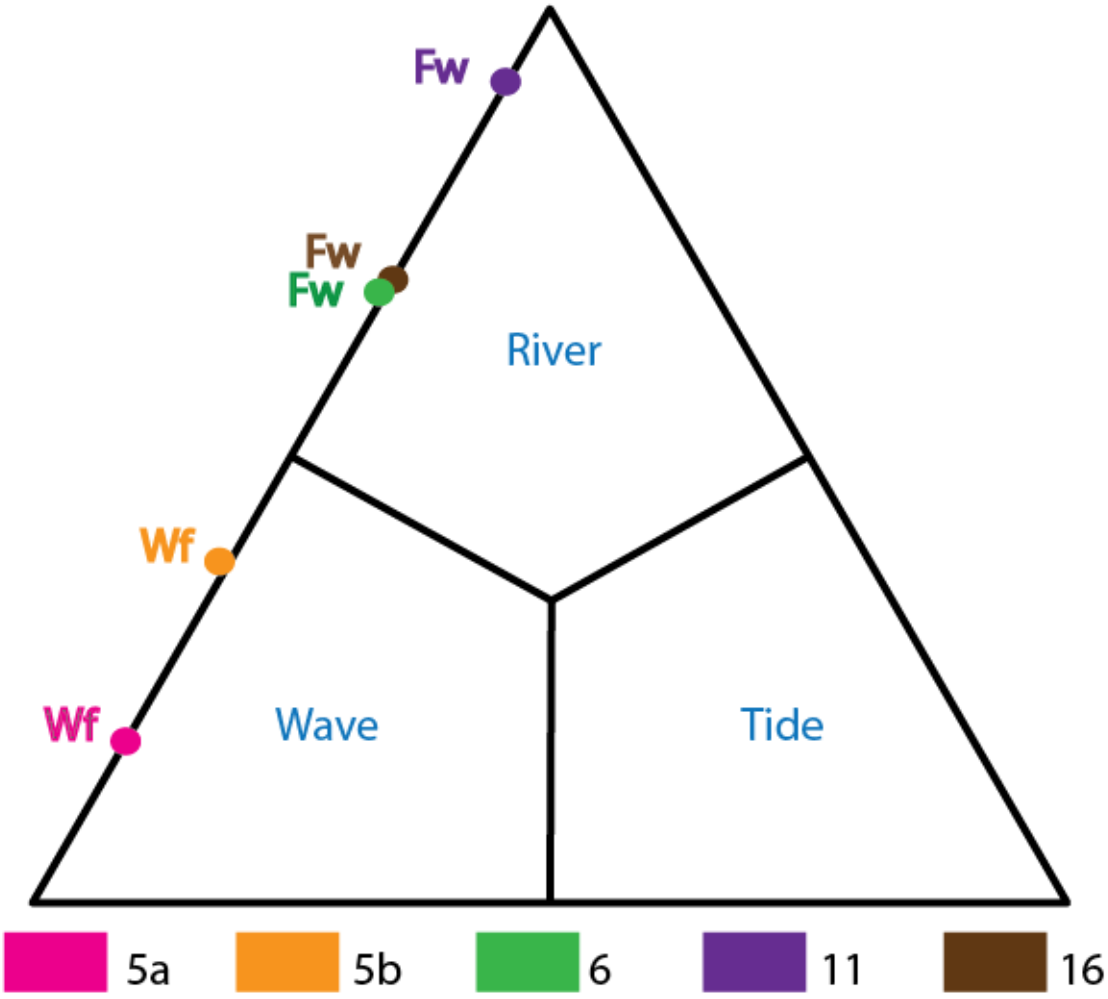


*Figure 7.2 Tripartite diagram showing the relative proportions of wave, fluvial and tidal influence within the heterolithic portions of each parasequence.*

## 8. Discussion

Tempestite deposits were the easiest formative process to recognize. HCS bedding, which may or may not be topped by wave ripples were the easiest way to recognize these deposits. Tempestites were not seen preserved in their full vertical succession as outlined by Harms et al. (1982). The relation of wave-rippled structures to only tempestite deposits is arguable. However ichnology studies on multiple locations have shown that it is possible to use bioturbation index to represent the presence of wave influence on deltas. This theory was tested by observing the percentages of completely bioturbated units within units which were storm-dominated, versus those which were river-dominated. This was shown to be true within all parasequences, except parasequence 11. Starved ripples can possibly be related to the influence of tides within the system. However due to the lack of any other tidal features such as herringbone cross bedding, tidal bundles, and reactivation surfaces, as well as their unidirectional shape, they were deducted to reflect the influence of turbidites within the system.

Turbidites, whether ignitive or sustained, proved to be a more challenging process to identify. Ignitive turbidites are rarely preserved in their entire succession, and sustained hyperpycnites, as well as ignitive turbidites can occur in repetitive Bouma $T_A$-$T_B$, and $T_B$-$T_C$ sequences. Less sustained hyperpcynite deposits, which had a waxing flow and the deposition of inversely graded beds, were the only process that allowed for their differentiation, since there seemed to be a large interplay between these two processes. No ignitive turbidites were positively identified due to poorly developed Bouma

sequences present within the sections. The differentiation did not seem to be too important and the dominant process for both successions to be deposited occurred within a fluvial setting. This therefore did not affect the quantitative plotting into the Galloway (1975) tripartite diagram.

Unknown beds did, however, leave some parts of the units questionable which lowered the accuracy of plotting of Galloway's tripartite diagram. This was negligible for parasequence 5, 6 and 16, but within parasequence 11, 26% of the beds were neither completely bioturbated, or able to positively group into a facies. Parasequence 11 was however clearly fluvial dominated, so this error seemed negligible also for this parasequence.

The results for each parasequence was compared with earlier work done by Li (2009), who looked at multiple parasequences and plotted then onto a tripartite diagram based on a larger scale mapping technique, but using multiple sections for each parasequence. The results of his work can be seen in Fig 8.1, and a comparative table seen in table 8.1.

| | **Parasequence 5a** | | **Parasequence 5b** | | **Parasequence 6** | | **Parasequence 11** | |
|---|---|---|---|---|---|---|---|---|
| | This Study | Li (2009) | This Study | Li (2009) | This Study | Li (2009) | This Study | Li (2009) |
| *Fluvial* | 4% | 8% | 29% | 29% | 72% | 29% | 92% | 19% |
| *Wave* | 96% | 90% | 71% | 67% | 28% | 67% | 8% | 78% |
| *Tidal* | 0% | 2% | 0% | 4% | 0% | 4% | 0% | 3% |

*Table 8.1 A comparison of wave, fluvial, and tidal influences as seen by Li (2009) versus this study.*

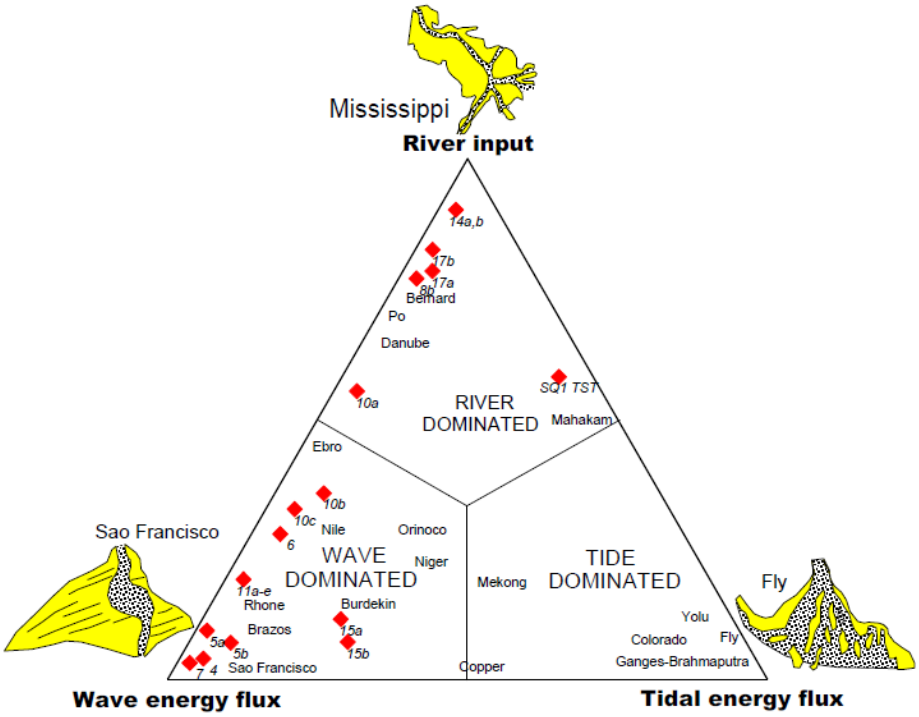


*Figure 8.1 Results of Li (2009) using multiple measured sections, as well as a larger scale mapping technique.*

From this comparison, it can be seen that there is no real differences between previous work for parasequences 5a and 5b, compared to this study. However, the numbers were quite different for those taken for parasequence 6 and 11.

Parasequence 6 is an asymmetrical delta. There is a wave-dominated upstream side and a river-dominated downstream side. The river-dominated section is fed mainly by a trunk channel and several distributary channels (Zhu, 2010). One area in which a mixed dominance can be seen is the Steamboat area, where the measured section from this study was taken. This can account for the difference in the statistical values taken from the two studies. Li (2009) accounted for multiple measured sections, taken at various

outcrop locations of parasequence 6, whereas this study only used one, from the river-dominated section of the parasequence.

Parasequence set 11 also has different statistical values, based on the similar ideas to that mentioned for parasequence 6 above. Parasequence Set 11 was mapped only in one location, and only for one of 5 parasequences which make up this parasequence set. Li (2009) based his statistics over an average of the 5 parasequences (11a-e) which make up this set, whereas this study looked at only one parasequence within the set, which was highly fluvial dominated, as opposed to the parasequence set 11 having an overall wave dominance.

This study also looked at the variations between wave, fluvial, and tidal dominance of the entire parasequence versus only the heterolithic portions within the parasequence (Figure 7.1 and Figure 7.2). These data showed that the heterolithic portions were more fluvial-influenced than the entire parasequence; however not enough to change the dominance of the overall process acting on the parasequence. All wave-dominated parasequences (parasequences 5a, 5b) were still wave-dominated whether the entire parasequence was mapped, or the heterolithic portions alone. This was also true for the river-dominated sections (parasequence 6, 11, and 16b). Higher fluvial influence within the heterolithic portions versus the entire parasequence was assumed to be due to the depth of fair-weather wave base. Since the thicker sandier portions at the top of the parasequences were assumed to be deposited above the fair-weather wave base, there was more wave action which acted during the deposition of these sands. These waves

change the overall proportions of wave energy within the parasequence, but are not enough to dominate in fluvial-dominated parasequences.

Application of this work to the thin-bed problem was done through the simulation of Gamma ray logs. This was done using parasequence 5b, and parasequence 6 for 0.15 meter intervals, and the actual data values to these simulated ones were compared (Figure 8.2 and 8.3).

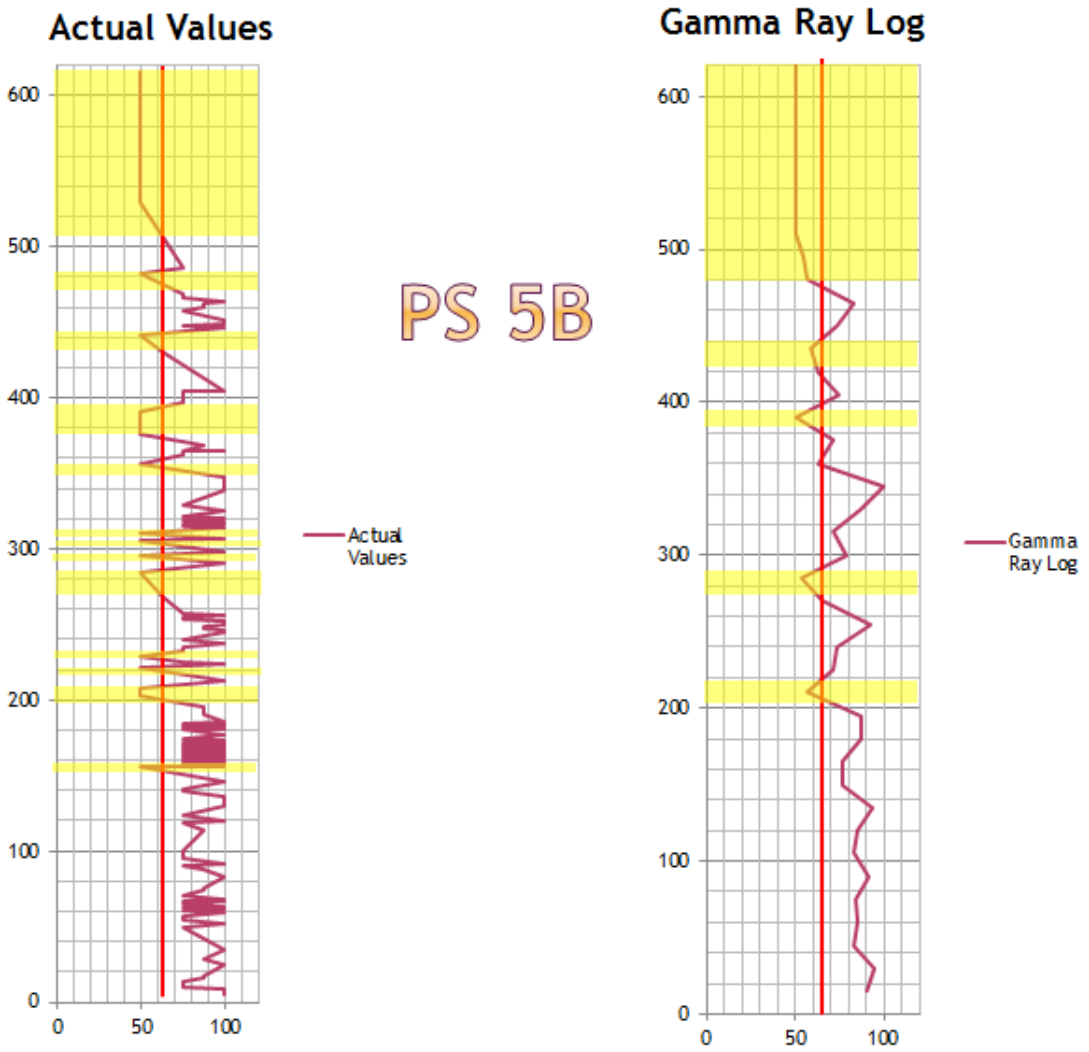


*Figure 8.2 Comparing the actual values of parasequence 5b (left) for an ideal log to a more realistic Gamma ray log (right) .Yellow areas represent sandy areas. (Scale in centimeters)*

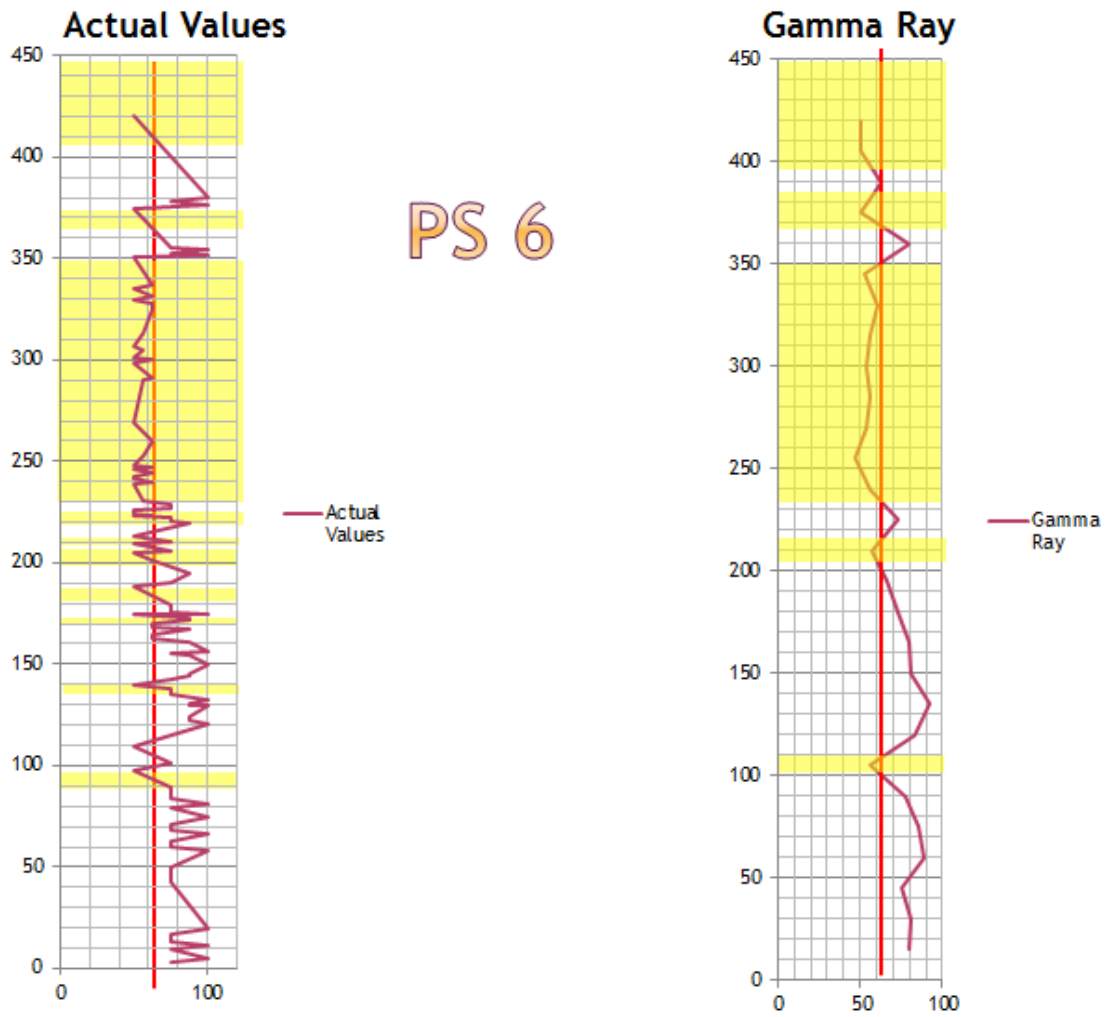


*Figure 8.3 Comparing the actual values of parasequence 6 (left) for an ideal log to a more realistic Gamma ray log (right). Yellow areas represent sandy areas (Scale in centimeters).*

Figure 1.3.2 can be compared to Figures 8.2, and 8.3 to show the actual variation between beds which can be imaged by a typical Gamma ray log, and thin-beds which are unable to do so. In Figure 8.3 around 200 centimeters, it can be seen that when there are small thin-bedded zones near each other, the Gamma ray log may average these to show an erroneous thicker sand unit than which is there. This can lead to drilling problems and underestimations if it is not accounted for.

## 9. Conclusions

Looking at the vertical facies successions and quantifying them on a millimeter to decimeter scale can quantitatively predict the formative processes to show the dominant process. This can further be used to accurately plot points onto the WTF tripartite diagram in order to determine the dominance of each process acting upon each parasequence. It can be seen that parasequence 5a is highly wave dominated, with 96% of the known facies being wave-dominated, and 4% being fluvial-dominated. Parasequence 5b was less wave-dominated than parasequence 5a, with 71% of the known facies being wave-dominated, 29% being fluvial-dominated. Parasequence 6 is fluvial dominated in a 70:30 ratio of fluvial to wave. There was no tidal influence seen within this parasequence. Parasequence 11 was seen to be the most highly fluvial-dominated, with 92% fluvial to 8% being wave-associated. Parasequence 16 was also found to be highly fluvial-dominated with 69% of the known facies being fluvial-dominated, and 31% wave-associated.

It can also be seen that mapping on a broader scale can sometimes produce similar results to those mapped on a smaller scale. This was also true when comparing the heterolithic portions of the sections to the entire parasequence. Heterolithic sections are more fluvial dominated, but does not change the dominant process which acts for the deposition of the parasequence.

With the proportions of normally graded beds as opposed to other facies, it can also be seen that deposition by suspension is a minor contribution to deposition of facies as

opposed to bedload transport. With the exception of parasequence 11, in which 30% of the beds were normally graded, all other parasequences observed had less than 10% of the deposition being normally graded beds, and hence over 90% of its deposition being due to bedload transport.

# REFERENCES

AINSWORTH, R.B., VAKARELOV, B.K., AND NANSON, R.A., 2011, Dynamic spatial and temporal prediction of changes in depositional processes on clastic shorelines: Toward improved subsurface uncertainty reduction and management, AAPG Bulletin, v. 95, no. 2, p. 267–297.

ARNOTT, R.W.C., AND HAND, B.M., 1989, Bedforms, primary structures and grain fabric in the presence of suspended sediment rain, Journal of Sedimentary Petrology, v. 59, p.1062-1069.

ASQUITH, G.B., 1990, Log Evaluation of Shaly Sandstones: A Practical Guide: Tulsa, OK (US), AAPG, 59 p.

AUGUSTINUS, P.F.E.G., 1989, Cheniers and chenier plains: a general introduction, Marine Geology, v. 90, p. 219–230.

BATES, R. L., AND JACKSON, J. A., 1984, Dictionary of Geological Terms, 3rd Edition: American Geological Institute, New York, Anchor Books, Doubleday, 571 p.

BHATTACHARYA, J. P., 2006, Deltas, in: Posamentier, H.W. and Walker, R.G., eds., Facies Models Revisited: Society for Sedimentary Geology (SEPM): Tulsa, OK, United States: Special Publication - Society for Sedimentary Geology, v. 84, p. 237-292.

BHATTACHARYA, J. P., AND WALKER, R. G., 1992, Deltas, in: R. G. Walker and N. P. James, eds., Facies Models: Response to Sea Level Change: St. John's, Newfoundland, Canada, Geological Association of Canada, p. 157–177.

BHATTACHARYA, J. P., AND MACEACHERN, J. A., 2009, Hyperpycnal rivers and prodeltaic shelves in the Cretaceous Seaway of North America: Journal of Sedimentary Research, v. 79, p. 184-209.

CAMPBELL, C. V., 1967, Lamina, lamina set, bed, and bedset: Sedimentology, v. 8, p. 7-26.

CATTANEO, A., TRINCARDI, F., ASIOLI, A., AND CORREGGIARI, A., 2007, The western Adriatic shelf clinoform: energy-limited bottomset, Continental Shelf Research, v. 27, p. 506–525.

CUMBAA, S.L., SHIMADA, K., AND COOK, T.D., 2010, Mid-Cenomanian vertebrate faunas of the Western Interior Seaway of North America and their evolutionary, paleobiogeographical, and paleoecological implications, Palaeogeography, Palaeoclimatology, Palaeoecology, v. 295, p.199-214.

DALRYMPLE, R.W., 1992, Tidal depositional systems, in: Walker, R.G., and James, N.P., eds., Facies Models: Response to Sea-Level Change: St. John's, Newfoundland, Canada, Geological Association of Canada, p. 195–218.

FIELDING, C.R., 2010, Planform and facies variability in asymmetric deltas: facies analysis and depositional architecture of the Turonian Ferron Sandstone in the

Western Henry Mountains, South-central Utah, U.S.A.: Journal of Sedimentary Research, v. 80, p. 455–479.

GALLOWAY, W.E., 1975, Process framework for describing the morphological and stratigraphical evolution of deltaic depositional systems, in: Broussard, M.L., ed., Deltas: Models for Exploration, 555 p.

GANI, M., AND BHATTACHARYA, J. P., 2007, Basic building blocks and process variability of a Cretaceous delta: internal facies architecture reveals a more dynamic interactions of river, wave, and tidal processes than is indicated by external shape, Journal of Sedimentary Research, v. 77, p. 284- 302.

GARDNER, M.H., 1995, Tectonic and eustatic controls on the stratal architecture of mid-Cretaceous stratigraphic sequences, central Western Interior Foreland Basin of North America, in: Dorobek S.L., and Ross, G.M., eds., Stratigraphic Evolution of Foreland Basins: SEPM, Special Publication 52, p. 243-281.

GARRISON, J.R., JR., AND VAN DEN BERGH, T.C.V., 2004, The high-resolution depositional sequence stratigraphy of the Upper Ferron Sandstone Last Chance Delta: an application of coal zone stratigraphy, in: Chidsey, T.C., Adams, R.D., and Morris, T.H., eds., Regional to Wellbore Analog for Fluvial–Deltaic Reservoir Modeling: The Ferron Sandstone of Utah: American Association of Petroleum Geologists, Studies in Geology, v. 50, p. 125-192.

GRAMMER, G. M., HARRIS, P. M., EBERLI, G. P., 2004, Integration of outcrop and modern analogs in reservoir modeling, AAPG Memoir, Tulsa, Okla: American Association of Petroleum Geologists, 138 p.

HAND, B.M., 1997, Inverse grading resulting from coarse-sediment transport lag, Journal of Sedimentary Research, v. 76, p. 124 – 129.

HARMS, J.C., AND FAHNESTOCK. R.K., 1965, Stratification, bed forms and flow phenomena (with an example from the Rio Grande), in: Middleton, G.V. ed., Primary Sedimentary Structures and their Hydrodynamic Interpretation. SEPM Special Publication 12, 84-l IS.

HARMS, J.C., SOUTHARD, J.B., SPERING, D.R., AND WALKER, R.G., 1975, Depositional environments as interpreted from primary sedimentary structures and stratification sequences, Society of Economic Paleontologists and Mineralogists, SEPM Short Course 2, Dallas, 153 p.

HARMS, J.C., SOUTHARD, J.B., AND WALKER, R.G., 1982, Structures and sequences in clastic rocks, Society of Economic Paleontologists and Mineralogists, Short Course 9, 249 p.

HE, S., KYSER, T.K., AND CALDWELL, W.G.E., Paleoenvironment of the Western Interior Seaway inferred from δ18O and δ13C values of molluscs from the Cretaceous Bearpaw marine cyclothem, Palaeogeography, Palaeoclimatology, Palaeoecology, v.217, p. 67-85.

HILL, P.S., FOX, J.M., CROCKETT, J.S., CURRAN, K.J., FRIEDRICHS, C.T., GEYER, W.R., MILLIGAN, T.G., OGSTON, A.S., PUIG, P., SCULLY, M.E., TRAYKOVSKI, P.A., AND WHEATCROFT, R.A., 2007, Sediment delivery to the seabed on continental margins, in: Nitrouer, C.A., Austin, J.A., Field, M.E, Kravitz, J.H., Syvitski, J.P.M., Wiberg, P.L. eds., Continental-Margin Sedimentation: from Sediment Transport to Sequence Stratigraphy, IAP Special Publication 37, Blackwell Publishing, Oxford.

KAUFFMAN, E.G., 1977, Upper Cretaceous cyclothems, biotas and environments, Rock Canyon Anticline, Pueblo, Colorado, Cretaceous Facies, Faunas and Paleoenvironments across the Western Interior Basin, Mountain Geologist, v.14 , p. 129–152.

KAUFFMAN, E.G., 1984, Paleobiogeography and evolutionary response dynamic in the Cretaceous Western Interior Seaway of North America, Jurassic–Cretaceous Biochronology and Biogeography of North America. Geological Association of Canada, Special Paper 27, p. 273–306.

KNELLER, B.C., AND BRANNEY, M.J., 1995, Sustained high-density turbidity currents and the deposition of thick massive sands, Sedimentology, v. 42, p. 607–616.

LAMBIASE, J.J., DAMIT, A.R., SIMMONS, M.D., ABDORRIAS, R., AND HUSSIN, A., 2003, A Depositional model and the stratigraphic development of modern and ancient tide-dominated deltas in NW Borneo, in: Sidi, F.H., Nummedal, D., Imbert, P., Darman, H., and Posamentier, H.W., eds., Tropical Deltas of Southeast Asia—Sedimentology, Stratigraphy, and Petroleum Geology: SEPM Special Publication 76, p. 109–123.

Li W., 2009, Valleys, facies, and sequence stratigraphy of the Ferron Notom delta, Capital Reef, Utah, Ph.D. Dissertation, University of Houston, Texas, USA

LOCK, B. E., BUTLER, R. W., AND FRANKLUND, R. T., 2009, Tempestite sedimentation: An example from the Del Rio Formation of West Texas: Gulf Coast Association of Geological Societies Transactions, v. 59, p. 463-476.

LOWE. D.R., 1976, Grain flows and grain flow deposits, Journal of Sedimentary Petrology, v.46, p.188- 199.

LOWE, D.R., 1982, Sediment gravity flows, II, Depositional models with special reference to the deposits of high-density turbidity currents, Journal of Sedimentary Petrology, v.52, p. 279-297.

MACEACHERN, J.A., BANN, K.L., BHATTACHARYA, J.P., AND HOWELL JR., C.D., 2005, Ichnology of deltas: Organisms responses to the dynamic interplay of rivers, waves, storms, and tides, in: Giosan, L., and Bhattacharya, J.P., eds., River Deltas – Concepts, Models, and Examples: Society for Sedimentary Geology, Special Publication 83, p. 49-85.

MACQUAKER, J. H. S., AND BOHACS, K. M., 2007, Geology, on the accumulation of mud, Science, v.318, p.1734–1735.

MACQUAKER, J.H.S., BENTLY, S.J., AND BOHACS, K.M., 2010, Wave-enhanced sediment-gravity flows and mud dispersal across continental shelves: Reappraising sediment

transport processes operating in ancient mudstone successions, Geology, v.38, no. 10, p. 947–950.

MCLANE, M., 1995, Sedimentology, Oxford University Press Edition, USA, 423 p.

MIDDLETON, G.V., 1967, Experiments on density and turbidity currents, III, Deposition of sediment, Canadian Journal of Earth Science. v.4, p. 475-505.

MULDER, T., AND SYVITSKI, J.P.M., 1995, Turbidity currents generated at river mouths during exceptional discharge to the world's oceans, Journal of Geology, v. 103, p. 285–298.

MULDER, T., SYVITSKI, J. P. M., AND SKENE, K.I., 1998, Modeling of erosion and deposition by turbidity currents generated by river mouths, Journal of Sedimentary Research, v. 68, p. 124-137.

MULDER, T., SYVITSKI, J.P.M., MIGEON, S., FAUGERES, J., AND SAVOYE, B., 2003, Marine hyperpycnal flows: initiation, behavior and related deposits. A review, Marine and Petroleum Geology, v. 20, p. 861-882.

MYROW, P.M., FISCHER, W., AND GOODGE, J.W., 2002, Wave-modified turbidites: combined-flow shoreline and shelf deposits, Cambrian, Central Transantarctic Mountains: Journal of Sedimentary Research, v. 72, p. 641-656.

MYROW, P.M. AND SOUTHARD, J.B., 1996, Tempestite deposition, Journal of Sedimentary Research, v.66, p. 875-887.

NAKAJIMA, T., 2006, Hyperpycnites deposited 700 km away from river mouths in the Central Japan Sea: Journal of Sedimentary Research, v. 76, p. 60–73.

NICHOLS, G., 1999, Sedimentology and Stratigraphy: London, Blackwell, 355 p.

PASSEY, Q. R., DAHLBERG, K. E., SULLIVAN, K. B., YIN, H.R., BRACKETT, A., XIAO, Y. H., AND GUZMÁN-GARCIA, A. G., 2006a, A clastic thin bed problem, in: Passey, Q.R., ed., Petrophysical Evaluation of Hydrocarbon Pore-thickness in Thinly Bedded Clastic Reservoirs: Volume AAPG Archie Series, No. 1, p. 1 – 15.

PASSEY, Q. R., DAHLBERG, K. E., SULLIVAN, K. B., YIN, H.R., BRACKETT, A., XIAO, Y. H., AND GUZMÁN-GARCIA, A. G., 2006b, Definitions and geologic occurrence of thin beds in clastics, in: Passey, Q.R., ed., Petrophysical Evaluation of Hydrocarbon Pore-thickness in Thinly Bedded Clastic Reservoirs , Volume AAPG Archie Series, No. 1, p. 27 – 39.

PETERSON, F., AND RYER, R.T., 1975, Cretaceous rocks in the Henry Mountains regions, Utah and their relation to neighboring regions, in: Fassett, J.E., and Wengerd, S.A., eds., Canyonlands Country: Four Corners Geological Society Guidebook, 8th Field Conference, p. 167-189.

PETTIJOHN, F.J., 1975, Sedimentary Rocks, Third Edition: New York, Harper & Row, 628 p.

PLINK-BJÖRKLUND, P. AND STEEL, R., 2004, Initiation of turbidity currents: Evidence for hyperpycnal flow turbidites in Eocene Central Basin of Spitsbergen, Sedimentary Geology, 165, p. 29-52.

POSAMENTIER, H.W., AND WALKER, R.G., 2006, Facies Models Revisited: Society for Sedimentary Geology (SEPM): Tulsa, OK, United States: Special Publication - Society for Sedimentary Geology, v. 84, p. 237-292.

PROTHERO, D.R., AND SCHWAB, F., 2004, Sedimentary Geology: An Introduction to Sedimentary Rocks and Stratigraphy, Second Edition: New York, W.H. Freeman and Company, 557 p.

RODRIGUEZ, A.B., HAMILTON, M.D., AND ANDERSON, J.B., 2000, Facies and evolution of the modern Brazos River, Texas: Wave versus flood influence, Journal of Sedimentary Research, v. 70, no. 2, p. 283–295.

ROTONDO, K.A., AND BENTLY, S.J., 2003, Marine dispersal of fluvial sediments as fluid muds: old concept, new significance, in: Scott, E.D., Bouma, A.H., and Bryant, W.R., eds., Siltstones, Mudstones and Shales: Depositional Processes and Characteristics: SEPM, CD-ROM, p. 24–49.

RYER, T.A., 2004, Previous studies of the Ferron Sandstone, in: Chidsey, T.C., Jr., Adams, R.D., and Morris, T.H., eds., Regional to Wellbore Analog for Fluvial-Deltaic Reservoir Modeling: The Ferron Sandtone of Utah: AAPG, Studies in Geology, v. 50, p. 3-38.

SHANMUGAM, G., 1996, Perception vs. reality in deep-water exploration, World Oil, v.217, p. 37-41.

SHANMUGAM. G., MOIOLA, R.J., 1995, Reinterpretation of depositional processes in a classic flysch sequence (Pennsylvanian Jackfork Group), Ouachita Mountains. Arkansas and Oklahoma, AAPG Bulletin, v.79, p.672-695.

SCHIEBER, J., AND J. B. SOUTHARD, 2009, Bed-load transport of mud by floccule ripples: Direct observation of ripple migration processes and their implications, Geology, v.37, p.483–486.

SCHIEBER, J., J. B. SOUTHARD, AND A. SCHIMMELMANN, 2010, Lenticular shale fabrics resulting from intermittent erosion of water-rich muds: Interpreting the rock record in the light of recent flume experiments, Journal of Sedimentary Research, v. 80, p.119–128.

SCHIEBER, J., J. B. SOUTHARD, AND K. THAISEN, 2007, Accretion of mudstone beds from migrating floccule ripples: Science, v. 318, p. 1760–1763.

SOYINKA, O.A. AND SLATT, R.M., Identification and micro-stratigraphy of hyperpycnites and turbidites in Cretaceous Lewis Shale, Wyoming, Sedimentology, v. 55, no. 5, p.1117–1133.

STAUFFER, P.H., 1967, Grain-flow deposits and their implications, Santa Ynez Mountains, California, Journal of Sedimentary Petrology, v.37, p.25-43.

SUTER, J.R., 2006 Clastic shelves, in: Posamentier, H.W., and Walker, R.G., eds., Facies Models Revisited: Society for Sedimentary Geology (SEPM): Tulsa, OK, United States: Special Publication - Society for Sedimentary Geology, v. 84, p. 237-292.

TA, T.K.O., NGUYEN, V.L., TATEISHI, M., KOBAYASHI, I., AND SAITO, Y., 2005, Holocene evolution and depositional models of the Mekong River Delta, southern Vietnam, in: Giosan, L., and Bhattacharya, J.P., eds., River Deltas: Concepts, Models, and Examples: Society for Sedimentary Geology, Special Publication 83, p. 453–466.

WALKER, R. G., DUKE, W. L., AND LECKIE, D. A., 1983, Hummocky stratification—Significance of its variable bedding sequences: Discussion: Geological Society of America Bulletin, v. 94, p. 1245-1249.

WILLIAMS, G.D. and STELCK, C.R., 1975, Speculations on the paleogeography of North America, in: Caldwell, W.G.E., ed., The Cretaceous System in the Western Interior of North America, Geological Association of Canada, Special Paper 13, p.1-20.

VAN WAGONER, J. C., MITCHUM, R. M., CAMPION, K. M., AND RAHMANIAN, V. D., 1990, Siliciclastic Sequence Stratigraphy in Well Logs, Cores, and Outcrops: AAPG Methods in Exploration Series, no. 7, 63 p.

WALKER, R.G., 1967, Turbidite sedimentary structures and their relationships to proximal and distal environments, Journal of Sedimentary Petrology, v.37, p.25-43.

WALSH, J.P., NITTROUER, C.A., PALINKAS, C.M., OGSTON, A.S., STERNBERG, R.W., AND BRUNSKILL, G.J., 2004, Clinoform mechanics in the Gulf of Papua, New Guinea, Continental Shelf Research, v. 24, p. 2487–2510.

ZENG, H., 2009, How thin is a thin bed? An alternative perspective, The Leading Edge, v. 28, no. 10, p. 1192-1197.

ZHU, Y., 2010, Sequence stratigraphy and facies architecture of the Cretaceous Ferron Notom Delta Complex, Central Utah, USA, Ph.D. Dissertation, University of Houston, Texas, USA

# APPENDIX

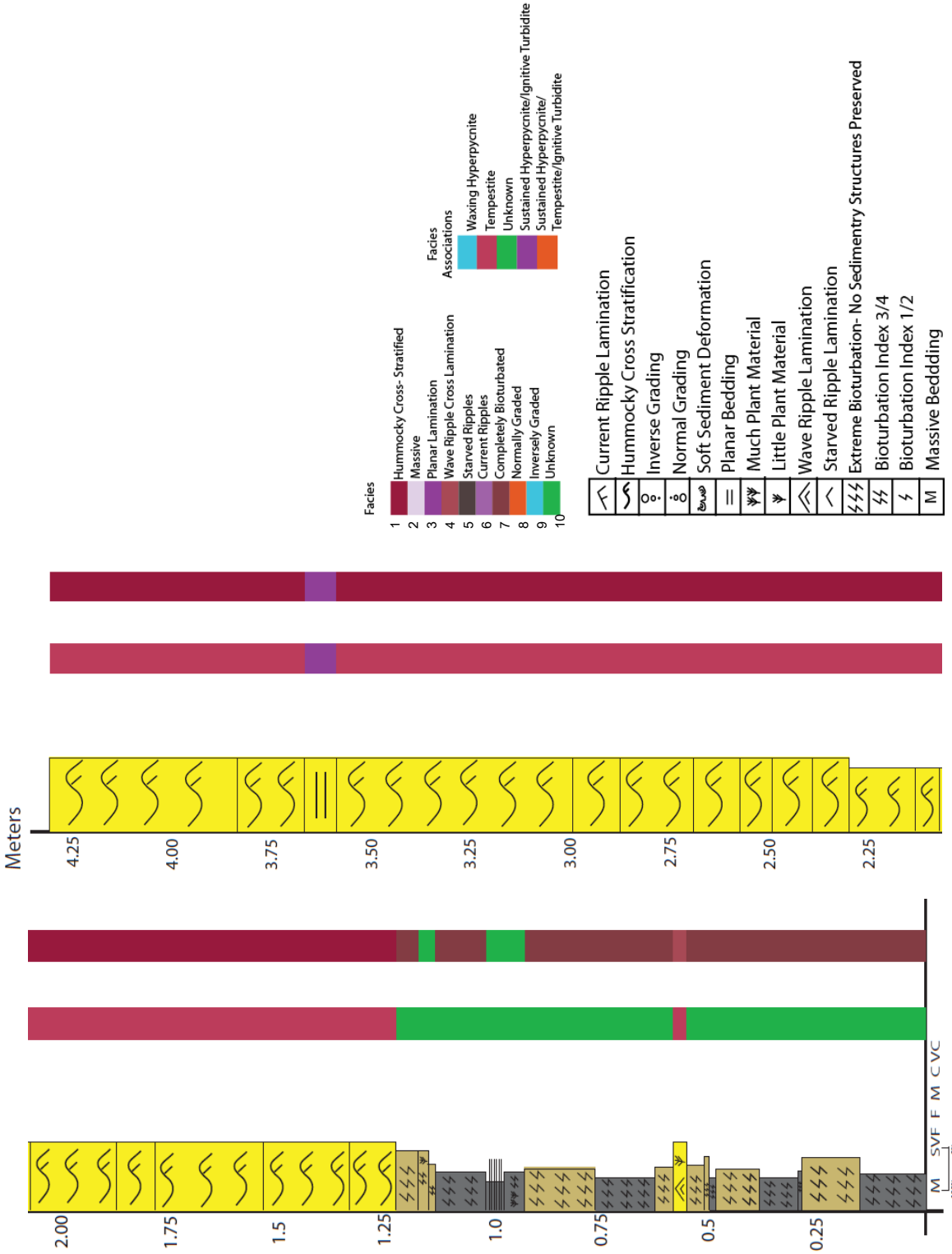


*Figure A1. Parasequence 5a. Left section taken as can be seen in Fig.3.4 with associated sedimentary structures, facies, and facies associations.*

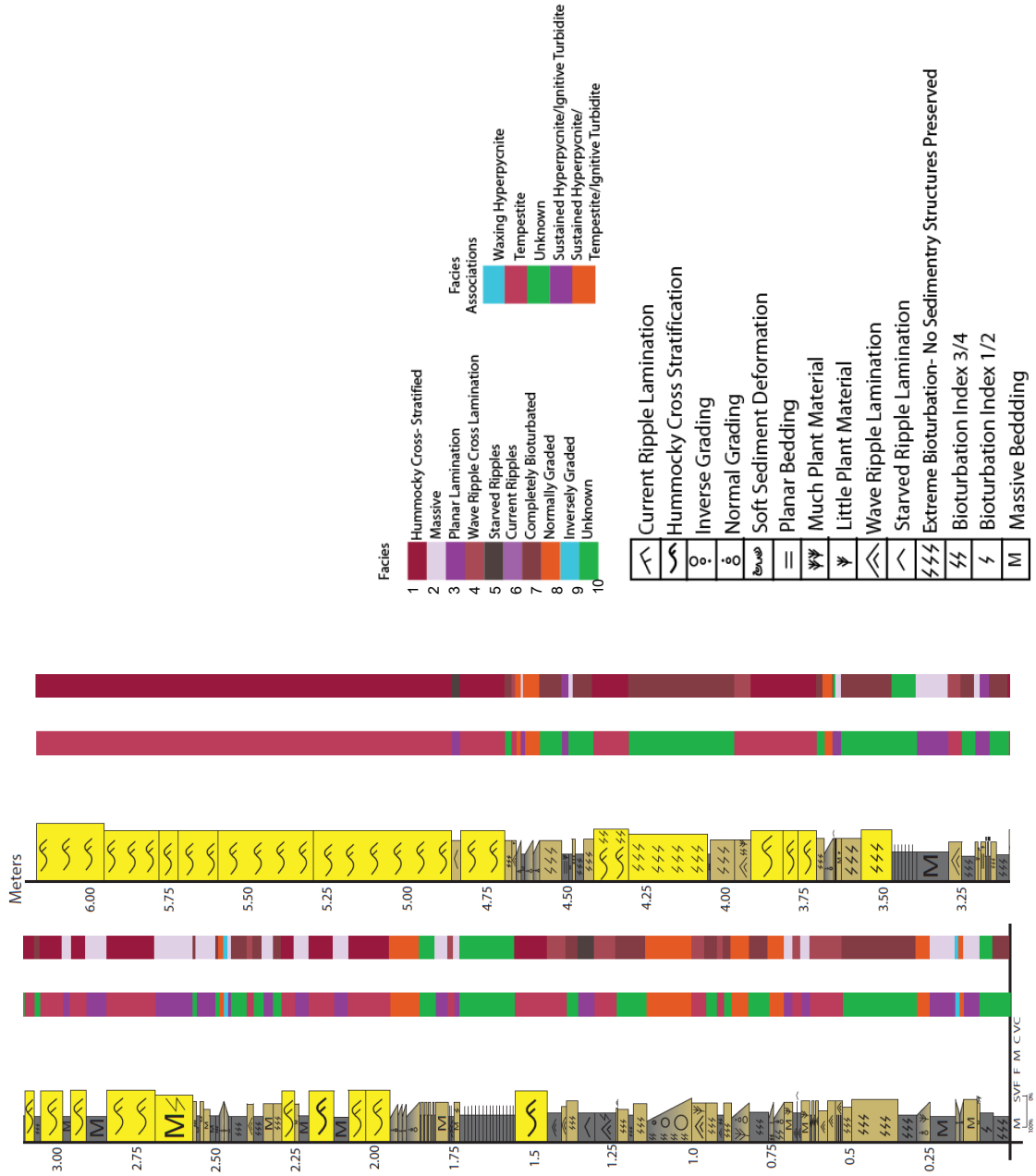


*Figure A2. Parasequence 5b. Left section taken as can be seen in Fig.3.4 with associated sedimentary structures, facies, and facies associations.*

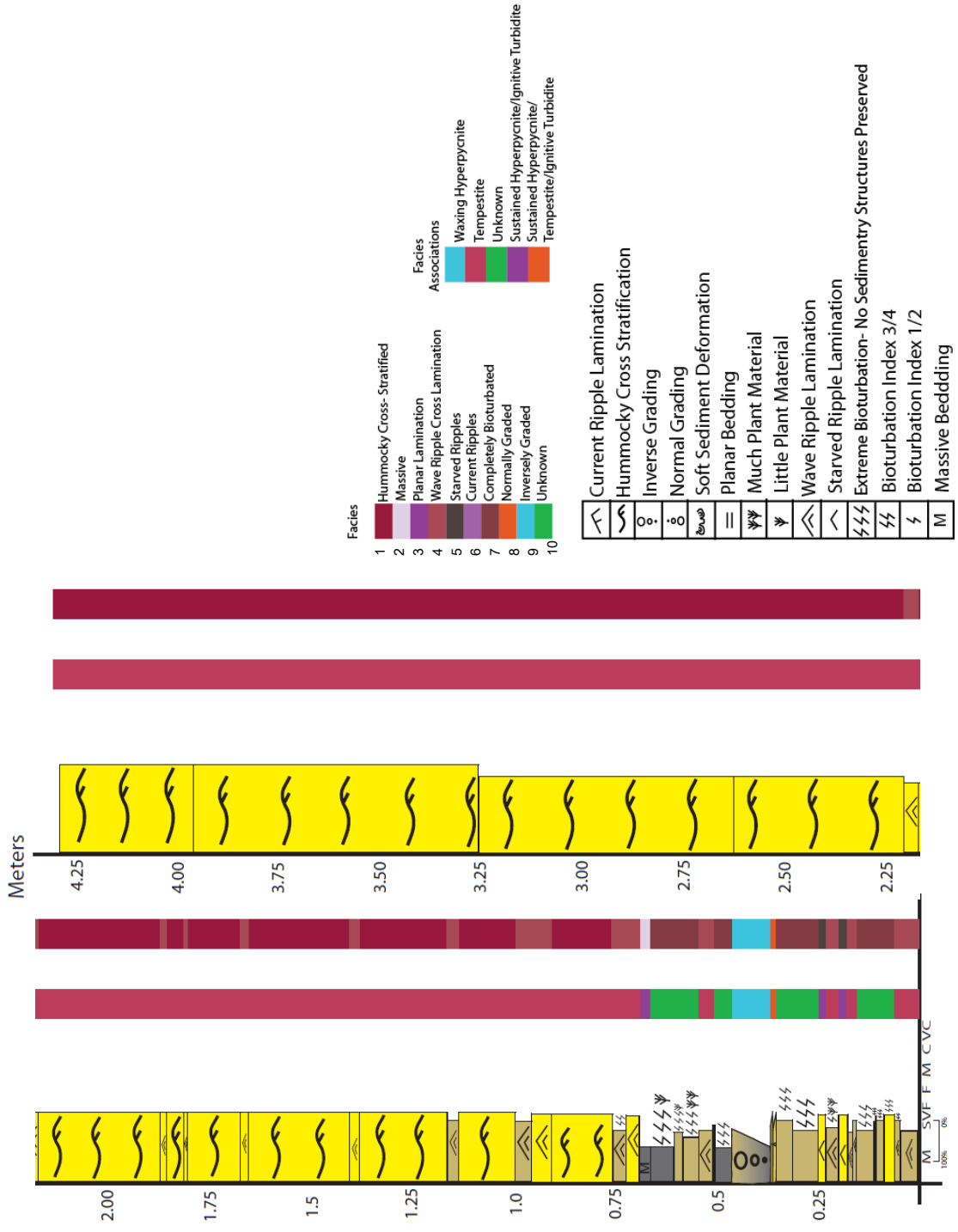


*Figure A3. Parasequence 5a. Right section taken as can be seen in Fig.3.4 with associated sedimentary structures, facies, and facies associations.*

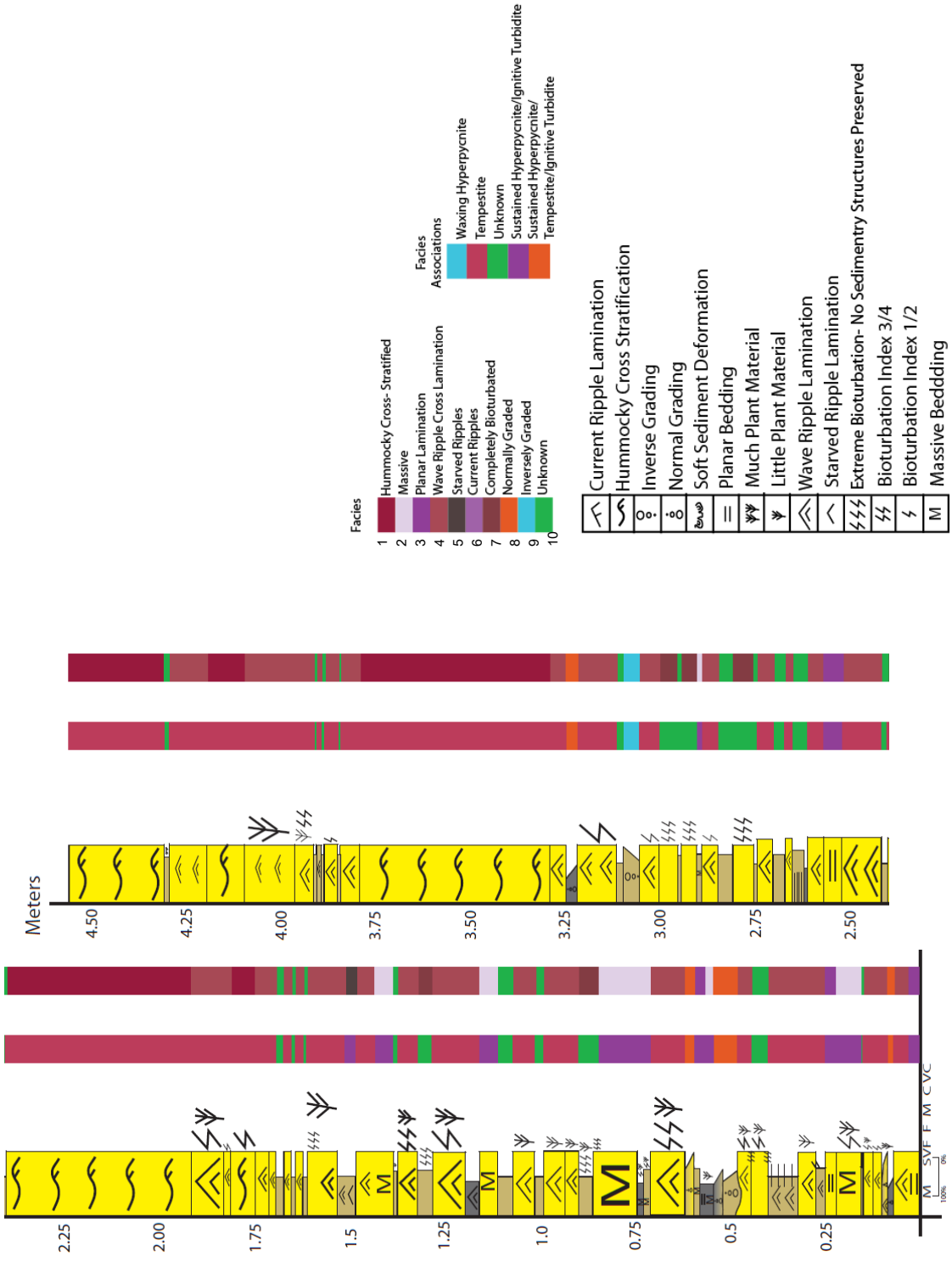


*Figure A4. Parasequence 5b. Right section taken as can be seen in Fig.3.4 with associated sedimentary structures, facies, and facies associations.*